Department of Physics and Astronomy

University of Heidelberg

Diploma thesis
in Physics
submitted by

Stephan Schnez

born in Ludwigshafen am Rhein

Year of submission: 2006

Bremsstrahlung in a Circularly Polarized Laser Field

This diploma thesis has been carried out **by Stephan Schnez** at the

Max Planck Institute for Nuclear Physics

under the supervision of

Professor Dr. Christoph H. Keitel

and

Privatdozent Dr. Ulrich D. Jentschura

Bremsstrahlung in a Circularly Polarized Laser Field

Abstract

In this diploma thesis, we evaluate the process of laser-assisted bremsstrahlung. In the usual, well-known bremsstrahlung process, an electron scatters off a Coulomb potential and spontaneously emits a photon. Here, the same process is considered, but in the presence of a strong, circularly polarized laser field. The intensities of the lasers we consider here are in the range of $10^{19}\,\mathrm{W/cm^2}$ to $10^{21}\,\mathrm{W/cm^2}$ so that a fully relativistic description is necessary. Consequently, we use a quantum-electrodynamical approach. In our formalism, we take the laser field into account by using the solutions of the Dirac equation coupled to an external field – the so-called Volkov solutions. Apart from the theoretical derivation of the laser-dressed bremsstrahlung cross section, the numerical evaluation of the resulting expression with the help of a self-written Fortran 90 programme is an essential part of the thesis at hand. One of the main results is that the cross section shows resonances at – depending on the scattering geometry – integer multiples of the laser frequency. In other words, we have *higher harmonic generation* in the bremsstrahlung process.

Contents

1 Introduction and Notation **1**
- 1.1 Introduction . . . 1
- 1.2 Units and Notation . . . 4
- 1.3 The Ponderomotive Energy . . . 6

2 Derivation of the Bremsstrahlung Cross Section **7**
- 2.1 Volkov Solutions of the Dirac Equation . . . 8
- 2.2 The Full, Laser-Dressed Electron Propagator . . . 11
- 2.3 The Vector Potentials $A_{\mathrm{Coul}}(x)$ and $A_{b,\lambda}(x)$ . . . 13
- 2.4 The S-Matrix and the Cross Section . . . 14
  - 2.4.1 Limit of Vanishing Laser Field $a \to 0$ . . . 18
  - 2.4.2 Integrated Cross Section . . . 19
- 2.5 Resonances and Higher Harmonic Generation . . . 19
- 2.6 Finite Peaks – the Imaginary Mass and Energy . . . 21
- 2.7 Explicit Calculation of the Cross Section . . . 23

3 The Numerical Evaluation **27**
- 3.1 Overview over the Whole Programme . . . 27
- 3.2 Implementation of the Minkowski Metric and the Dirac Algebra . . . 29
- 3.3 The Numerical Integration over $\mathrm{d}\Omega_f$ . . . 30
- 3.4 Calculation of the Differential Cross Section . . . 33
- 3.5 Calculation of the Imaginary Mass and Energy Shift . . . 36
- 3.6 Numerical Tests of the Validity of the Code . . . 37

4 Results **41**
- 4.1 Comparison between the Free and the Laser-Dressed Electron Propagator . . . 41
- 4.2 Comparison with and without Imaginary Mass and Energy . . . 43
- 4.3 Differential Cross Sections . . . 43
- 4.4 Total Cross Sections . . . 47
- 4.5 The Peculiar Behaviour for a Varying Laser Intensity . . . 49

5 Summary and Outlook **53**

A Derivation of the Bethe-Heitler Cross Section **57**

B Classical Motion of an Electron **63**

C The Role of the Interference Term **67**

D Dirac Algebra and the Free Dirac Spinor **69**

E Bessel Functions and Generalized Bessel Functions **71**

F Derivation of $S_{fi}^{(1)}$ **77**

G Main Structure of the Programme **83**

Chapter 1

Introduction and Notation

1.1 Introduction

"A solution looking for a problem."
General perception of the first lasers in the scientific community

Quantum electrodynamics (QED) deals with the quantized electromagnetic field. It is the most precise physical theory mankind has advanced so far. For example, Landé's g factor of the electron – the gyromagnetic ratio – is predicted to be[1]

$$\frac{g-2}{2} = 0.001\,159\,652\,140 \pm 0.000\,000\,000\,028$$

according to QED. The most recent experiments give [2]

$$\frac{g_{\text{exp}}-2}{2} = 0.001\,159\,652\,180\,85(76).$$

This is a most remarkable agreement between theory and experiment to an accuracy greater than one part in a billion. Transition frequencies of hydrogen and deuterium were recently calculated to an even higher precision [3].

QED-processes are in most cases calculated according to a diagram-technique originally developed by R. P. Feynman. Feynman diagrams are a graphical representation of the expansion of the S-matrix in powers of the fine-structure constant α. However, for a free electron, the first-order process (commonly referred to as the elementary QED-vertex since all higher-order Feynman diagrams consist of combinations of this vertex, see figure (1.1)) is forbidden by four-momentum conservation. This will be proven briefly. The four-momenta of the initial and final electron are $p_{i,f} = (E_{i,f}, \vec{p}_{i,f})$, and the corresponding four-momentum of the photon is $k = \left(\omega, \vec{k}\right)$ (for questions due to units, please consult the next section). Thus, one would get at the vertex

$$k = p_i - p_f \Rightarrow k^2 = (p_i - p_f)^2 \stackrel{!}{=} 0$$

[1] J. Schwinger did a first calculation to second order in 1948 and found $(g-2)/2 = \alpha/(2\pi)$. Today's theoretical prediction includes terms up to four loops; see [1].

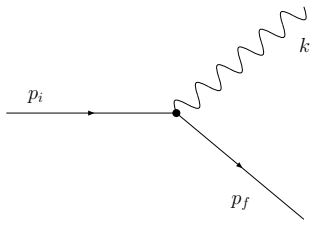

Figure 1.1: The elementary QED-vertex corresponds to photon emission or absorption by a free electron or positron. Here and in all other Feynman diagrams, the time evolves from left to right. Hence, the QED-vertex depicted here shows photon emission by an electron. This process is forbidden by four-momentum conservation.

for a real photon. On the other hand, we have:

$$\begin{aligned}(p_i - p_f)^2 &= p_i^2 + p_f^2 - 2p_i p_f = 2m_e^2 - 2E_i E_f + 2\vec{p}_i\vec{p}_f \\ &= 2m_e^2 - 2E_i^2 + 2\omega E_i + 2\vec{p}_i^{\,2} - 2\vec{k}\vec{p}_i \\ &= 2\omega E_i - 2\omega E_i \underbrace{\sqrt{1 - \frac{m_e^2}{E_i^2}}}_{<1} \cos\alpha \\ &> 0.\end{aligned}$$

with $E_i^2 = p_i^2 + m_e^2$ and $\alpha = \angle(\vec{k}, \vec{p}_i)$. The square root could only be equal to 1 if $E_i \to \infty$, i.e. the electron moves with the velocity of light. This is of course not possible because the electron is not massless. Hence, we get a contradiction; the process is not allowed consequently.

A second-order process is the emission of *bremsstrahlung*; the corresponding Feynman diagrams are depicted in figure (1.2). In contrast to the first-order process we just considered, bremsstrahlung is not forbidden by four-momentum conservation. The reason is that the intermediate electron, i.e. the electron between the two vertices, does not have to fulfill the on-shell condition $p^2 = m_e^2$. Bremsstrahlung occurs whenever a charged particle is deflected by the Coulomb field of a nucleus. The Coulomb force acting on the charged particle leads to the emission of a photon. This is also well-known from classical electrodynamics. A fully relativistic calculation of this process using the means of QED was done by H. Bethe and W. Heitler [4].

In 1935, D. M. Volkov solved the Dirac equation for a spin-1/2-particle in an external (i.e. classical), electromagnetic plane-wave field [5]. This achievement laid the foundation for a cal-

Figure 1.2: Bremsstrahlung is a second-order process. The incoming electron first interacts with the Coulomb potential of a nucleus (dashed line with cross) and then emits the bremsstrahlung photon or vice versa. These two processes interfere coherently.

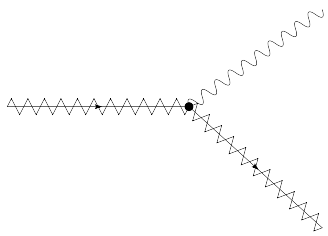

Figure 1.3: The elementary QED-process is not forbidden anymore if it takes place in an external laser field for which we introduce the nonstandard notation of a zigzag-line. We will refer to this process as laser-dressed Compton scattering.

culation of QED-processes in these fields by using the so-called *Volkov states* as initial and final states. However, back in those days, monochromatic plane-wave fields were just of theoretical interest; an experimental realisation of such a field was impossible. Things changed in 1960 when Theodore Maiman built a special light source using *l*ight *a*mplification by *s*timulated *e*mission of *r*adiation – a so-called laser [6]. Experimental physicists started to investigate the behaviour of charged particles in monochromatic external fields. Consequently, theoretical interest also arose. With the discovery of *higher harmonic generation* of radiation, this new field became even more fascinating. Higher harmonic radiation is radiation which is emitted during a process in a laser field whose frequency ω_e is an integer multiple of the laser frequency ω: $\omega_e = n\omega, n = 1, 2, 3 \ldots$ A well-written account of atomic physics with high-intensity lasers including the historical development is the review article [7].

The external field can be seen as a pool which "provides" energy and momentum. Consequently, the first-order process which is forbidden by four-momentum conservation in the vacuum will be allowed in an external field. The Feynman diagram for this *laser-dressed* or *laser-assisted Compton scattering*[2] can be seen in figure (1.3). This is the first process taking place in an external field which was analysed using QED ([8, 9], and recently [10]). However, a numerical evaluation of the results is very hard because in the expressions appear infinite sums over so-called *generalized Bessel functions*.

For a couple of years now, modern computers are fast enough to tackle this problem. Simultaneously, lasers became that powerful that the ponderomotive energy[3] U_p of an electron in the laser field is of the order of its rest mass: $U_p \gtrsim m_e c^2$. In order to describe these processes correctly, calculations have to be carried out relativistically.

In this diploma thesis, we will now go over to a second-order process – namely bremsstrahlung – and analyse its features if the process is exposed to an external, circularly polarized plane-wave field (see figure (1.4)). The derivation of the cross section will be done fully relativistically, taking into account the laser-dressed electron propagator. Then, the result will be evaluated numerically by a Fortran 90 programme. In fact, the numerical analysis of the cross section is quite demanding because we will encounter several infinite sums in the expression of the cross section. Thus, an analytical approach for the evaluation is impossible. Finally, numerical results both for the differential cross section and the integrated one over the direction of the outgoing electron will be presented for different scattering geometries. We will see that we have emission of higher harmonics. Since the Bethe-Heitler formula is the counterpart to the laser-dressed

[2]Compton scattering is the inelastic scattering of a photon off an electron. However, this is the special case of photon emission by an electron in an external field if this field contains just one photon. Therefore, this much more general process is called laser-dressed Compton scattering in scientific articles.

[3]This is the average classical kinetic energy of a particle in an external field. This concept will be explained in more detail below.

Figure 1.4: Bremsstrahlung can also take place in an external field. Then not only the initial and final electron states, but also the electron propagator are modified by the interaction with the field.

case discussed here, we will present a full and detailed re-derivation of this nontrivial result in appendix A. In fact, for a vanishing laser field or, equivalently, arguments of the Bessel functions equal to zero, the laser-dressed cross section goes over into the Bethe-Heitler cross section as it will be discussed in section 2.4.1. In a further appendix C, we will shortly discuss the role of the interference term of bremsstrahlung and laser-dressed Compton scattering. Since both processes have the same initial and final states, one could assume that they interfere with each other. However, we will show that this is not the case.

1.2 Units and Notation

"It has been a mystery ever since it was discovered . . . , and all good theoretical physicists put this number up on their wall and worry about it."
R. P. Feynman about the fine-structure constant α

In the following thesis, natural units will be used if not stated otherwise explicitly. Thus, we have $\hbar = c = \epsilon_0 = 1$. As an example, we may consider the connection between the unit charge e and the fine-structure constant α:

$$\alpha = \frac{e^2}{4\pi\epsilon_0\hbar c} \approx \frac{1}{137.036} \qquad \rightarrow \qquad \alpha = \frac{e^2}{4\pi} \approx \frac{1}{137.036}.$$

Moreover, one easily finds:

$$\hbar = 1 \Rightarrow [J] = \frac{1}{[t]} = \text{MeV};$$
$$c = 1 \Rightarrow [s] = [t] = \text{MeV}^{-1}.$$

This leads to the following conversion factors from natural to SI-units:

$$\hbar = 6.585 \times 10^{-22}\,\text{MeV s} \Rightarrow \text{s} = 1.519 \times 10^{21}\,\text{MeV}^{-1}$$
$$\hbar c = 1.975 \times 10^{-13}\,\text{MeV m} \Rightarrow \text{m} = 5.063 \times 10^{12}\,\text{MeV}^{-1}$$
$$c^2 = E_0/m_e = \frac{0.511\,\text{MeV}}{9.1094 \times 10^{-31}\,\text{kg}} \Rightarrow \text{kg} = 5.610 \times 10^{29}\,\text{MeV}$$

A very important quantity is the *intensity* I of a laser. It is defined as the energy density times its velocity, i.e. it is the energy flux: $I = (\mathrm{d}E/\mathrm{d}V)c$. For circular polarization, we find $I = a^2\omega^2$ with a being the amplitude of the laser four-potential and ω being the laser frequency.

Hence $[I] = \text{MeV}^4$ in natural units, whereas $[I] = \text{W/cm}^2$ in SI-units. Thus, the conversion factor between the intensity in SI- and natural units is[4]

$$I\left[\frac{\text{W}}{\text{cm}^2}\right] = 6.239 \times 10^{29} \frac{\text{W/cm}^2}{\text{MeV}^4} a^2\omega^2$$

with a and ω given in MeV.

According to most textbooks, Greek letters in connection with the *Minkowski notation* denote indices running from 0 to 3, Latin letters denote the spatial components only. Hence, they run from 1 to 3. The metric tensor is

$$g^{\mu\nu} = g_{\mu\nu} = \begin{pmatrix} 1 & 0 & 0 & 0 \\ 0 & -1 & 0 & 0 \\ 0 & 0 & -1 & 0 \\ 0 & 0 & 0 & -1 \end{pmatrix}.$$

It relates contravariant and covariant four-vectors. For example, for the contravariant four-momentum $p^\mu = (E, \vec{p})$, one gets the covariant four-momentum by

$$p_\mu = \sum_{\nu=0}^{3} g_{\mu\nu} p^\nu = g_{\mu\nu} p^\nu = (E, -\vec{p}).$$

As in the example above, Einstein's summation convention is also used. The four-vector product is denoted by a dot: $p \cdot k = g^{\mu\nu} p_\mu k_\nu = p^0 k^0 - \vec{p}\vec{k}$.

According to the most common notation, the Dirac adjoint will be denoted by a bar and is by definition

$$\begin{aligned} \overline{u} &= u^\dagger \gamma^0 \qquad \text{for a spinor } u, \\ \overline{M} &= \gamma^0 M^\dagger \gamma^0 \qquad \text{for a } 4\times4\text{-matrix } M. \end{aligned}$$

The dagger † is of course the hermitean conjugate. E.g., we get for the Dirac adjoint of a wave function $\psi = Mu$, which is the product of a matrix with a spinor,

$$\overline{\psi} = \overline{Mu} = (Mu)^\dagger \gamma^0 = u^\dagger M^\dagger \gamma^0 = u^\dagger \gamma^0 \gamma^0 M^\dagger \gamma^0 = \overline{u}\overline{M}.$$

For explicit calculations, we will use the Dirac representation of the γ-matrices:

$$\gamma^0 = \begin{pmatrix} 1 & 0 & 0 & 0 \\ 0 & 1 & 0 & 0 \\ 0 & 0 & -1 & 0 \\ 0 & 0 & 0 & -1 \end{pmatrix}, \quad \gamma^1 = \begin{pmatrix} 0 & 0 & 0 & 1 \\ 0 & 0 & 1 & 0 \\ 0 & -1 & 0 & 0 \\ -1 & 0 & 0 & 0 \end{pmatrix},$$

$$\gamma^2 = \begin{pmatrix} 0 & 0 & 0 & -i \\ 0 & 0 & i & 0 \\ 0 & i & 0 & 0 \\ -i & 0 & 0 & 0 \end{pmatrix}, \quad \gamma^3 = \begin{pmatrix} 0 & 0 & 1 & 0 \\ 0 & 0 & 0 & -1 \\ -1 & 0 & 0 & 0 \\ 0 & 1 & 0 & 0 \end{pmatrix}.$$

In contrast to many textbooks, the Feynman dagger will not be denoted by $\not{p} = \gamma^\mu p_\mu$, but by $\hat{p} = \gamma^\mu p_\mu$ for any four-vector p. The reason is quite simple: While $\not{p}$ looks good, the "Feynman daggered" four-potential A – namely $\not{A}$ – is hard to read. The hat $\hat{}$ is a common notation in laser-physics.

[4] This is not correct for linear polarization because then the energy and intensity of the laser depends on the phase of the laser. Therefore, for linear polarization, one uses the average value over one laser cycle. This leads to a factor 1/2.

1.3 The Ponderomotive Energy

The ponderomotive energy of a charged particle in an external laser field is the non-relativistic average kinetic energy of the particle in one cycle. Hence, it is defined by

$$U_p = \frac{e^2 E_0^2}{4 m_e \omega^2}.$$

Here, E_0 is the peak of the electric field, ω the laser frequency. In the case of circular polarization, we have $A_\mu = a(\varkappa^1_\mu \cos\phi + \varkappa^2_\mu \sin\phi)$ with $\phi = k^\mu x_\mu$ (see below). We obtain the electric field by $\vec{E} = -\frac{\partial}{\partial t}\vec{A} - \vec{\nabla} A^0$ to be $\vec{E} = a\omega(\vec{\varkappa}^1 \sin\phi - \vec{\varkappa}^2 \cos\phi)$. Thus, we can calculate the ponderomotive energy:

$$U_p = \frac{e^2 a^2}{4 m_e}.$$

If the ponderomotive energy of a particle is of the order of its rest mass, a fully relativistic description of a process is necessary since the non-relativistic approximation breaks down. The laser intensity a at which this regime starts is easily calculated:

$$\begin{aligned} U_p = \frac{e^2 a^2}{4 m_e} &\gtrsim m_e \\ \Rightarrow a = \frac{2 m_e}{e} &= 3.38\,\mathrm{MeV} \end{aligned}$$

Typical intensities we will consider are $a = 10\,\mathrm{MeV}$, $20\,\mathrm{MeV}$, $30\,\mathrm{MeV}$.

Chapter 2

Derivation of the Bremsstrahlung Cross Section

"God runs electromagnetics by wave theory on Monday, Wednesday, and Friday, and the Devil runs them by quantum theory on Tuesday, Thursday, and Saturday."
Sir William Bragg

One of the main tasks of this thesis is – as stated above in the introduction – the derivation of the cross section for a bremsstrahlung process of a relativistic electron in a circularly polarized laser field. This will be done in this section. For such processes, the differential cross section is given by the well-known formula [11, 12]

$$\mathrm{d}\sigma = \frac{1}{\frac{|\vec{v}_i|}{V}T}|S_{fi}|^2 \frac{V\mathrm{d}^3k_b}{(2\pi)^3}\frac{V\mathrm{d}^3p_f}{(2\pi)^3}. \tag{2.1}$$

$\vec{v}_i$ is the velocity of the incoming electron. Hence, $|\vec{v}_i|/V$ corresponds to the incoming particle flux because we will normalize the wave functions in such a way that there is exactly one particle per unit volume V. The last two fractions give the number of final states within the range of momentum d^3k_b and d^3p_f, respectively. S_{fi} is the S-matrix element. If we have an initial state $|\Phi(-\infty)\rangle = |i\rangle$ long before a scattering occcurs ($t_i = -\infty$) and $|\Phi(\infty)\rangle$ is the state into which the initial state evolves at $t = \infty$, then the S-matrix relates $|\Phi(\infty)\rangle$ to $|\Phi(-\infty)\rangle$ and is defined by

$$|\Phi(\infty)\rangle = S|\Phi(-\infty)\rangle = S|i\rangle.$$

The scattering can lead to many different final states $|f\rangle$. The transition probability that after the scattering the particle is in the state $|f\rangle$ is given by $|\langle f|\Phi(\infty)\rangle|^2$ and the corresponding probability amplitude is

$$\langle f|\Phi(\infty)\rangle = \langle f|S|i\rangle \equiv S_{fi}.$$

Therefore, we can interpret the scattering cross section as a transition probability per particle and per unit time divided by the incoming particle flux.

In principle, the S-matrix can be calculated arbitrarily accurately. However in reality, it is an expansion in powers of the fine-structure constant α. Thus the calculation must be aborted after a few terms. The summands of the expansion can be depicted by so-called Feynman diagrams. They can be calculated using the standard technics developed by Feynman. For the bremsstrahlung process, which is under consideration here, there are two diagrams $S_{fi}^{(1)}$ and $S_{fi}^{(2)}$.

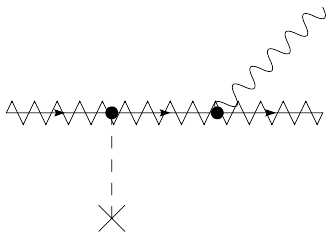

Figure 2.1: Bremsstrahlung amplitude $S_{fi}^{(1)}$

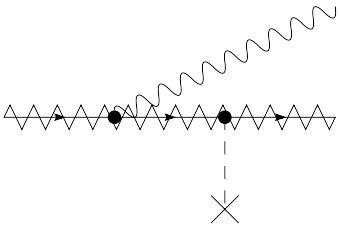

Figure 2.2: Bremsstrahlung amplitude $S_{fi}^{(2)}$

Both have the same ingoing (namely one electron with four-momentum p_i) and outgoing states (one electron with four-momentum p_f and an emitted bremsstrahlung photon with k_b). This means that the two processes $S_{fi}^{(1)}$ and $S_{fi}^{(2)}$ will interfere quantum mechanically and a distinction which of the two processes takes place is not possible. Therefore, the two Feynman diagrams must be added up coherently: $S_{fi} = S_{fi}^{(1)} + S_{fi}^{(2)}$. One can infer from the diagrams that the wave function of an electron in the laser field and the full, laser-dressed electron propagator as well as the vector potentials of both the nucleus and the emitted bremsstrahlung photon are needed in order to evaluate the Feynman diagrams correctly. This will be done in the next three chapters. Afterwards, the S-matrix will be calculated and then the differential cross section (2.1) will be evaluated.

We know from non-relativistic quantum mechanics that recollision effects of the electron with the nucleus in a laser field are the decisive reason for higher harmonic generation [13, 7]. We may wonder whether this is also true in the relativistic case. If this is the case, then the laser-dressed bremsstrahlung cross section as shown in the Feynman diagrams $S_{fi}^{(1)}$ and $S_{fi}^{(2)}$ will not be a good approximation since we just take one electron-nucleus interaction into account. However, we will show in appendix B that the electron which is exposed to a very intense laser field will not recollide with the nucleus. Thus, in the relativistic regime with an unbound electron, higher harmonic generation is not due to recollision effects.

2.1 Volkov Solutions of the Dirac Equation in a Circularly Polarized Field

The process which will be considered here is the scattering of a spin-1/2-particle at relativistic energies. For such processes, Dirac's equation must be used. The external monochromatic laser field is described by a 4-potential A_μ. Since we will only consider plane waves, A_μ depends on space and time only via the product $\phi = k^\mu \cdot x_\mu = \omega t - \vec{k}\vec{x}$ with $k = \left(\omega, \vec{k}\right)$ being the wave vector of the external field and x_μ the corresponding position vector. According to Einstein's famous law $E^2 = m^2 + \vec{p}^2$ and since photons do not have any rest mass, one immediately obtains that

$$k^\mu k_\mu = \omega^2 - \vec{k}^2 = 0.$$

The external laser field $A_\mu \equiv A_\mu(\phi)$ is coupled to the Dirac equation in the normal way. Thus, the relativistic wave equation for an electron in an external field looks:

$$\left[\hat{p} - e\hat{A}(\phi) - m_e\right] \psi(x) = 0$$

The solutions were originally derived by Volkov [5]. An instructive derivation can be found in [11]. The Volkov solutions can thus be written down as follows[1]

$$\psi_{p,r}(x) = \sqrt{\frac{m_e}{\tilde{E}V}} \left(1 + \frac{e\hat{k}\hat{A}(\phi)}{2(k\cdot p)}\right) u_r(p)\, e^{iS_p[\phi]}$$

with

$$S_p[\phi] = -p\cdot x - \int_0^\phi \left(e\frac{p\cdot A(\phi')}{k\cdot p} - e^2\frac{A^2(\phi')}{2(k\cdot p)}\right) \mathrm{d}\phi'.$$

p is the momentum of the electron, and r labels the spinor index. The spinors $u_r(p)$, which appear in the Volkov solutions, are the same spinors as in the free Dirac equation. Therefore, they also obey the relation $[\hat{p} - m_e]\, u_r(p) = 0$.

In this thesis, we will only deal with a *circularly polarized plane-wave field*. Such fields are described by the following expression [12]:

$$A_\mu(\phi) = a\left(\varkappa_\mu^1 \cos\phi + \varkappa_\mu^2 \sin\phi\right)$$

with the laser polarization vectors $\varkappa_\mu^1$ and $\varkappa_\mu^2$. At this point, it is important to make some remarks on the gauge we will use throughout this thesis. A nice feature of the *Lorenz gauge* $\partial_\mu A^\mu = 0$ is its Lorentz-covariance. However, it is still possible to restrict this gauge class further. Thus, we can set $A^0 = 0$ and $\vec{\nabla}\vec{A} = 0$. This gauge is called *radiation gauge*. In this gauge, photons can have only two polarization states $\lambda = 1, 2$. Both are transversal and purely space-like $(\varkappa^\mu)^{1,2} = (0, \vec{\varkappa}^{1,2})$. Keeping this in mind, it is easy to derive the following important relations and normalization conditions:

$$\vec{\varkappa}^i\vec{k} = 0 \quad \Rightarrow \quad k^\mu A_\mu = 0, \tag{2.2}$$

$$\varkappa^{1\,\mu}\cdot\varkappa_\mu^2 = 0, \tag{2.3}$$

$$\varkappa^{i\,\mu}\cdot\varkappa_\mu^i = -1, \qquad \vec{\varkappa}^i\vec{\varkappa}^i = 1, \tag{2.4}$$

$$A^\mu A_\mu = -a^2.$$

Obviously, the radiation gauge is not Lorentz-covariant and only valid in one particular Lorentz-frame. On the other hand, the Lorentz-covariance of the formalism will be broken later on anyway by carrying out the calculation in the rest frame of the nucleus. Thus, we are free to choose a gauge which is noncovariant and helpful for our calculations.

The phase integration in $S_p[\phi]$ is elementary in the circularly polarized case and yields

$$S_p[\phi] = -q\cdot x + \xi\sin\phi + \eta\cos\phi - \eta.$$

Here, we introduced the abbreviations

$$\xi = -\frac{eap\cdot\varkappa^1}{k\cdot p}, \qquad \eta = \frac{eap\cdot\varkappa^2}{k\cdot p}$$

(for later use: ξ_j and η_j respectively correspond to ξ, η with momentum p_j.). We also defined the *effective momentum* of the electron in the laser field:

$$q^\mu := p^\mu + \frac{e^2a^2}{2k\cdot p}k^\mu, \qquad q^\mu = \left(\tilde{E}, \vec{q}\right), \qquad \tilde{E} = q^0. \tag{2.5}$$

[1] The normalization factor, especially the meaning of $\tilde{E}$, will be discussed in a few lines below

We note that $k \cdot q = k \cdot p$ and $\varkappa^{1,2} \cdot q = \varkappa^{1,2} \cdot p$. As a result, ξ and η can also be expressed in terms of the effective momentum q:

$$\xi = -\frac{eaq \cdot \varkappa^1}{k \cdot q}, \qquad \eta = \frac{eaq \cdot \varkappa^2}{k \cdot q}.$$

The effective momentum directly leads to an *effective mass* m_e^* which is defined by

$$m_e^{*2} := q^2 = m_e^2 + e^2 a^2.$$

Therefore, we get a modified relativistic energy-momentum relation:

$$\tilde{E}^2 = |\vec{q}|^2 + m_e^{*2}.$$

If we want to impose the box normalization condition onto the wave function, we demand that the average particle density amounts to one particle in the volume V. This condition leads to a slightly different normalization factor compared to the field free case; it now depends on the *effective energy* $\tilde{E}$ and looks $\sqrt{m_e/(\tilde{E}V)}$. This explains the prefactor in (2.1).

Plugging the effective momentum into the expression for the wave function $\psi_{p,r}(x)$, we get

$$\begin{aligned}\psi_{p,r}(x) =& \sqrt{\frac{m_e}{\tilde{E}V}} \Big(\exp\left[i\xi \sin\phi + i\eta\cos\phi\right] + \\ & \frac{ea\hat{k}\hat{\varkappa}^1}{2k\cdot p} \cos\phi \exp\left[i\xi\sin\phi + i\eta\cos\phi\right] + \\ & \frac{ea\hat{k}\hat{\varkappa}^2}{2k\cdot p} \sin\phi \exp\left[i\xi\sin\phi + i\eta\cos\phi\right] \Big) \times \\ & u_r(p) e^{-iq\cdot x - i\eta}.\end{aligned}$$

Having a closer look at this expression, we see that we can rewrite it using the generalized Bessel functions $B^0, B^1,$ and B^2. These are derived in the appendix E. Thus, we finally end up with[2]

$$\begin{aligned}\psi_{p,r}(x) =& \sqrt{\frac{m_e}{\tilde{E}V}} \sum_{s=-\infty}^{\infty} \underbrace{\left\{ B_s^0(\xi,\eta) + \frac{ea\hat{k}\hat{\varkappa}^1}{2k\cdot p} B_s^1(\xi,\eta) + \frac{ea\hat{k}\hat{\varkappa}^2}{2k\cdot p} B_s^2(\xi,\eta) \right\}}_{=:U(s,\xi,\eta,a,k,p)} \times \\ & u_r(p)\, e^{-i\eta - i(q-sk)\cdot x}.\end{aligned} \tag{2.6}$$

For calculating the Dirac adjoint $\overline{\psi}$, we use relation (D.2) from the appendix D:

$$\begin{aligned}\overline{\psi}_{p,r}(x) =& \sqrt{\frac{m_e}{\tilde{E}V}} \sum_{s=-\infty}^{\infty} \overline{u}_r(p) \underbrace{\left\{ B_s^{0*}(\xi,\eta) + \left(\hat{\varkappa}^1 B_s^{1*}(\xi,\eta) + \hat{\varkappa}^2 B_s^{2*}(\xi,\eta)\right) \frac{ea\hat{k}}{2k\cdot p} \right\}}_{=:\overline{U}(s,\xi,\eta,a,k,p)} \times \\ & e^{+i\eta + i(q-sk)\cdot x}\end{aligned}$$

[2] We could write down the expression for the Volkov wave function without using generalized Bessel functions as it is done in [11] or according to (E.9). However we think that the structure of our expressions are reflected in a nicer way when we keep the generalized Bessel functions. Moreover in the linear case, it is not possible to reduce the generalized Bessel functions to normal Bessel functions. So we can compare our results more easily with the linear case.

We observe:

1. For $a \to 0$, we recover the solution for the free Dirac particle (using $J_s(0) = \delta_{s,0}$):

$$\psi_{\text{free}}(x) = \sqrt{\frac{m_e}{EV}} u_r(p) e^{-ip\cdot x}.$$

2. Linearly polarized light $A_\mu = a\epsilon_\mu \cos\phi$ is not a special case of circularly polarized light $A_\mu = a(\varkappa_\mu^1 \cos\phi + \varkappa_\mu^2 \sin\phi)$ since $\varkappa^2$ cannot be zero ($\varkappa^{2\mu} \cdot \varkappa_\mu^2 = -1$).

2.2 The Full, Laser-Dressed Electron Propagator

We already pointed out at the beginning of this section that we also have to calculate the full, laser-dressed electron propagator in addition to the Volkov solutions. In general, propagators are the Green's functions to the equation of motion. Therefore, the free electron propagator S_F is the Green's function to the free Dirac equation

$$\left(i\hat{\partial} - m_e\right) S_F(x_2, x_1) = \delta^{(4)}(x_2 - x_1).$$

The solution is

$$S_F(x_2, x_1) = \int \frac{\mathrm{d}^4 p}{(2\pi)^4} \frac{\hat{p} + m_e}{p^2 - m_e^2 + i\epsilon} e^{-ip(x_2 - x_1)}.$$

Accordingly, the laser-dressed electron propagator $G(x_2, x_1)$ is given by

$$\left(i\hat{\partial} - e\hat{A} - m_e\right) G(x_2, x_1) = \delta^{(4)}(x_2 - x_1).$$

In order to find G, one could solve this linear differential equation. This can be done by considering the second-order Dirac equation and is shown in [14].

However, we will pursue another, more elegant way according to [15, 16]. For this purpose, we rewrite the Volkov solution in the following way:

$$\psi_{p,r}(x) = E_p(x) u_r(p)$$

with

$$E_p(x) = \left(1 + \frac{e\hat{k}\hat{A}(\phi)}{2k\cdot p}\right) \times \exp\left[-ip\cdot x - i\int_0^\phi \left(\frac{ep\cdot A(\phi')}{k\cdot p} - \frac{e^2 A^2(\phi')}{2k\cdot p}\right) \mathrm{d}\phi'\right].$$

Consequently,

$$\overline{E}_p(x) = \left(1 + \frac{e\hat{A}(\phi)\hat{k}}{2k\cdot p}\right) \times \exp\left[ip\cdot x + i\int_0^\phi \left(\frac{ep\cdot A(\phi')}{k\cdot p} - \frac{e^2 A^2(\phi')}{2k\cdot p}\right) \mathrm{d}\phi'\right].$$

We note that there is no normalization as in (2.1). According to [16], the matrix $E_p(x)$ fulfills the following orthogonality and completeness relations:

$$\int \frac{\mathrm{d}^4x}{(2\pi)^4}\overline{E}_p(x)E_{p'}(x) = \delta^{(4)}(p-p'),$$
$$\int \frac{\mathrm{d}^4p}{(2\pi)^4}E_p(x)\overline{E}_p(x') = \delta^{(4)}(x-x'). \tag{2.7}$$

Whereas the first of these two relations is quite obvious, the second one is not as evident. An elaborate treatment on the question of orthogonality and completeness of the Volkov solutions can be found in [17].

Moreover, we can derive

$$\begin{aligned}\left(-i\hat{\partial}+i\hat{\partial}-e\hat{A}-m_e\right)E_p(x)u_r(p) &= \left(-E_p(x)\hat{p}+E_p(x)\hat{p}-e\hat{A}E_p(x)-m_eE_p(x)\right)u_r(p)\\ &= \left(-E_p(x)\hat{p}-e\hat{A}E_p(x)\right)u_r(p).\end{aligned}$$

We remember that $E_p(x)$ is a matrix and hence does not commute with other matrices in general. Since $u_r(p)$ is the free Dirac spinor, we could use the relation $(\hat{p}-m_e)u_r(p)=0$. We also used $\hat{\partial}\hat{A}(\phi)\hat{k} = \hat{k}\hat{A}'(\phi)\hat{k} = 0$. On the other hand, $\left(i\hat{\partial}-e\hat{A}-m_e\right)E_p(x)u_r(p)=0$. Thus, we can write $-i\hat{\partial}E_p(x)u_r(p) = \left(-E_p(x)\hat{p}-e\hat{A}E_p(x)\right)u_r(p)$ which is equivalent to

$$\left(i\hat{\partial}-e\hat{A}(\phi)\right)E_p(x) = E_p(x)\hat{p}. \tag{2.8}$$

With these expressions, we can easily prove the following statement: The laser-dressed Green's function looks [16]:

$$\begin{aligned}G(x_2,x_1) &= \int \frac{\mathrm{d}^4p}{(2\pi)^4}E_p(x_2)\frac{\hat{p}+m_e}{p^2-m_e^2+i\epsilon}\overline{E}_p(x_1)\\ &= \int \frac{\mathrm{d}^4p}{(2\pi)^4}\left(1+\frac{e\hat{k}\hat{A}(\phi_2)}{2k\cdot p}\right)\frac{\hat{p}+m_e}{p^2-m_e^2+i\epsilon}\left(1+\frac{e\hat{A}(\phi_1)\hat{k}}{2k\cdot p}\right)\times\\ &\quad \exp\left[-ip(x-x')-i\int_{\phi_1}^{\phi_2}\left(\frac{ep\cdot A(\tilde{\phi})}{k\cdot p}-\frac{e^2A^2(\tilde{\phi})}{2k\cdot p}\right)\mathrm{d}\tilde{\phi}\right].\end{aligned}$$

Here $\phi_{1,2} = k\cdot x_{1,2}$. In words, this means that the laser-dressed Green's function is more or less the free propagator inserted between the Volkov solutions of the Dirac equation in an external field.

$$\begin{aligned}(i\hat{\partial}-e\hat{A}-m_e)G(x_2,x_1) &= \int \frac{\mathrm{d}^4p}{(2\pi)^4}E_p(x_2)\,(\hat{p}-m_e)\,\frac{1}{\hat{p}-m_e}\overline{E}_p(x_1) \qquad \text{using (2.8)}\\ &= \int \frac{\mathrm{d}^4p}{(2\pi)^4}E_p(x)\overline{E}_p(x')\\ &= \delta^{(4)}(x_2-x_1) \qquad \text{using (2.7)}\end{aligned}$$

Herewith it is proven that $G(x_2,x_1)$ really is the laser-dressed electron propagator. For $a=0$, we immediately recover the free electron propagator since in this case $E_p(x) = \exp[-ipx]$.

We can rewrite the above expression for the propagator using the generalized Bessel functions. All this happens in exactly the same way as in the previous section. Thus, we get

$$\begin{aligned} G(x_2,x_1) = \int \frac{\mathrm{d}^4p}{(2\pi)^4} \sum_{s,s'=-\infty}^{+\infty} & \left\{ B_s^0(\xi,\eta) + \frac{ea\hat{k}}{2k\cdot p}\left(\hat{\varkappa}^1 B_s^1(\xi,\eta) + \hat{\varkappa}^2 B_s^2(\xi,\eta)\right)\right\} \times \\ & \frac{\hat{p}+m_e}{p^2-m_e^2+i\epsilon}\left\{ B_{s'}^{0\,*}(\xi,\eta) + \left(\hat{\varkappa}^1 B_{s'}^{1\,*}(\xi,\eta) + \hat{\varkappa}^2 B_{s'}^{2\,*}(\xi,\eta)\right)\frac{ea\hat{k}}{2k\cdot p}\right\} \times \\ & \exp\left[-iq\,(x_2-x_1) + ik\,(sx_2 - s'x_1)\right]. \end{aligned}$$

We substitute $p^\mu = q^\mu - \frac{e^2a^2}{2k\cdot p}k^\mu$ for the integration variable in order to get a nicer dependence of the exponent on the variable of integration. The jacobian for this coordinate transformation is:

$$\begin{aligned} J &= \det\left(\frac{\partial q^\mu}{\partial p^\nu}\right) = \epsilon^{\mu\nu\rho\sigma}\frac{\partial q^0}{\partial p^\mu}\frac{\partial q^1}{\partial p^\nu}\frac{\partial q^2}{\partial p^\rho}\frac{\partial q^3}{\partial p^\sigma} \\ &= \epsilon^{\mu\nu\rho\sigma}\left(\delta^{0\mu} + \frac{e^2a^2k_\mu k^0}{2(k\cdot p)^2}\right)\left(\delta^{1\nu} + \frac{e^2a^2k_\nu k^1}{2(k\cdot p)^2}\right)\times \\ &\quad \left(\delta^{2\rho} + \frac{e^2a^2k_\rho k^2}{2(k\cdot p)^2}\right)\left(\delta^{3\sigma} + \frac{e^2a^2k_\sigma k^3}{2(k\cdot p)^2}\right) \\ &= \epsilon^{0123} + \left(\frac{e^2a^2}{2(k\cdot p)^2}\right)^4 \epsilon^{\mu\nu\rho\sigma}k_\mu k_\nu k_\rho k_\sigma k^0 k^1 k^2 k^3 \\ &= 1 \end{aligned}$$

by virtue of the completely antisymmetric tensor $\epsilon^{\mu\nu\rho\sigma}$ with $\epsilon^{0123} = +1$. Thus $\mathrm{d}^4p = \frac{1}{J}\mathrm{d}^4q = \mathrm{d}^4q$. After renaming $q \to p$, we finally end up with

$$\begin{aligned} G(x_2,x_1) = \int \frac{\mathrm{d}^4p}{(2\pi)^4} \sum_{s,s'=-\infty}^{+\infty} & \left\{ B_s^0(\xi,\eta) + \frac{ea\hat{k}}{2k\cdot p}\left(\hat{\varkappa}^1 B_s^1(\xi,\eta) + \hat{\varkappa}^2 B_s^2(\xi,\eta)\right)\right\} \times \\ & \frac{\hat{p}-\frac{e^2a^2}{2k\cdot p}\hat{k}+m_e}{p^2-m_e^{*2}+i\epsilon}\left\{ B_{s'}^{0\,*}(\xi,\eta) + \left(\hat{\varkappa}^1 B_{s'}^{1\,*}(\xi,\eta) + \hat{\varkappa}^2 B_{s'}^{2\,*}(\xi,\eta)\right)\frac{ea\hat{k}}{2k\cdot p}\right\} \times \\ & \exp\left[-ip(x_2-x_1) + ik(sx_2 - s'x_1)\right] \end{aligned} \tag{2.9}$$

with the effective mass $m_e^* = \sqrt{m_e^2 + e^2a^2}$. We remember that $k\cdot p = k\cdot q$. Obviously, the poles are shifted to the effective mass shell, as it is evident from the occurence of the denominator $p^2 - m_e^{*2} + i\epsilon$.

2.3 The Vector Potentials $A_{\mathbf{Coul}}(x)$ and $A_{b,\lambda}(x)$

Before we can start to calculate the elements $S_{fi}^{(1)}$ and $S_{fi}^{(2)}$, we still have to make some remarks on the two electromagnetic four-potentials $A_{b,\lambda}$ of the emitted bremsstrahlung photon and A_{Coul} of the nucleus.

The bremsstrahlung photon wave function is given by

$$A_{b,\lambda}^\mu = \frac{1}{\sqrt{2\omega_b V}}\epsilon_{b,\lambda}^\mu\left(e^{-ik_b\cdot x} + e^{ik_b\cdot x}\right)$$

according to [12]. The normalization factor $\frac{1}{\sqrt{2\omega_b V}}$ is due to a finite normalization volume V also explained in [12]. If one compares this expression with the second-quantized field operator for the transverse part of the electromagnetic vector potential with discrete modes

$$\vec{A}(t,\vec{x}) = \sum_{\vec{k}\lambda} \frac{1}{\sqrt{2|\vec{k}|V}} \vec{\epsilon}_\lambda(\vec{k}) \left(a_{\vec{k}\lambda} e^{-ik\cdot x} + a^\dagger_{\vec{k}\lambda} e^{ik\cdot x} \right),$$

one immediately sees that the emission of a bremsstrahlung photon (i.e. the "creation" of a photon) is connected with the positive exponential $\exp[ik_b \cdot x]$ [18]. Thus, the four-potential of the emitted bremsstrahlung photon reads

$$A^\mu_{b,\lambda} = \frac{1}{\sqrt{2\omega_b V}} \epsilon^\mu_{b,\lambda} e^{ik_b\cdot x}. \tag{2.10}$$

The polarization vector $\epsilon_{b,\lambda}$ with $\lambda = 1,2$ fulfills the equivalent relations as $\varkappa^{1,2}$, namely

$$\begin{aligned} \epsilon_{b,\lambda} \cdot \epsilon_{b,\lambda'} &= -\delta_{\lambda\lambda'}, \\ k_b \cdot \epsilon_{b,\lambda} &= 0. \end{aligned} \tag{2.11}$$

The incoming electron interacts with the Coulomb field A_{Coul} of a nucleus. We assume the nucleus to be infinitely heavy so that the whole calculation is done in the *Born approximation*, i.e. recoil effects of the nucleus are neglected. Instead the nucleus serves as an absorber or source of momentum. Hence, the four-potential of the Coulomb field is given by $A_{\mathrm{Coul}}(x) = \left(A^0_{\mathrm{Coul}}(x), \vec{0}\right)$ with $A^0_{\mathrm{Coul}}(x)$ being the normal Coulomb potential

$$A^\mu_{\mathrm{Coul}}(x) = -\frac{Ze}{4\pi|\vec{x}|}\delta^{\mu 0}.$$

However, it is more convenient to use the Fourier representation of the Coulomb potential for the calculation

$$A^\mu_{\mathrm{Coul}}(x) = \int \frac{\mathrm{d}^4 q}{(2\pi)^4} A^\mu_{\mathrm{Coul}}(q) e^{-iq\cdot x} \tag{2.12}$$

with [12]

$$A^\mu_{\mathrm{Coul}}(q) = 2\pi\delta\left(q^0\right)\left[-\frac{Ze}{\vec{q}^2}\right]\delta^{\mu 0}. \tag{2.13}$$

We already mentioned that the use of the radiation gauge breaks the Lorentz-covariance of the formalism. Obviously, Lorentz-covariance would have been broken anyway by using this particular Coulomb potential which is only correct in the rest frame of the nucleus. Therefore, the whole calculation takes place in this particular frame.

2.4 The S-Matrix and the Cross Section

We can now start to calculate the S-matrix of laser-dressed bremsstrahlung. Starting point is the same S-matrix as for the laser-free case, namely equation (A.1). Obviously, we have to substitute Volkov states and the laser-dressed Green's function for the free states and the free

electron propagator:

$$\begin{aligned}
S_{fi} &= S_{fi}^{(1)} + S_{fi}^{(2)} \\
&= e^2 \int \mathrm{d}^4x_1 \int \mathrm{d}^4x_2\, \overline{\psi}_f(x_2) \left\{ \left(-i\hat{A}_{b,\lambda}(x_2)\right) iG(x_2,x_1) \left(-i\hat{A}_{\mathrm{Coul}}(x_1)\right) + \right. \\
&\quad \left. \left(-i\hat{A}_{\mathrm{Coul}}(x_2)\right) iG(x_2,x_1) \left(-i\hat{A}_{b,\lambda}(x_1)\right) \right\} \psi_i(x_1) \\
&= e^2 \int \mathrm{d}^4x_1 \int \mathrm{d}^4x_2 \overline{u}_r(p_f)\overline{E}_{p_f}(x_2) \times \\
&\quad \left\{ \left(-i\hat{A}_{b,\lambda}(x_2)\right) \left(i\frac{1}{(2\pi)^4} \int \mathrm{d}^4p E_p(x_2) \frac{\hat{p}+m_e}{p^2-m_e^2+i\epsilon} \overline{E}_p(x_1) \right) \left(-i\hat{A}_{\mathrm{Coul}}(x_1)\right) + \right. \\
&\quad \left. \left(-i\hat{A}_{\mathrm{Coul}}(x_2)\right) \left(i\frac{1}{(2\pi)^4} \int \mathrm{d}^4p E_p(x_2) \frac{\hat{p}+m_e}{p^2-m_e^2+i\epsilon} \overline{E}_p(x_1) \right) \left(-i\hat{A}_{b,\lambda}(x_1)\right) \right\} \times \\
&\quad E_{p_i}(x_1) u_r(p_i).
\end{aligned} \tag{2.14}$$

Already from this expression, one can conclude that we will get peaks in the S-matrix (and thus also in the cross section) whenever the denominator of the propagator equals zero, i.e. if the virtual electron is "on shell" (becomes real). This leads to a nice interpretation: Whenever there are peaks in the cross section resulting from the propagator, the cross section is in fact the multiplication of two first-order processes. These processes are laser-assisted Compton scattering [8] and deflection of an electron by a Coulomb field [19].

As one might guess the calculation and simplification of this term is quite demanding, e.g. one has to take into account several identities involving the Dirac algebra and generalized Bessel functions. On the other hand, there is not much insight during the calculation from a physical point of view. Therefore, we will do the simplification of the term $S_{fi}^{(1)}$ explicitly in the appendix F. A completely analogous calculation then yields $S_{fi}^{(2)}$.

Thus, the expression for S_{fi} looks like

$$\begin{aligned}
S_{fi} =& 2\pi i \frac{Ze^3 m_e}{\sqrt{2\omega_b \tilde{E}_i \tilde{E}_f V^3}} \exp[i(\eta_f - \eta_i)] \sum_{n,s=-\infty}^{\infty} \frac{\delta^{(1)}\left(q_n^0\right)}{\vec{q}_n^2} \overline{u}_{r_f}(p_f) \times \\
& \left[F_{-n-s}^{f,p_{n,s}}(\xi_p - \xi_f, \eta_p) \frac{\hat{p}_{n,s} - \frac{e^2a^2}{2k\cdot p_{n,s}}\hat{k} + m_e}{p_{n,s}^2 - m_e^{*2} + i\epsilon} \overline{G}_{-s}^{i,p_{n,s}}(\xi_p, \eta_p) + \right. \\
& \left. G_{-n-s}^{f,p'_{n,s}}(\xi_{p'} - \xi_f, \eta_{p'}) \frac{\hat{p}'_{n,s} - \frac{e^2a^2}{2k\cdot p'_{n,s}}\hat{k} + m_e}{p_{n,s}'^2 - m_e^{*2} + i\epsilon} \overline{F}_{-s}^{i,p'_{n,s}}(\xi_{p'}, \eta_{p'}) \right] u_{r_i}(p_i)
\end{aligned} \tag{2.15}$$

with

$$\begin{aligned}
F_m^{j,q}(\xi,\eta) =& \left(\hat{\epsilon}_{b,\lambda} + \frac{ea}{2k\cdot p_j}\frac{ea}{2k\cdot q}\hat{k}\hat{\epsilon}_{b,\lambda}\hat{k} \right) B_m^0(\xi,\eta) + \\
& \left(\frac{ea}{2k\cdot q}\hat{\epsilon}_{b,\lambda}\hat{k}\hat{\varkappa}^1 + \frac{ea}{2k\cdot p_j}\hat{\varkappa}^1\hat{k}\hat{\epsilon}_{b,\lambda} \right) B_m^1(\xi,\eta) + \\
& \left(\frac{ea}{2k\cdot q}\hat{\epsilon}_{b,\lambda}\hat{k}\hat{\varkappa}^2 + \frac{ea}{2k\cdot p_j}\hat{\varkappa}^2\hat{k}\hat{\epsilon}_{b,\lambda} \right) B_m^2(\xi,\eta)
\end{aligned} \tag{2.16}$$

and

$$\begin{aligned} G_m^{j,q}(\xi,\eta) = &\left(\gamma^0 + \frac{ea}{2k\cdot p_j}\frac{ea}{2k\cdot q}\hat{k}\gamma^0\hat{k}\right) B_m^0(\xi,\eta) + \\ &\left(\frac{ea}{2k\cdot q}\gamma^0\hat{k}\hat{\varkappa}^1 + \frac{ea}{2k\cdot p_j}\hat{\varkappa}^1\hat{k}\gamma^0\right) B_m^1(\xi,\eta) + \\ &\left(\frac{ea}{2k\cdot q}\gamma^0\hat{k}\hat{\varkappa}^2 + \frac{ea}{2k\cdot p_j}\hat{\varkappa}^2\hat{k}\gamma^0\right) B_m^2(\xi,\eta). \end{aligned} \tag{2.17}$$

j can take the values $j = i, f$ in order to differ between incoming and outgoing electron. In our notation, the momentum transfer onto the nucleus q gained an index n since it is dependent on the sum over n: $q \equiv q_n$. Thus, F describes the emission of the bremsstrahlung photon, whereas the interaction between the electron and the nucleus is formulated in G.

During the calculation of S_{fi}, δ-functions occur which ensure momentum conservation:

$$\vec{q}_f = \vec{q}_i + n\vec{k} - \vec{k}_b + \vec{q}_n.$$

The intermediate electron momenta $p_{n,s}$ and $p'_{n,s}$ are defined by

$$\begin{aligned} p_{n,s} &= q_f - (n+s)k + k_b = q_i - sk + q_n, \\ p'_{n,s} &= q_i - sk - k_b = q_f - (n+s)k - q_n. \end{aligned} \tag{2.18}$$

It should already be stressed here that $\xi_p, \eta_p, \xi_{p'}$, and $\eta_{p'}$, which enter as arguments into the expression of the S-matrix, are not dependent on s; $\xi_{p'}$ and $\eta_{p'}$ even not on n. This can easily be seen by having a look at their definition:

$$\begin{aligned} \xi_p &= -\frac{eap_{n,s}\cdot\varkappa^1}{k\cdot p_{n,s}} = -\frac{ea\,(q_f-(n+s)k+k_b)\cdot\varkappa^1}{k\cdot(q_f-(n+s)k+k_b)} \\ &= -\frac{ea\left(q_f\cdot\varkappa^1 + k_b\cdot\varkappa^1\right)}{k\cdot q_f + k\cdot k_b}, \\ \xi_{p'} &= -\frac{ea\left(q_i\cdot\varkappa^1 - k_b\cdot\varkappa^1\right)}{k\cdot q_i - k\cdot k_b}, \\ \eta_p &= \frac{ea\left(q_f\cdot\varkappa^2 + k_b\cdot\varkappa^2\right)}{k\cdot q_f + k\cdot k_b}, \\ \eta_{p'} &= \frac{ea\left(q_i\cdot\varkappa^2 - k_b\cdot\varkappa^2\right)}{k\cdot q_i - k\cdot k_b}. \end{aligned}$$

So, we can finally write down the S-matrix in full beauty and length. Using (2.1), it should be straightforward to derive the differential cross section in consideration. However, one may ask whether it is correct to use the factor $\frac{V\mathrm{d}^3p_f}{(2\pi)^3}$ in (2.1). The whole bremsstrahlung process takes place in the laser field, so it may look consistent to replace p_f by the effective momentum of the electron in the laser field q_f. The differential cross section will then read

$$\mathrm{d}\sigma = \frac{1}{\frac{|\vec{v}_i|}{V}T}|S_{fi}|^2\frac{V\mathrm{d}^3k_b}{(2\pi)^3}\frac{V\mathrm{d}^3q_f}{(2\pi)^3}. \tag{2.19}$$

We remember the definition of the effective momentum: $q^\mu = p^\mu + \frac{e^2a^2}{2k\cdot p}k^\mu$. Since we have a fixed laser frequency ω, it follows that $\mathrm{d}^3k = 0$ and consequently that the phase space of the

free momentum p and the effective momentum q are equal: $\mathrm{d}^3p_f = \mathrm{d}^3q_f$. Now, $\vec{v}_i$ has to be understood as the *effective velocity* of the electron within the laser field.

Another thing needs to be explained in more detail: When we calculate $|S_{fi}|^2$, we get the square of a δ-function. From a mathematical point of view, this is not a well-defined quantity. However, we can make this expression plausible when we assume that the whole process lasts only a finite time T. At the end, we take the limit $T \to \infty$. Then we can write for the energy-conserving δ-function

$$2\pi\delta\left(\tilde{E}_f - \tilde{E}_i - n\omega + \omega_b\right) = \lim_{T\to\infty}\int_{-T/2}^{T/2}\mathrm{d}t\,\exp\left[i\left(\tilde{E}_f - \tilde{E}_i - n\omega + \omega_b\right)t\right].$$

For $\tilde{E}_f = \tilde{E}_i + n\omega - \omega_b$, it follows

$$2\pi\delta\left(0\right) = \lim_{T\to\infty}\int_{-T/2}^{T/2}\mathrm{d}t = \lim_{T\to\infty} T.$$

Thus, it is justified to substitute

$$\left(\delta\left(\tilde{E}_f - \tilde{E}_i - n\omega + \omega_b\right)\right)^2 \to \frac{T}{2\pi}\delta\left(\tilde{E}_f - \tilde{E}_i - n\omega + \omega_b\right). \tag{2.20}$$

Before we will finally plug all expresssions into the formula for the cross section, we have to remember some constants and relations:

$$\begin{aligned}
\alpha &= \frac{e^2}{4\pi} \qquad \text{fine-structure constant,}\\
\tilde{E}_i|\vec{v}_i| &= \frac{1}{\sqrt{1-\vec{v}_i^{\,2}}}m_e^*|\vec{v}_i| = |\vec{q}_i|,\\
\mathrm{d}^3k_b &= |\vec{k}_b|^2\mathrm{d}|\vec{k}_b|\mathrm{d}\Omega_b = \omega_b^2\mathrm{d}\omega_b\mathrm{d}\Omega_b,\\
\mathrm{d}^3q_f &= |\vec{q}_f|^2\mathrm{d}|\vec{q}_f|\mathrm{d}\Omega_f,\\
\tilde{E}_f\mathrm{d}\tilde{E}_f &= |\vec{q}_f|\mathrm{d}|\vec{q}_f|.
\end{aligned}$$

We consider an unpolarized electron beam. Then, we can use the elegant trace formalism which was introduced by *H. B. G. Casimir* in 1933 [20]. For any 4×4-matrix Γ, the following relation is true [12]:

$$\sum_{r_i,r_f=1,2}\left|\overline{u}_{r_f}(p_f)\Gamma u_{r_i}(p_i)\right|^2 = \mathrm{Tr}\left[\Gamma\frac{\hat{p}_i + m_e}{2m_e}\overline{\Gamma}\frac{\hat{p}_f + m_e}{2m_e}\right]. \tag{2.21}$$

r_i and r_f are the spin polarization indices. Summing over spin polarizations and using the above relation, we get

$$\begin{aligned}
\sum_{r_i,r_f}|S_{fi}|^2 =& \frac{4\pi^2Z^2e^6m_e^2}{2\omega_b\tilde{E}_i\tilde{E}_fV^3}\sum_n\sum_{n'}\delta^{(1)}\left(\tilde{E}_f - \tilde{E}_i - n\omega + \omega_b\right)\delta^{(1)}\left(\tilde{E}_f - \tilde{E}_i - n'\omega + \omega_b\right)\times\\
&\frac{1}{\vec{q}_n^{\,2}}\frac{1}{\vec{q}_{n'}^{\,2}}\mathrm{Tr}\left[\left(\sum_s Q_{n,s}^{\lambda}\right)\frac{\hat{p}_i + m_e}{2m_e}\left(\sum_{s'}\overline{Q}_{n,s'}^{\lambda}\right)\frac{\hat{p}_f + m_e}{2m_e}\right]
\end{aligned}$$

with

$$\begin{aligned} Q^{\lambda}_{n,s} =& F^{f,p_{n,s}}_{-n-s}(\xi_p - \xi_f, \eta_p)\frac{\hat{p}_{n,s} - \frac{e^2a^2}{2k\cdot p_{n,s}}\hat{k} + m_e}{p^2_{n,s} - m^{*2}_e + i\epsilon}\overline{G}^{i,p_{n,s}}_{-s}(\xi_p, \eta_p) + \\ & G^{f,p'_{n,s}}_{-n-s}(\xi_{p'} - \xi_f, \eta_{p'})\frac{\hat{p}'_{n,s} - \frac{e^2a^2}{2k\cdot p'_{n,s}}\hat{k} + m_e}{p'^2_{n,s} - m^{*2}_e + i\epsilon}\overline{F}^{i,p'_{n,s}}_{-s}(\xi_{p'}, \eta_{p'}). \end{aligned} \tag{2.22}$$

Because of the two δ-functions, only terms with $n = n'$ contribute and just one δ-function remains according to (2.20). Plugging all results into (2.19) and summing over photon polarization as well, we get the unpolarized differential cross section $\mathrm{d}\overline{\sigma} = \sum_{r_i,r_f,\lambda}\mathrm{d}\sigma$. Moreover, the averaging over incoming spins yields a factor $1/2$.

$$\begin{aligned} \frac{\mathrm{d}\overline{\sigma}}{\mathrm{d}\Omega_f\mathrm{d}\Omega_b\mathrm{d}\omega_b} &= \frac{4\pi^2Z^2e^6m_e^2V^3\omega_b^2}{4\omega_b\tilde{E}_i\tilde{E}_fV^3(2\pi)^6|\vec{v}_i|2\pi(2m_e)^2}\sum_{\lambda=1,2}\sum_n\delta^{(1)}\left(\tilde{E}_f - \tilde{E}_i - n\omega + \omega_b\right)\times \\ &\quad \frac{|\vec{q}_f|^2\mathrm{d}q_f}{|\vec{q}_n|^4}\mathrm{Tr}\left[\left(\sum_s Q^{\lambda}_{n,s}\right)(\hat{p}_i + m_e)\left(\sum_{s'}\overline{Q}^{\lambda}_{n,s'}\right)(\hat{p}_f + m_e)\right] \\ &= \frac{\alpha(Z\alpha)^2\omega_b}{8\pi^2}\frac{1}{|\vec{q}_i|}\sum_{\lambda=1,2}\sum_n\frac{|\vec{q}_f|}{|\vec{q}_n|^4}\delta^{(1)}(\tilde{E}_f - \tilde{E}_i - n\omega + \omega_b)\times \\ &\quad \mathrm{Tr}\left[\left(\sum_s Q^{\lambda}_{n,s}\right)(\hat{p}_i + m_e)\left(\sum_{s'}\overline{Q}^{\lambda}_{n,s'}\right)(\hat{p}_f + m_e)\right]\mathrm{d}\tilde{E}_f. \end{aligned}$$

Since we are not interested in the dependence of the cross section on the energy $\tilde{E}_f$ of the outgoing electron, we integrate over $\tilde{E}_f$. Together with the δ-function in the cross section, this yields the energy conservation

$$\tilde{E}_f = \tilde{E}_i + n\omega - \omega_b.$$

Thus, the cross section for bremsstrahlung in a circularly polarized field is finally derived:

$$\begin{aligned} \frac{\mathrm{d}\overline{\sigma}}{\mathrm{d}\Omega_f\mathrm{d}\Omega_b\mathrm{d}\omega_b} =& \frac{\alpha(Z\alpha)^2\omega_b}{8\pi^2}\frac{1}{|\vec{q}_i|}\sum_{\lambda=1,2}\sum_n\frac{|\vec{q}_f|}{|\vec{q}_n|^4}\times \\ & \mathrm{Tr}\left[\left(\sum_s Q^{\lambda}_{n,s}\right)(\hat{p}_i + m_e)\left(\sum_{s'}\overline{Q}^{\lambda}_{n,s'}\right)(\hat{p}_f + m_e)\right]\Theta(\tilde{E}_f - m^*_e). \end{aligned} \tag{2.23}$$

The step function appears to make sure that the energy of the outgoing electron is always greater than its rest mass. This is in close analogy to the Bethe-Heitler formula. We see that the cross section is differential in the energy of the bremsstrahlung photon and in the directions of both the final electron and the emitted photon.

2.4.1 Limit of Vanishing Laser Field $a \to 0$

Expression (2.23) is fairly complicated. To check whether it is a reasonable result, the easiest possibility is to "turn off" the laser field. Then, we should retrieve the Bethe-Heitler cross section. So, let us consider the case $a \to 0$. Trivially, $q_f = p_f$ and $q_i = p_i$. Obviously, all ξ's and η's equal zero then. Subsequently, $F^{j,p_{n,s}}_n(0,0) = \hat{\epsilon}_{b,\lambda}B^0_n(0,0) = \hat{\epsilon}_{b,\lambda}\delta_{n,0}$ and similarly

$G_n^{j,p_{n,s}}(0,0) = \gamma^0\delta_{n,0}$. From this, it follows that

$$Q_{n,s}^{\lambda} = \hat{\epsilon}_{b,\lambda}\delta_{-n-s,0}\frac{\hat{p}_{n,s}+m_e}{p_{n,s}^2-m_e^2+i\epsilon}\gamma^0\delta_{-s,0} + \gamma^0\delta_{-n-s,0}\frac{\hat{p}'_{n,s}+m_e}{p'^2_{n,s}-m_e^2+i\epsilon}\hat{\epsilon}_{b,\lambda}\delta_{-s,0}.$$

Here, we used (D.1) from appendix D. Because of the Kronecker-δ's in the cross section, the infinite sums break down. Only the terms with $n = s = s' = 0$ survive. In order to go on, we make use of the completeness relation for the photon polarization vectors $\epsilon_{b,\lambda}^{\mu}$ [12]:

$$\sum_{\lambda=1,2}\epsilon_{b,\lambda}^{\mu}\epsilon_{b,\lambda}^{\nu} = -g^{\mu\nu} + \text{gauge terms}.$$

The gauge terms drop out in the field-free case when we calculate any observables. Thus, we can write down the cross section in the limit $a = 0$:

$$\frac{\mathrm{d}\overline{\sigma}}{\mathrm{d}\Omega_b\mathrm{d}\Omega_f\mathrm{d}\omega_b} = -\frac{\alpha(Z\alpha)^2\omega_b}{8\pi^2}\frac{|\vec{p}_f|}{|\vec{p}_i|}\frac{1}{|\vec{q}|^4}\Theta(E_i-m_e-\omega_b)\times \mathrm{Tr}\left[\left(\gamma^{\mu}\frac{\hat{p}_f+\hat{k}_b+m_e}{2p_f\cdot k_b}\gamma^0+\gamma^0\frac{\hat{p}_i-\hat{k}_b+m_e}{-2p_i\cdot k_b}\gamma^{\mu}\right)(\hat{p}_i+m_e)\times \left(\gamma^0\frac{\hat{p}_f+\hat{k}_b+m_e}{2p_f\cdot k_b}\gamma_{\mu}+\gamma_{\mu}\frac{\hat{p}_i-\hat{k}_b+m_e}{-2p_i\cdot k_b}\gamma^0\right)(\hat{p}_f+m_e)\right].$$

This is already the Bethe-Heitler cross section as we can see by comparison with the formula in appendix A.

2.4.2 Integrated Cross Section

The cross section (2.23) derived up to here is differential in the energy of the bremsstrahlung photon and in the solid angles of both the electron and the photon. However, from an experimental point of view, this is difficult to measure since the photons and the electrons have to be detected in coincidence. Moreover, the main focus is put on the bremsstrahlung photon; the electron is just used to "create" it, what it "does" afterwards is of not so much interest. So, we will integrate over $\mathrm{d}\Omega_f$ in order to get a cross section only dependent on the energy of the bremsstrahlung photon and its direction of emission:

$$\frac{\mathrm{d}\overline{\sigma}}{\mathrm{d}\Omega_b\mathrm{d}\omega_b} = \int\mathrm{d}\Omega_f\frac{\mathrm{d}\overline{\sigma}}{\mathrm{d}\Omega_b\mathrm{d}\Omega_f\mathrm{d}\omega_b}. \tag{2.24}$$

Obviously, this integration can only be done numerically in the general case of equation (2.23) since it is an integration over Bessel functions. The numerical integration routine will be discussed in more detail when the Fortran 90 programme is explained in section 3.3. We note that in the field-free case (i.e. for the Bethe-Heitler formula) an analytical integration is possible. The result is shown in appendix A.

2.5 Resonances and Higher Harmonic Generation

Resonances of the cross section are generated when the denominators of the propagators (2.22) become zero (or at least close to zero). Thus, the conditions for resonances are

$$p_{n,s}^2 - m_e^{*2} = 0 \qquad \text{and} \qquad p'^2_{n,s} - m_e^{*2} = 0.$$

We define two four-vectors $\tilde{n}$ and $\tilde{n}_b$ by $k = \omega\tilde{n}$ and $k_b = \omega_b\tilde{n}_b$. The first relation of the two equations above can then be rewritten as

$$\begin{aligned}(q_f - (n+s)\omega\tilde{n} + \omega_b\tilde{n}_b)^2 - m_e^{*2} &= 0\\ -(n+s)\omega q_f\cdot\tilde{n} + \omega_b q_f\cdot\tilde{n}_b - (n+s)\omega\omega_b\tilde{n}\cdot\tilde{n}_b &= 0.\end{aligned}$$

We solve this expression for ω_b and scale it with the laser frequency ω. This yields the condition for resonances of our cross section:

$$\frac{\omega_b}{\omega} = \frac{(n+s)q_f\cdot\tilde{n}}{q_f\cdot\tilde{n}_b - (n+s)k\cdot\tilde{n}_b}. \tag{2.25}$$

The equivalent calculation for the second relation gives:

$$\frac{\omega_b}{\omega} = \frac{sq_i\cdot\tilde{n}}{-q_i\cdot\tilde{n}_b + sk\cdot\tilde{n}_b}. \tag{2.26}$$

In general, one speaks of higher harmonics if the frequency of the emitted photon is an integer multiple of the laser frequency or, in mathematical terms, if $\omega_b/\omega = n$ with $n \in \mathbb{N}$. A closer look at (2.25) and (2.26) reveals that there will be higher harmonics if $\tilde{n}_b = \tilde{n}$. The two equations simplify to

$$\frac{\omega_b}{\omega} = n + s \qquad \text{and} \qquad \frac{\omega_b}{\omega} = -s.$$

However, for an arbitrary direction of the emitted bremsstrahlung photon, we can estimate the spacing between two resonances easily. We neglect the $k\cdot\tilde{n}_b$-term since it is only a small contribution and get

$$\Delta\left(\frac{\omega_b}{\omega}\right) = \frac{q_f\cdot\tilde{n}}{q_f\cdot\tilde{n}_b} \qquad \text{and} \qquad \Delta\left(\frac{\omega_b}{\omega}\right) = \frac{q_i\cdot\tilde{n}}{q_i\cdot\tilde{n}_b}. \tag{2.27}$$

Let us consider the resonance frequency ω_b in the rest frame of the electron. The electron moves with a velocity of $|\vec{v}_{i,f}| = |\vec{q}_{i,f}|/\tilde{E}_{i,f}$. The relativistic Doppler shift is

$$\omega' = \gamma\omega\left(1 - |\vec{v}|\cos\theta\right).$$

Here, ω' is the frequency in the moving frame (i.e. the rest frame of the electron), ω the frequency in the laboratory frame, and θ is the angle in the laboratory frame between $\vec{v}$ and $\vec{k}$. In the following, $\theta_{el} = \angle\left(\vec{v},\vec{k}\right)$ and $\theta_{eb} = \angle\left(\vec{v},\vec{k}_b\right)$. We thus get

$$\begin{aligned}\omega' &= \gamma\omega\left(1 - |\vec{v}|\cos\theta_{el}\right),\\ \omega_b' &= \gamma\omega_b\left(1 - |\vec{v}|\cos\theta_{eb}\right).\end{aligned}$$

We will just consider the case (2.25); the other one is treated in exactly the same manner and yields obviously an equivalent result.

$$\begin{aligned}\frac{\omega_b'}{\omega'} &= \frac{\omega_b}{\omega}\frac{1 - |\vec{v}_2|\cos\theta_{eb}}{1 - |\vec{v}_2|\cos\theta_{el}}\\ &= (n+s)\frac{\tilde{E}_f - |\vec{q}_f|\cos\theta_{el}}{\tilde{E}_f - |\vec{q}_f|\cos\theta_{eb} - (n+s)k\cdot\tilde{n}_b}\frac{1 - |\vec{v}_2|\cos\theta_{eb}}{1 - |\vec{v}_2|\cos\theta_{el}} \qquad \text{using (2.25).}\end{aligned}$$

$\tilde{E}_f$ is of the order of 10 MeV, whereas ω is of the order of 10^{-6} MeV. Therefore, we can neglect the term $k \cdot \tilde{n}_b$ in the denominator as long as the number $(n+s)$ of the resonance is not too large. Then, the two fractions cancel each other, and we end up with

$$\frac{\omega_b'}{\omega'} = n + s.$$

As we will see later, the number of resonances $(n+s)$ is in all relevant cases not greater than $\mathcal{O}(10^3)$. So, we can conclude that all resonances are higher harmonics in the rest frame of the electron, but not in the laboratory frame.

2.6 Finite Peaks – the Imaginary Mass and Energy

Whenever we have a resonance peak of our cross section (i.e. the intermediate electron "goes on shell"), the value of the cross section is infinite. This is due to the fact that at a resonance the virtual electron becomes real and the denominator is equal to zero as we saw in the previous section. However, infinities do not show up in nature. We have to consider higher-order Feynman diagrams of the electron propagator in order to suppress this unphysical behaviour. The next higher-order Feynman diagram, the so-called electron self-energy (here laser-dressed), is shown in figure (2.3). The calculation of the contribution of the electron self-energy yields a shift of the electron mass in the propagator. This calculation is very demanding. However, making use of the so-called *Cutkowsky rule*, it is comparatively easy to calculate the imaginary mass shift of the electron mass. This was done for the first time by [15]. The imaginary mass shift of the electron is given by [21]

$$m_e \to m_e - i\Gamma_m \quad \text{with} \quad \Gamma_m = \frac{\tilde{p}^0}{2m_e} W_\gamma. \tag{2.28}$$

We remark that this is a nonstandard notation; in the literature $\Gamma_m/2$ is commonly used instead of Γ_m. However, we will use the same notation as in [15, 21]. $\tilde{p}^0$ is the zero-component (i.e. the energy) of the four-momentum of the intermediate electron; in our case, it is $\tilde{p}^0 = p^0_{n,s}$ or $\tilde{p}^0 = p'^0_{n,s}$. W_γ is the total probability of photon emission, i.e. of laser-dressed Compton scattering:

$$\begin{aligned} W_\gamma &= \int \frac{\left| \text{  } \right|^2}{VT} \frac{V\mathrm{d}^3 k_b}{(2\pi)^3} \frac{V\mathrm{d}^3 q_f}{(2\pi)^3} \\ &= \int \frac{\left| e \int \mathrm{d}^4 x \, \overline{\psi}_f(x) \left(-i \hat{A}_{c,\lambda}(x) \right) \psi_i(x) \right|^2}{VT} \frac{V\mathrm{d}^3 k_b}{(2\pi)^3} \frac{V\mathrm{d}^3 q_f}{(2\pi)^3} \end{aligned}$$

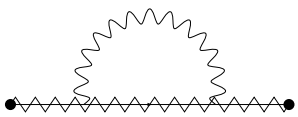

Figure 2.3: The so-called self-energy of the electron is due to (in lowest order) a virtual photon which is emitted and then reabsorbed by the electron. This process leads to a mass shift of the electron mass.

The index c in $A_{c,\lambda}$ denotes that we talk about a Compton photon and not about a bremsstrahlung photon (as in $A_{b,\lambda}$) anymore. Of course, ψ_i and ψ_f are Volkov wave functions.

W_γ is calculated in [11] for circular polarization. So, we will just state the result here[3]:

$$\begin{aligned} W_\gamma &= \frac{\alpha m_e^2}{4\tilde{p}^0}\sum_{s=1}^{\infty}\int_0^{u_s}\frac{\mathrm{d}u}{(1+u)^2}\times \\ &\quad \left\{-4J_s^2(z)+\zeta^2\left(2+\frac{u^2}{1+u}\right)\left(J_{s+1}^2(z)+J_{s-1}^2(z)-2J_s^2(z)\right)\right\} \\ &=: \frac{\alpha m_e^2}{4\tilde{p}^0}\tilde{W}_\gamma(k\cdot\tilde{p}) \end{aligned} \tag{2.29}$$

with[4]

$$\zeta=\frac{ea}{m_e},\qquad u_s=2s\frac{k\cdot\tilde{p}}{m_e^{*2}},\qquad z=2s\frac{\zeta}{\sqrt{1+\zeta^2}}\sqrt{\frac{u}{u_s}\left(1-\frac{u}{u_s}\right)}.$$

As we will see later in 3.5, $\tilde{W}_\gamma(k\cdot\tilde{p})$ is a function linear in $k\cdot\tilde{p}$ (at least in our range of paramters). Therefore it can be written as $\tilde{W}_\gamma(k\cdot\tilde{p})=b_a(k\cdot\tilde{p})$. The slope b_a of the straight line depends on a. For example, we will find $b_{20}=240\,\mathrm{MeV}^{-2}$.

However, with the implementation of the imaginary mass in our formalism, an imaginary energy has to be introduced as well to make the formalism consistent again:

$$\tilde{E}\to\tilde{E}-i\Gamma_{\tilde{E}}.$$

Again, we do not use the standard notation $\tilde{E}\to\tilde{E}-i\Gamma_{\tilde{E}}/2$. We found that the effective four-momentum also fulfills the Einstein-relation $q^2=m_e^{*2}$. By introducing only the imaginary mass shift, this relation would be violated. We will choose $\Gamma_{\tilde{E}}$ in such a way that this relation also holds with the imaginary mass shift. With $m_e^{*2}\to(m_e-i\Gamma_m)^2+e^2a^2\approx m_e^{*2}-2im_e\Gamma_m$, we write

$$\begin{aligned} \left(\tilde{E}-i\Gamma_{\tilde{E}}\right)^2 &= m_e^{*2}-2im_e\Gamma_m+\vec{q}^2 \\ \tilde{E}^2-2i\tilde{E}\Gamma_{\tilde{E}} &= m_e^{*2}-2im_e\Gamma_m+\vec{q}^2 \\ \Rightarrow\Gamma_{\tilde{E}} &= \frac{m_e}{\tilde{E}}\Gamma_m. \end{aligned} \tag{2.30}$$

We define the shifted effective momentum $q^\Gamma=\left(\tilde{E}-i(m_e/\tilde{E})\Gamma_m,\vec{q}\right)$.

In the numerator of the propagators (2.22), both the electron mass and the effective momentum appear, but the imaginary shifts are so small compared to the other values that they can be neglected. However, the denominator equals zero when the electron is "on shell". Therefore, even small correction terms must not be neglected. Thus, in the denominators, we have to replace

$$\begin{aligned} p_{n,s}^2-m_e^{*2}\to\quad & \left(q_f^\Gamma-(n+s)k+k_b\right)^2-m_e^{*2}+2im_e\Gamma_m \\ =&2\left[-(n+s)q_f\cdot k+q_f\cdot k_b-(n+s)k\cdot k_b+i\frac{m_e}{\tilde{E}_f}\Gamma_m\left((n+s)\omega-\omega_b\right)\right] \end{aligned} \tag{2.31}$$

[3] In [11], e^2 equals the fine-structure constant α. This is not true in our system of units. The formula in [11] is changed accordingly.

[4] In [11] eq. (101,17), there is a misprint in the definition of z which becomes obvious by dimensional considerations. It also contradicts [21]. The treatment in [11] becomes consisten with [21] (taking the appropriate limit) and with dimensional considerations when we neglect m_e^2 in the definition of z.

and

$$\begin{aligned} {p'_{n,s}}^2 - m_e^{*2} \to \quad & \left(q_i^\Gamma - sk - k_b\right)^2 - m_e^{*2} + 2im_e\Gamma_m \\ =& 2\left[-sq_i\cdot k - q_i\cdot k_b + sk\cdot k_b + i\frac{m_e}{\tilde{E}_i}\Gamma_m\left(s\omega+\omega_b\right)\right]. \end{aligned}$$

Γ_m can be rewritten as

$$\Gamma_m = \frac{\tilde{p}^0}{2m_e}W_\gamma = \frac{\tilde{p}^0}{2m_e}\frac{\alpha m_e^2}{4\tilde{p}^0}b_a(k\cdot\tilde{p}) = \frac{\alpha m_e}{8}b_a(k\cdot\tilde{p}). \tag{2.32}$$

What is the interpretation of the imaginary energy? To get some insight, we replace q with q^Γ in the Volkov state (2.6). We find

$$\begin{aligned} \psi^\Gamma_{p,r}(x) &= \psi_{p,r}(x)e^{-\Gamma_{\bar{E}}t}, \\ |\psi^\Gamma_{p,r}(x)|^2 &= |\psi_{p,r}(x)|^2 e^{-2\Gamma_{\bar{E}}t}. \end{aligned}$$

Thus, the Volkov state becomes a decaying state. This is not very amazing because the electron in the laser field shows a level structure – the levels are labelled by the number s of absorbed or emitted laser photons in (2.6). Transitions between these levels are possible.

2.7 Explicit Calculation of the Cross Section – the Scattering Geometry

The scattering geometry we consider is depicted in figure (2.4). Since one expects the most interesting physics from a head-on collision of the electrons and the laser photons, we assume the incoming electrons and the laser photons to counterpropagate. The x-axis is defined by the direction $\vec{p}_i$. After the scattering process, the outgoing electrons are deflected by an angle $\theta_f = \angle(\vec{q}_i, \vec{q}_f)$. The bremsstrahlung photon is emitted by an angle $\theta_b = \angle\left(\vec{q}_i, \vec{k}_b\right)$. In order to describe the directions of the outgoing electron and the bremsstrahlung photon exactly, we also need the azimuthal angles ρ_f for the final electron and ρ_b for the bremsstrahlung photon. They are defined according to figure (2.5). Now, we can easily write down explicit expressions for the different four-vectors:

$$\begin{aligned} q_i &= \left(\tilde{E}_i, \sqrt{\tilde{E}_i^2 - m_e^{*2}}, 0, 0\right), \\ q_f &= \left(\tilde{E}_f, \sqrt{\tilde{E}_f^2 - m_e^{*2}}\cos\theta_f, \sqrt{\tilde{E}_f^2 - m_e^{*2}}\sin\theta_f\cos\rho_f, \sqrt{\tilde{E}_f^2 - m_e^{*2}}\sin\theta_f\sin\rho_f\right), \\ k &= (\omega, -\omega, 0, 0), \\ k_b &= (\omega_b, \omega_b\cos\theta_b, \omega_b\sin\theta_b\cos\rho_b, \omega_b\sin\theta_b\sin\rho_b). \end{aligned}$$

We also have to find expressions for the polarization vectors $\varkappa^1, \varkappa^2$ and $\epsilon_{b,1}, \epsilon_{b,2}$. Since the ϵ_b's have to fulfill the relations (2.11), we can choose

$$\begin{aligned} \epsilon_{b,1} &= (0, 0, -\sin\rho_b, \cos\rho_b), \\ \epsilon_{b,2} &= (0, -\sin\theta_b, \cos\theta_b\cos\rho_b, \cos\theta_b\sin\rho_b). \end{aligned}$$

The $\varkappa$'s obey the equivalent relations (2.2), (2.3), and (2.4). The first and simplest choice for an explicit representation would be $\varkappa^1 = (0,0,1,0)$ and $\varkappa^2 = (0,0,0,1)$. However, it turns out that

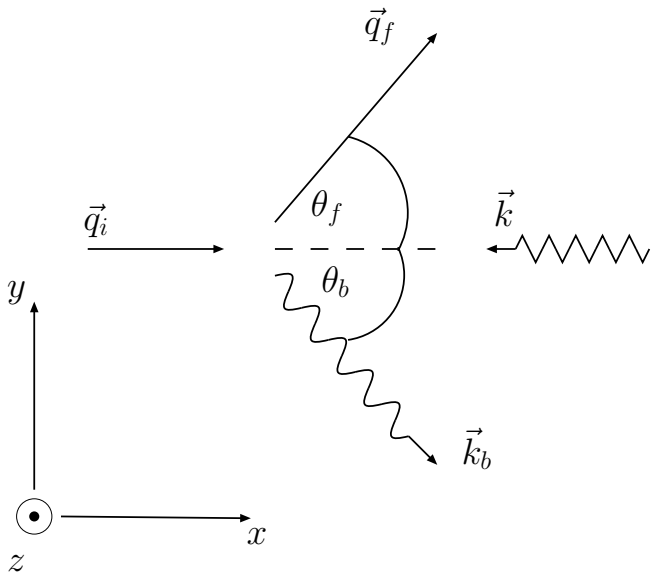

Figure 2.4: In our scattering geometry, the incoming electron with q_i and laser photons with k are counterpropagating. The directions of the final electron and the bremsstrahlung photon can be determined in each case with two angles. In this projection on the xy-plane, only the polar angles θ_f and θ_b are visible.

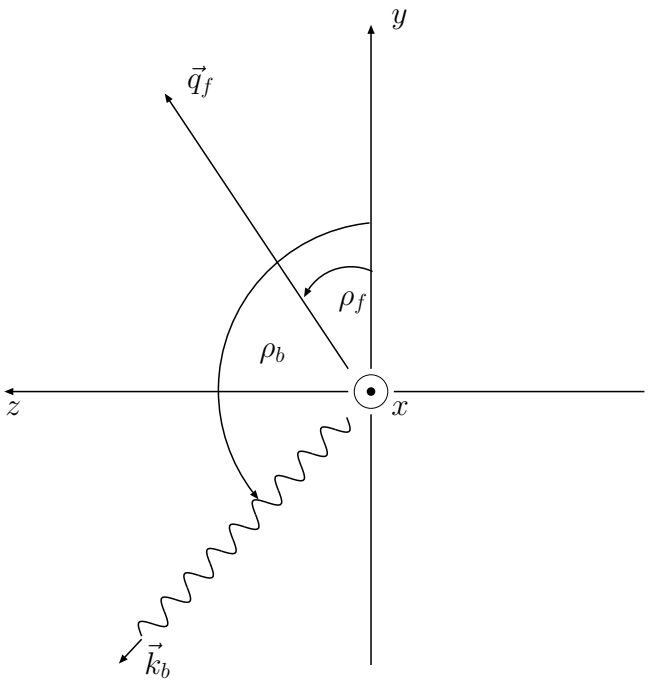

Figure 2.5: A projection of the scattering geometry on the yz-plane shows the azimuthal angles ρ_f of the final electron and ρ_b of the bremsstrahlung photon.

it is more convenient to use a slightly more complicated representation, namely

$$\begin{aligned}\varkappa^1 &= (0, 0, \cos\rho_f, \sin\rho_f)\,,\\ \varkappa^2 &= (0, 0, -\sin\rho_f, \cos\rho_f)\,.\end{aligned}$$

The reason for this choice will be given in a few lines below.

Apart from the fact that we expect the most interesting physics from a head-on collision of electrons and photons, it also yields the nice result $\xi_i = \eta_i = 0$:

$$\begin{aligned}\xi_i &= -\frac{ea\overbrace{q_i\cdot\varkappa^1}^{=0}}{q\cdot k} = 0;\\ \eta_i &\propto q_i\cdot\varkappa^2 = 0.\end{aligned}$$

Moreover – and this is due to the more complicated choice of the $\varkappa$'s –, we even find that $\eta_f = 0$:

$$\begin{aligned}\eta_f &\propto q_f\cdot\varkappa^2\\ &= -\sqrt{\tilde{E}_f^2 - m^{*2}}\,(-\sin\theta_f\cos\rho_f\sin\rho_f + \sin\theta_f\sin\rho_f\cos\rho_f)\\ &= 0.\end{aligned}$$

Thus, this little difference in choosing an explicit representation of the polarization vectors $\varkappa^1$ and $\varkappa^2$ will make a huge difference in evaluating the cross section formular numerically. For example, we can derive much easier formulars for the sum rules of the generalised Bessel functions (see appendix E). It should be stressed however that this simplification is a special feature of circular polarization and our scattering geometry.

Chapter 3

The Numerical Evaluation: Discussion of the Fortran Code

After having derived an expression for the bremsstrahlung cross section (2.23), it is now our main task to evaluate this expression. Obviously, this can only be done numerically. In this section, a Fortran 90 programme will be described which is capable of doing this. Moreover, numerical and other difficulties will be addressed and solved.

Why do we use Fortran 90 and not, for example, C++? Of course, this would be possible, too. However, a nice feature of Fortran is that both complex numbers and matrix calculation are already implemented. We do not have to write our own class or download something to "upgrade" Fortran as in the case of C++. Moreover, there is a general agreement in the community – although this has not been analysed thoroughly – that Fortran is approximately a factor of 2 faster than C.

This chapter is organised in the following way: In the first section, we will give an overview over the whole programme with the help of a simplified flowchart. Then, the implementation of the special features of the Minkowski metric and the Dirac algebra are described. Afterwards, we will have a closer look at the numerical integration and the calculation of the differential cross section. At the end of this chapter, we will shortly explain how the imaginary mass and energy is calculated and perform some numerical tests of our code. For a closer investigation of our code, we refer to appendix G where the main programme and the calculation of the propagators are presented.

In the following, everything which is printed in a `typewriter font` is quoted from the Fortran 90 programme.

3.1 Overview over the Whole Programme

The simplified flowchart shown in figure (3.1) depicts the organization of the programme. All functions and subroutines which can be seen in the flowchart have their counterpart in the source code in appendix G. We note that we will present the programme for the calculation of spectra, i.e. the cross section is presented as a function of the bremsstrahlung frequency ω_b. For other kinds of graphs, minor modifications must be implemented. Nevertheless, this does not effect the overall structure of the programme.

In an outer loop, ω_b is increased step by step. After each cycle, the result is written to a file which can then be imported by another programme (in our case XMGrace) to create the graphs.

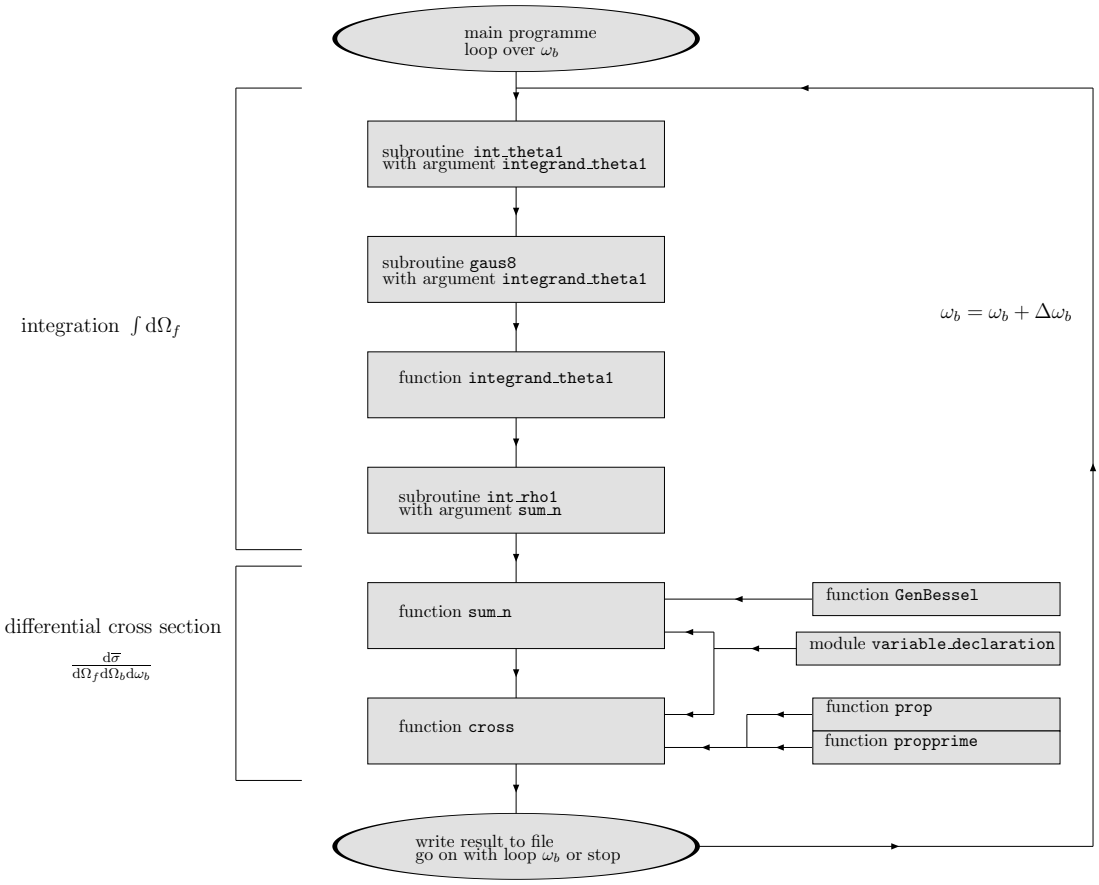

Figure 3.1: A simplified flowchart depicts the organization of the Fortran programme for the evaluation of the cross section.

During each cycle, the differential cross section (2.23) is numerically integrated over the direction of the outgoing electron in order to yield the total cross section (2.24). In the programme, this is organised in the following way: We assign a function (called `integrand_theta1`) to the routine which performs the θ_f-integration. `integrand_theta1` itself is the differential cross section integrated over ρ_f or, in other words, performs the numerical integration over ρ_f. Hence, the function calculating the differential cross section is assigned to `integrand_theta1` as an argument. The two numerical integrations will be discussed in more detail below.

The calculation of the differential cross section is split up into two functions, namely `sum_n` and `cross`. These two functions will also be explained below. We remark that the Bessel functions are calculated in the module `Besselfunctions_GenBesselfunctions`. The declaration of variables and constants is bundled in a further module called `variable_declaration`.

3.2 Implementation of the Minkowski Metric and the Dirac Algebra into Fortran 90

In particle physics, expressions involving traces can in most cases be simplified considerably by using methods of the Dirac algebra and relations for traces. A similar approach was done in [18]. However, it turns out that we do not have any simplifications in the laser-dressed case. So, it is advantageous to choose an explicit representation of the γ-matrices. We choose, as already stated at the beginning of this thesis, the Dirac representation.

All constants (constant matrices) we need, i.e. the unit matrix, the metric tensor g and the γ-matrices $\gamma^0, \gamma^1, \gamma^2, \gamma^3$, are defined in an extra module called `variable_declaration.f90`. For example, the definition for γ^2 in the Dirac representation looks

```
complex(kind=QD), dimension (0:3,0:3), parameter:: gamma2 = reshape&
((/(0._QD,0._QD),(0._QD,0._QD),(0._QD,0._QD),-(0._QD,1._QD),&
(0._QD,0._QD),(0._QD,0._QD),(0._QD,1._QD),(0._QD,0._QD),&
(0._QD,0._QD),(0._QD,1._QD),(0._QD,0._QD),(0._QD,0._QD),&
-(0._QD,1._QD),(0._QD,0._QD),(0._QD,0._QD),(0._QD,0._QD)/),&
(/4,4/),order=(/2,1/))
```

`complex` just means that we define a complex number. In Fortran, complex numbers are given by two numbers in brackets: `(a,b)` $\equiv a + bi$. The `kind`-statement specifies the precision; `QD` can take the values 8 and 16 corresponding to double and quadruple precision, respectively. The command `dimension(0:3,0:3)` generates a 4×4-matrix with indices running from 0 to 3. The `reshape`- and `order`-commands (which is a new feature of Fortran 90) assure that the components are correctly assigned. One has to be careful since it easily happens that the rows and columns of the matrix are interchanged. `parameter` tells the compiler that this "variable" is a constant which cannot be changed throughout the programme. The rest of the command assignes the values to each component of the matrix called `gamma2`. For example, `-(0._QD,1._QD)` corresponds to the value $-i$ with precision `QD`. All other definitions look more or less the same – be it a variable then without the `parameter`-command, be it a scalar then without the `dimension(...)`-command.

Now let us turn our attention to the functions we need for the upcoming four-dimensional calculations. They are all internally defined.

The following function calculates the Feynman dagger of a four-vector p:

```
function slash(p) result (slash_p)
  implicit none
  real(kind=QD), intent(in), dimension(0:3) :: p
  complex(kind=QD), dimension(0:3,0:3) :: slash_p

  slash_p=gamma0*p(0)-(gamma1*p(1)+gamma2*p(2)+gamma3*p(3))
end function slash
```

As an argument, the function `slash` receives the four-vector p. The return value is called `slash_p` and is defined in this function as a complex 4×4-matrix. In the last but one line of the function, the value $\hat{p} = \gamma^0 p^0 - (\gamma^1 p^1 + \gamma^2 p^2 + \gamma^3 p^3)$ is assigned to `slash_p`.

The function `diracadj` is used for calculating the Dirac adjoint $\overline{M}$ of a matrix M:

```
function diracadj(M) result (Mbar)
  implicit none
  complex(kind=QD), intent(in), dimension(0:3,0:3) :: M
  complex(kind=QD), dimension(0:3,0:3) :: Mbar
```

```
    Mbar = matmul(matmul(gamma0, conjg(transpose(M))), gamma0)
  end function diracadj
```

Here, we make use of Fortran's abilities to manipulate matrices: `conjg(transpose(M))` $\equiv (M^t)^* = M^\dagger$. The matrix multiplication of two matrices A and B is denoted by the command `matmul(A,B)` $\equiv AB$. Hence, `Mbar = matmul(matmul(gamma0,`$M^\dagger$`, gamma0)` $\equiv \gamma^0 M^\dagger \gamma^0 = \overline{M}$.

The function `g` with the two arguments `x` and `y` is obviously the Fortran representation of the scalar product $x \cdot y = x^\mu y_\mu$:

```
function g(x,y)
  implicit none
  real(kind=QD), intent(in), dimension(0:3) :: x,y
  real(kind=QD) :: g

  g=x(0)*y(0)-(x(1)*y(1)+x(2)*y(2)+x(3)*y(3))
end function g
```

After the previous considerations and explanations, this function is straightforward. According to our metric, this function assigns the value $x^\mu y_\mu = x^0y^0 - (x^1y^1 + x^2y^2 + x^3y^3) \equiv$ `x(0)*y(0)-(x(1)*y(1)+x(2)*y(2)+x(3)*y(3))` to `g`.

Although this is not part of four-dimensional calculations, we will present a function for calculating the norm of a three-dimensional vector (only spatial components) here:

```
function norm(vec)
  implicit none
  real(kind=QD), intent(in), dimension (1:3) :: vec
  real(kind=QD) :: norm

  norm=sqrt(sum(vec**2))
end function norm
```

`vec**2` just squares each component of the vector which are then sumed up by the command `sum`: `sum(vec**2)=sum(vec(1)`^{2}`,vec(2)`^{2}`,vec(3)`^{2}`)=vec(1)`^{2}+`vec(2)`^{2}+`vec(3)`^{2}.

3.3 The Numerical Integration over $\mathrm{d}\Omega_f$

"God does not care about our mathematical difficulties. He integrates empirically."
Albert Einstein

We can rewrite $\mathrm{d}\Omega_f$ as $\mathrm{d}\Omega_f = \sin\theta_f \mathrm{d}\theta_f \mathrm{d}\rho_f$. So, we perform an integration over the polar angle θ_f and the azimuthal angle ρ_f.

For the θ_f-integration, we use a Gaussian integration routine which is part of the integration library `intlib.f90`. The subroutine `gaus8` integrates real functions over finite intervals using an adaptive algorithm [22]. This finite interval is $[0, \pi]$ for the polar integration. However, as we can see in figure (3.2), the differential cross section decreases very fast with increasing θ_f. The explanation for this behaviour is very easy. We remember that the momentum transfer onto the nucleus is given by $\vec{q}_n = \vec{q}_f - \vec{q}_i - n\vec{k} + \vec{k}_b$. So, if $\vec{q}_f \parallel \vec{q}_i$, the momentum transfer will be very small and hence the cross section very big because of $\mathrm{d}\overline{\sigma} \propto 1/|\vec{q}_n|^4$. On the other hand, if $\vec{q}_f \nparallel \vec{q}_i$,

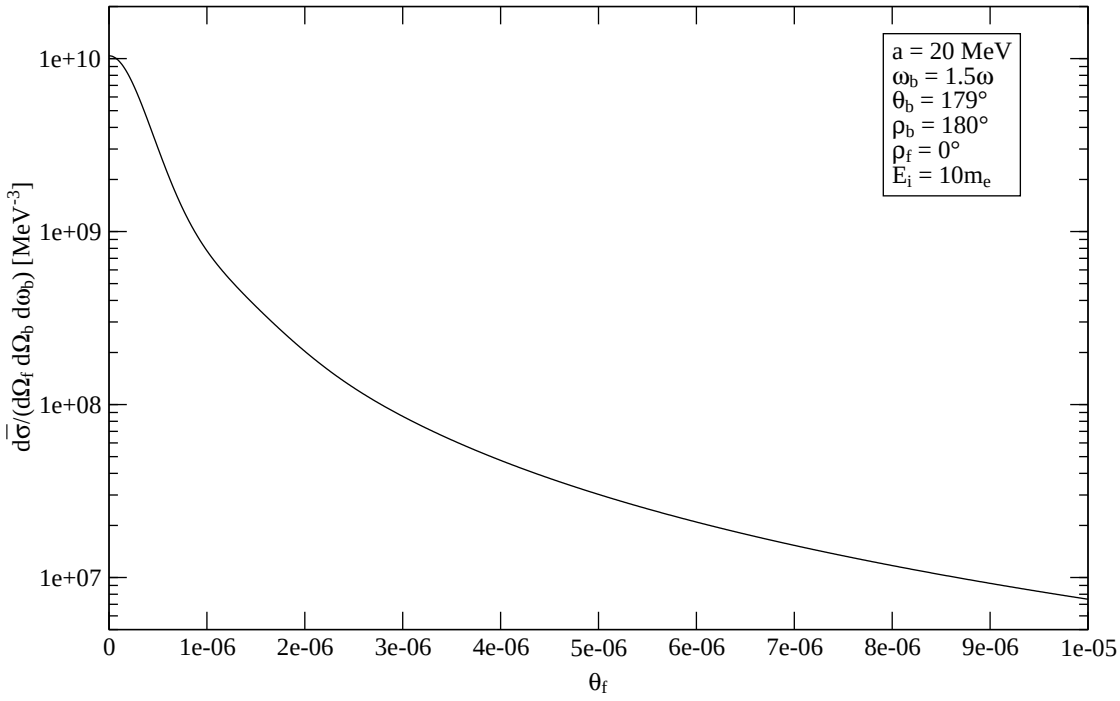

Figure 3.2: The differential cross falls off rapidly with increasing polar angle θ_f. This feature can be exploited to speed up the numerical integration.

$|\vec{q}_n|$ can get much larger, and the cross section is consequently strongly suppressed. Therefore, it is enough to integrate over θ_f from 0 to approximately 10^{-4}.[1]

Whenever we call the routine `int_theta1(integrand_theta1,0._QD,0.0001_QD)` in the main programme, these limits are used. `int_theta1` itself then calls the earlier mentioned routine `gaus8`. As an argument, we assign the function `integrand_theta1`:

```
function integrand_theta1(theta1)
  ...
  a = 0._QD
  b = pi

  call int_rho1(sum_n, a, b, theta1)
  integrand_theta1 = 2._QD * result * sin(theta1)

  return
end function integrand_theta1
```

`integrand_theta1` calls the routine `int_rho1`. This routine integrates over the azimuthal angle ρ_f, i.e. it does the integration $\int_a^b \mathrm{d}\rho_f \, \mathtt{sum\_n}(\rho_f, \theta_f)$. Here, we use a Romberg integration. The Romberg method uses the trapezoidal rule and subinterval halving [22]. As we can see in `integrand_theta1`, the integration interval is just $[0, \pi]$ and not up to 2π as one would expect.

[1] In figure (3.2), we set $a = 20\,\mathrm{MeV}$, $\omega_b = 1.5\omega$, and $\theta_b = 179°$; however, varying these numbers have almost no effect on this particular behaviour.

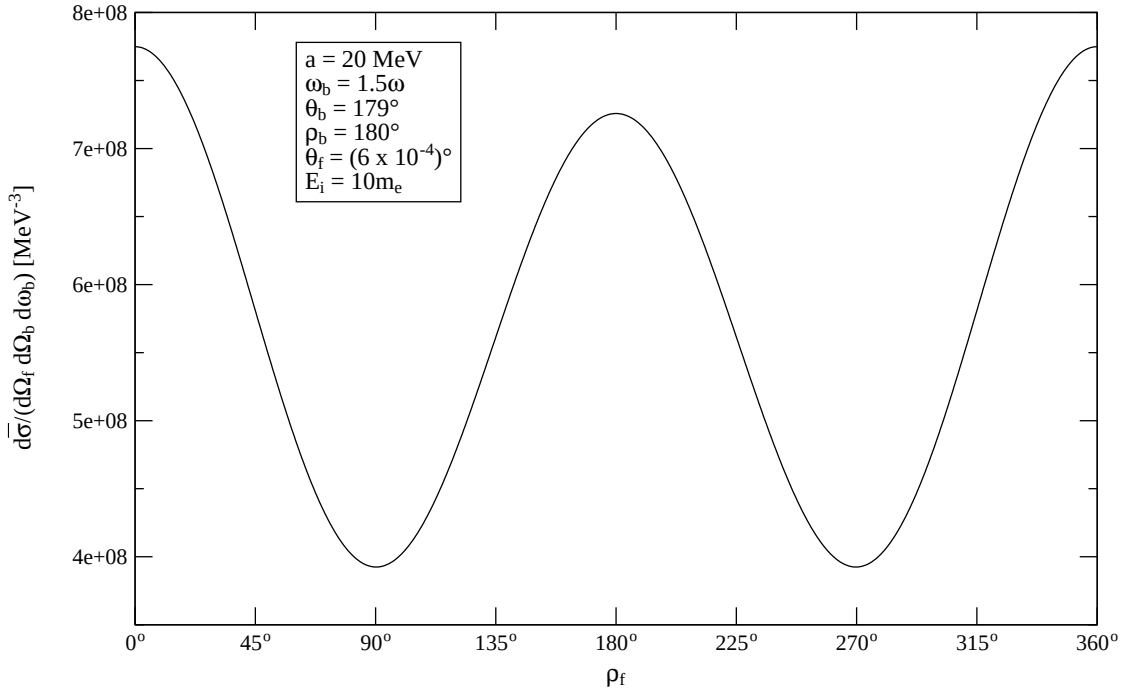

Figure 3.3: The differential cross section in dependence on ρ_f is symmetric around $\rho_f = \rho_b$. Therefore, the integration over ρ_f simplifies.

This is due to a special symmetry in our scattering geometry and a feature of circular polarization. We have only two characteristic directions, namely the direction of the laser photon $\vec{k}/\omega$ and the direction of the emitted bremsstrahlung photon $\vec{k}_b/\omega_b$. Why do we have only these two? $\vec{q}_i/|\vec{q}_i|$ is antiparallel to $\vec{k}/\omega$ and thus does not yield a new characteristic direction (this is due to our scattering geometry). Finally, $\vec{A}$ or, respectively, $\vec{E}$ and $\vec{B}$ do not contribute either since we consider a circularly polarized field (so, our argumentation does not hold for linear polarization). Therefore, the plane spanned by the vectors $\vec{k}$ and $\vec{k}_b$ is a plane of symmetry or, to be more explicit, the value of the cross section on one side of the plane is the same as on the opposite side of the plane. Thus, we have to integrate the differential cross section from $\rho_b - \pi$ to ρ_b (from 0 to π if we choose $\rho_b = \pi$) and take the resulting value times two. Figure (3.2) clearly reflects our considerations: ρ_f was set to π; hence, the differential cross section in dependence on ρ_f is symmetric around π.

The value of the azimuthal integration is stored in the variable `result`. `integrand_theta1` returns the value `2._QD * result * sin(theta1)`. The factor 2 is due to the symmetry we just explained. The second factor `sin(theta1)` $\equiv \sin\theta_f$ comes from the expression of the solid angle we mentioned at the beginning of this section.

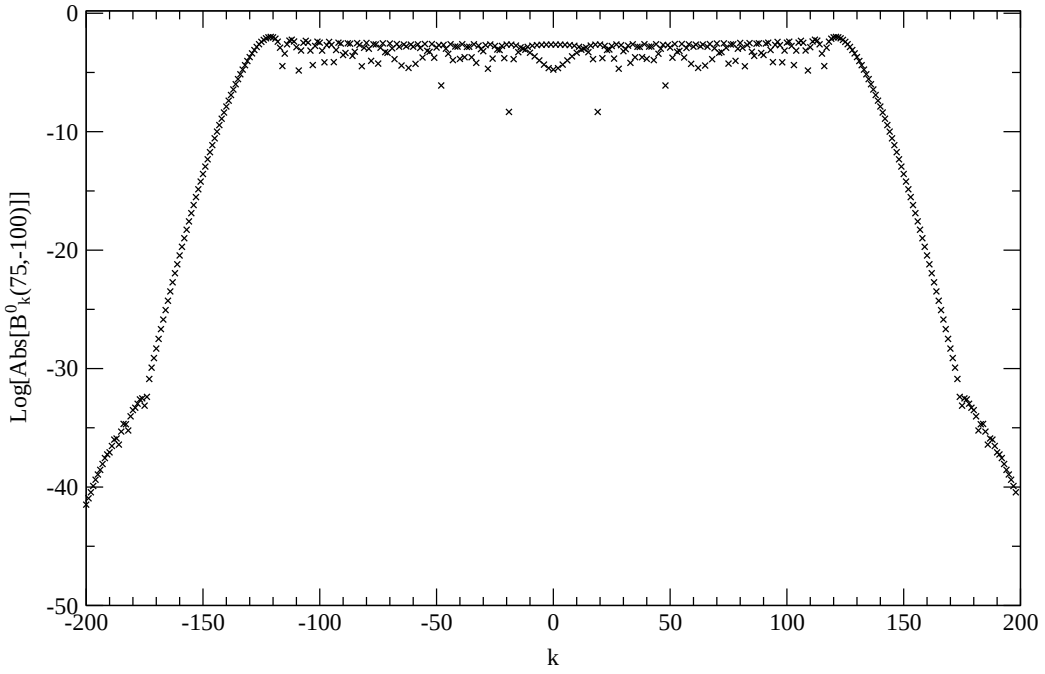

Figure 3.4: The progression of the generalized Bessel function B_k^0 as a function of the index k shows a clear cutoff (here we printed the function $\log\left|\left(B_k^0(75,-100)\right)\right|$). The theoretical cutoff is at $k = \pm 175$.

3.4 Calculation of the Differential Cross Section – the Functions `sum_n` and `cross`

The functions `sum_n` and `cross` calculate the differential cross section (2.23) in dependence on the solid angle of the outgoing electron $\mathrm{d}\Omega_f = \sin\theta_f \mathrm{d}\theta_f \mathrm{d}\rho_f \equiv \sin(\texttt{theta1})\mathrm{d}(\texttt{theta1})\mathrm{d}(\texttt{rho1})$. In `cross`, we find the calculation of the trace $\mathrm{Tr}\,[\dots]$ with the two sums over s and s'. The result is returned to `sum_n` where we have the n- and λ-sum among other things.

At this point, we want to emphasize again that the sums over n, s, and s' theoretically run from $-\infty$ to ∞. A numerical evaluation of an infinite sum is obviously not possible. Therefore, we have to find certain summation limits so that the "infinite" sum can be done in a finite time intervall. From a physical point of view, these sums have to converge since otherwise the cross section would be infinite – an unphysical behaviour! Mathematical, this convergence is due to the fact that Bessel functions tend to zero very fast if the index becomes greater than the argument (see appendix E). We can use that in order to derive summation limits for the summation variables n, s, and s' which appear as indices of the generalized Bessel functions. To this end, we go back to the definition of B_k^0 in order to find $k_{\mathrm{max,min}}$ so that

$$\sum_{k=-\infty}^{\infty} B_k^0(\xi,\eta)\,(\dots) \approx \sum_{k=k_{\min}}^{k_{\max}} B_k^0(\xi,\eta)\,(\dots)\,.$$

This is easily done:

$$\begin{aligned}\sum_{k=-\infty}^{\infty} B_k^0(\xi,\eta)\,(\dots) &= \sum_{k=-\infty}^{\infty}\sum_{n=-\infty}^{\infty} i^k J_{n-k}(\xi)J_n(\eta)\,(\dots)\\ &\approx \sum_{k=-\infty}^{\infty}\sum_{n=-|\eta|}^{|\eta|} i^k J_{n-k}(\xi)J_n(\eta)\,(\dots)\\ &\approx \sum_{k=-(|\xi|+|\eta|)}^{|\xi|+|\eta|}\sum_{n=-|\eta|}^{|\eta|} i^k J_{n-k}(\xi)J_n(\eta)\,(\dots)\,.\end{aligned}$$

Thus we find $k_{\max} = -k_{\min} = |\xi| + |\eta|$. We can see these summation limits as a cutoff of the generalized Bessel function B_k^0 in figure (3.4).

We can apply this rule to obtain the summation limits for the n- and s-sum. According (2.22), we set $s_{\max} = \max\left(|\xi_p| + |\eta_p|, |\xi_{p'}| + |\eta_{p'}|\right)$ and, using this result, $n_{\max} = \max(|\xi_p - \xi_f| + |\eta_p|, |\xi_{p'} - \xi_f| + |\eta_{p'}|) + s_{\max}$.

```
function sum_n(rho1, theta1)
  ...
  kappa1 = ...
  kappa2 = ...
  xipprime = ...
  etapprime = ...

  do n= -nmax,nmax
     if (step(Etilde2-mstar)) then

        q2 = ...
        p2 = ...
        qn = ...
        xi2 = ...
        eta2 = ...
        xip = ...
        etap = ...

        smax = ...
        nmax_test = ...
        ...

        allocate (bessel1(0:2, -abs(n)-smax:abs(n)+smax))
        ...
        bessel1(:,:) = GenBessel(abs(n)+smax,xip-xi2,etap)
        ...

        do lambda = 1,2
          sum_n = sum_n + cross(n,lambda,smax)
        end do

        deallocate (bessel1)
```

```
          ...
          end if
       end if
    end do
    sum_n = sum_n*finestructure*(finestructure*Z)**2*wb/&
            (8._QD*pi**2*norm(q1(1:3)))

  end function sum_n

!-----------------------------------------------------------------
  function cross(n, lambda, smax) result (intres)
    ...
    integer :: s, r1, r2
    ...
    do s = -smax, smax
       qsum = qsum + prop(n,s,lambda) + propprime(n,s,lambda)
    end do

    qbarsum = diracadj(qsum)

! spinor outgoing electron----------------------------------------
    u2(1,0) = (1._QD,0._QD)
    u2(1,1) = (0._QD,0._QD)
    ...
    u2 = u2 * Sqrt((p2(0)+m)/(2._QD*m))
! ----------------------------------------------------------------

    do r1 = 1,2
       do r2 = 1,2
          testcom = (dot_product(matmul(conjg(u2(r2,:)),gamma0),&
                    matmul(qsum,u1(r1,:))))
          intres=intres+ testcom*conjg(testcom)
       end do
    end do
    intres = intres * norm(q2(1:3))/norm(qn(1:3))**4
  end function cross
```

As stated above, in `sum_n` we find the n-summation running from `-nmax` up to `nmax`. For each n, we can now calculate the values for almost all quantities we need to go on: q_f, p_f, q_n, ξ_f, η_f and, since they are not s-dependent, ξ_p, η_p, $\xi_{p'}$, and $\eta_{p'}$. In a next step, we allocate an array with dimensions according to our summation limits in which we store the values of the generalized Bessel functions. We can do this at this particular point and do not have to wait until we perform the loop for the s-summation because the generalized Bessel functions do not depend on s. This is a great advantage since the calculation of them is numerically demanding. We then proceed by doing the summation over the two possible photon polarizations $\lambda = 1, 2$. Within this loop, we call the function `cross`: `sum_n = sum_n + cross(n,lambda,smax)`. We see that the return value `sum_n` is incremented for each cycle of the nested loops over n and λ by the return value of the function `cross`. At the end, we deallocate the array and multiply `sum_n` with the prefactors in (2.23).

The function `cross` is fairly intuitive; therefore, we will not discuss the details as the s-

loop. However, one point is remarkable: In the derivation of the cross section, we made use of the trace formalism (2.21). During the numerical evaluation, it turns out that the trace is numerically unstable for certain parameters. Therefore, we evaluate the cross section by doing the sums over the spinors u_{r_i} and u_{r_f} explicitly. The explicit representation of the spinors can be found in appendix D. In the following, we present some result for the differential cross section using the trace- and the spinor-formalism ($a = 4\,\mathrm{MeV}$, $\theta_f = \rho_f = 0°$, $\theta_b = 179°, \rho_b = 180°$):

ω_b/ω	trace	spinor
0.8	$-5.7 \times 10^{16}\,\mathrm{MeV}^{-3}$	$7.0 \times 10^{15}\,\mathrm{MeV}^{-3}$
0.9	$5.4 \times 10^{15}\,\mathrm{MeV}^{-3}$	$5.2 \times 10^{15}\,\mathrm{MeV}^{-3}$
1.0	$-2.7 \times 10^{16}\,\mathrm{MeV}^{-3}$	$3.2 \times 10^{15}\,\mathrm{MeV}^{-3}$
1.1	$1.0 \times 10^{16}\,\mathrm{MeV}^{-3}$	$2.4 \times 10^{15}\,\mathrm{MeV}^{-3}$
1.2	$1.3 \times 10^{16}\,\mathrm{MeV}^{-3}$	$2.1 \times 10^{15}\,\mathrm{MeV}^{-3}$
1.3	$-7.4 \times 10^{14}\,\mathrm{MeV}^{-3}$	$1.5 \times 10^{15}\,\mathrm{MeV}^{-3}$

Negative cross sections make no sense. However, these strange results are due to a too low precision of the internal processes or, equivalently, to cancellation effects in the sums.

Now, we presented the main parts of the programme for calculating the total cross section (2.24). Of course, for different plots the programme will be changed accordingly. However, the basic structure of the programme will always be the same. If we are interested in the differential cross section, then we can use the same programme and directly call the function `sum_n`. We just do not integrate over $\mathrm{d}\Omega_f$.

3.5 Calculation of the Imaginary Mass and Energy Shift

In order to be able to include the imaginary mass and energy shift in our evaluation, we have to calculate (2.29), or, to be more precise,

$$\tilde{W}_\gamma(k\cdot p) = \sum_{s=1}^{\infty} \int_0^{u_s} \frac{\mathrm{d}u}{(1+u)^2} \left\{ -4J_s^2(z) + \zeta^2 \left(2 + \frac{u^2}{1+u}\right) \left(J_{s+1}^2(z) + J_{s-1}^2(z) - 2J_s^2(z)\right) \right\}.$$

For each a, $\tilde{W}_\gamma$ is calculated with a separate programme. This will not be discussed here because it does not use any new concepts. The infinite sum over s can be truncated by the same rules which were presented in the previous section. However, the convergence is worse since the argument z of the Bessel functions increases with the increase of the index s as well. Nevertheless, the sum converges – anthing else makes no sense because we talk about the propability of photon emission – but we have to include many more terms; s is, depending on a, of the order of $\mathcal{O}(10^4)$.

In a loop, $(k \cdot p)$ is increased from 0 to approximately $10^{-4}\,\mathrm{MeV}^2$ – this is the typical range of values in the propagator. The programme then returns the value $\tilde{W}_\gamma(k \cdot p)$. In this range, $\tilde{W}_\gamma$ is a linear function of $(k \cdot p)$ as we can see in figure (3.5). Thus, we can approximate $\tilde{W}_\gamma$ by a regression line of the form $\tilde{W}_\gamma(k \cdot p) \approx b_a(k \cdot p)$. b_a will then be used for the calculation of the imaginary mass and energy shift according to (2.30) and (2.32).

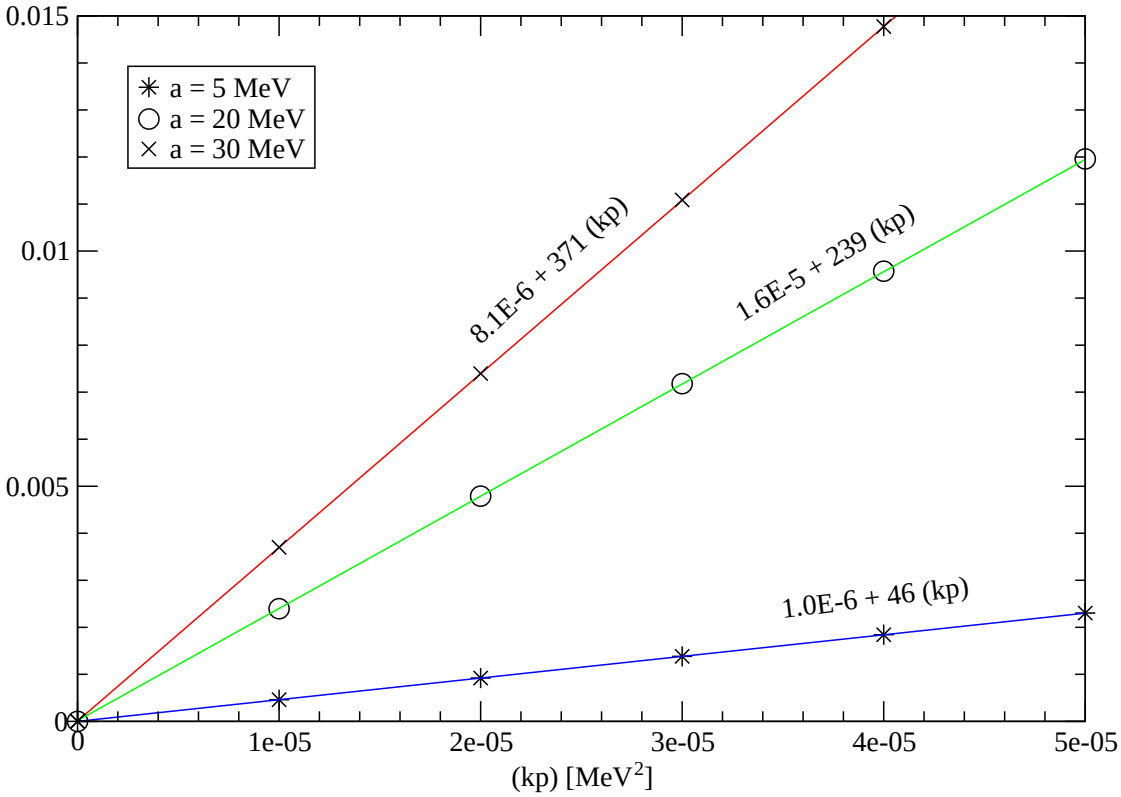

Figure 3.5: The calculation of some values of the function $\tilde{W}_\gamma(k \cdot p)$ is fairly complicated and takes some time. It turns out that it can be approximated by a linear function (in colour) to a very high accuracy in the range of our interest.

According to figure (3.5), we find

a [MeV]	b_a [MeV^{-2}]
1	3.4
5	46
10	110
20	240
30	371
40	499

3.6 Numerical Tests of the Validity of the Code

In all spectra we will present later, we will show the corresponding cross section without an external field (i.e. the Bethe-Heitler cross section) as a comparison. As we saw above, the Bethe-Heitler cross section is a special case of our more general cross section; namely for the case $a \to 0$. Since we have an analytic expression for the Bethe-Heitler cross section, we can compare the results of our programme for $a \to 0$ with the results of that expression in order to test the

validity of our Fortran code[2].

So, in a first step, we compare the results of the differential cross section (2.23) with the Bethe-Heitler cross section (A.2). Further information on the specific parameters for the energy of the incoming electron and the laser frequency will be given below. In this section, we want to compare the two results to make us believe in our programmes. We arbitrarily choose $\theta_f = 0°$, $\rho_f = 0°$, $\theta_b = 90°$, and $\rho_b = 180°$.

As we can see from some exemplary numbers in the tabular below and from the top graph (3.6), the agreement between the limit of our cross section and the Bethe-Heitler cross section is almost perfect. In fact, this calculation was done with double precision; a higher (quadruple) precision yields results which are in perfect agreement with each other.

ω_b/ω	laser-dressed cross section with $a = 0$	Bethe-Heitler cross section
1.0	$5.868 \times 10^9\,\mathrm{MeV}^{-3}$	$5.905 \times 10^9\,\mathrm{MeV}^{-3}$
1.5	$1.751 \times 10^9\,\mathrm{MeV}^{-3}$	$1.750 \times 10^9\,\mathrm{MeV}^{-3}$
5.0	$47.232 \times 10^6\,\mathrm{MeV}^{-3}$	$47.242 \times 10^6\,\mathrm{MeV}^{-3}$
10.0	$5.905 \times 10^6\,\mathrm{MeV}^{-3}$	$5.905 \times 10^6\,\mathrm{MeV}^{-3}$
20.0	$738.157 \times 10^3\,\mathrm{MeV}^{-3}$	$738.160 \times 10^3\,\mathrm{MeV}^{-3}$

In a next step, we want to check the numerical integration over the solid angle $\mathrm{d}\Omega_f$. As a test function, we again use the laser-dressed cross section (2.23) with $a = 0$. If we integrate it numerically, we should obtain the same result as from the analytically integrated Bethe-Heitler formula (A.3). We again present some values for the same scattering geometry:

ω_b/ω	numerical integration	analytical integration
1.0	$0.128\,\mathrm{MeV}^{-3}$	$0.128\,\mathrm{MeV}^{-3}$
2.0	$6.370 \times 10^{-2}\,\mathrm{MeV}^{-3}$	$6.262 \times 10^{-2}\,\mathrm{MeV}^{-3}$
5.0	$2.414 \times 10^{-2}\,\mathrm{MeV}^{-3}$	$2.346 \times 10^{-2}\,\mathrm{MeV}^{-3}$
10.0	$1.121 \times 10^{-2}\,\mathrm{MeV}^{-3}$	$1.117 \times 10^{-2}\,\mathrm{MeV}^{-3}$
20.0	$5.222 \times 10^{-3}\,\mathrm{MeV}^{-3}$	$5.303 \times 10^{-3}\,\mathrm{MeV}^{-3}$

We find a very close agreement between the numerical and analytical integration. This is obvious from both the above tabular and from the bottom diagram (3.6). Therefore, our numerical integration works perfectly. We could again achieve an even better agreement by increasing the precision (using quadruple precision).

We want to shortly summarize these two checks. First, we compared only the differential cross sections with each other. Since we showed theoretically that in the limit $a \to 0$ the laser-dressed cross section and the Bethe-Heitler formula will agree with each other, this numerical test is a check whether the Fortran programme works properly. At least in the limit $a \to 0$, this is the case. Then, we integrated the differential cross section over $\mathrm{d}\Omega_f$ in the limit $a \to 0$. Since we now know that the function to be integrated, namely the differential cross section, is correct, this is a check whether the numerical integration works correctly. The comparison with the analytic integration shows that the numerical integration passes this test, too.

[2]The programmes which are written to evaluate the Bethe-Heitler cross section are fairly simple and will not be presented in this thesis.

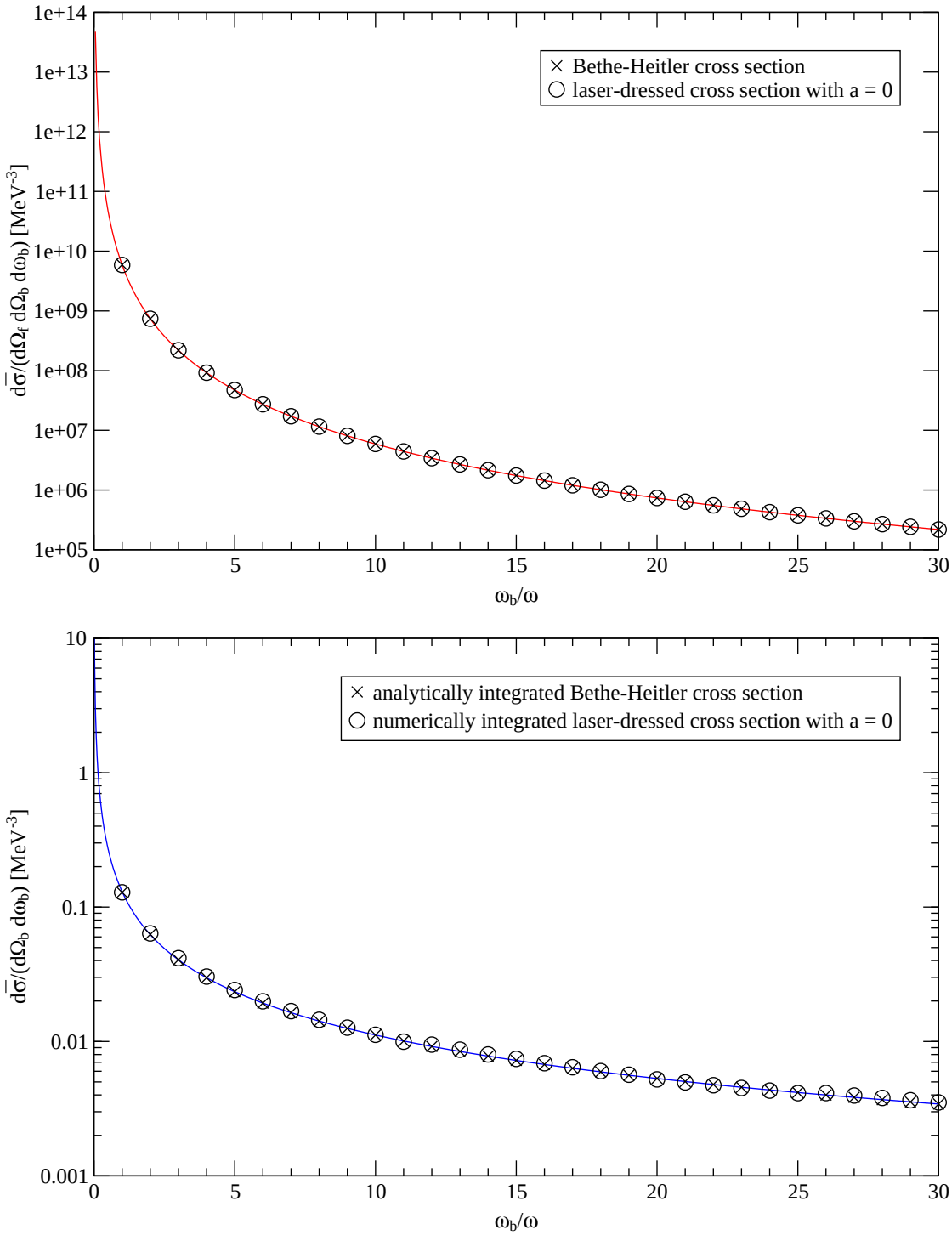

Figure 3.6: The comparison between the Bethe-Heitler and the laser-dressed cross section with $a = 0$ shows clearly that not only theoretically but also numerically the laser-dressed bremsstrahlung cross section coincides with the Bethe-Heitler cross section for a vanishing laser field. This is also a numerical test of the validity of the code. In the top diagram, we see the differential cross section, whereas it is integrated over the solid angle $\mathrm{d}\Omega_f$ in the bottom diagram.

Chapter 4

Results

Although we could choose an arbitrary laser frequency, we set $\omega = 1.1698 \times 10^{-6}\,\mathrm{MeV}$ in all calculations. This corresponds to a wavelength of 1060 nm of the laser. Hence, it is a typical neodymium laser. Moreover, the energy of the incoming electron is in all cases $E_i = 10m_e$. So, despite the fact that a fully relativistic description of the process is necessary because of the high-intensity laser, we also need a relativistic description since the (undressed) electron itself is highly relativistic. Possible differences from these conventions will be stated at that point explicitly.

The laser intensity I is defined as the energy flux: $I = \frac{\mathrm{d}E}{\mathrm{d}V}c$ with $c \equiv 1$ in natural units. The energy is $E = \frac{1}{2}\int_V \mathrm{d}^3x \left(\vec{E}^2 + \vec{B}^2\right)$. The $\vec{E}$- and $\vec{B}$-field can be calculated from $\vec{E} = -\frac{\partial \vec{A}}{\partial t} - \vec{\nabla}A^0$ and $\vec{B} = \vec{\nabla} \times \vec{A}$. This leads to $I = (a\omega)^2$. We give the values of the intensity in SI-units for different amplitudes a:

$a[\,\mathrm{MeV}]$	$I[\mathrm{W/cm^2}]$
5	2.13×10^{19}
10	8.54×10^{19}
20	3.41×10^{20}
30	7.68×10^{20}

First we will compare and analyse the differences between the free and the laser-dressed electron propagator as well as the differences between the cross sections with and without the imaginary mass shift. This is probably mainly of theoretical interest. Then, in a next step, we will present "normal" spectra – normal in the sense that we plot the cross section versus the frequency ω_b of the emitted bremsstrahlung photon. We will scale ω_b with the frequency ω of the laser – hence, the value at the x-axis is ω_b/ω. At the end of this section, some peculiarities of the bremsstrahlung cross section will be discussed.

If not stated otherwise explicitly, we always choose $\rho_b = 180°$ and $\rho_f = 0°$ (if we consider differential cross sections; otherwise we integrate over ρ_f anyway).

4.1 Comparison between the Free and the Laser-Dressed Electron Propagator

One might assume that the free electron propagator is a good approximation for the laser-dressed one we derived above. An intuitive explanation for this assumption is the following: The

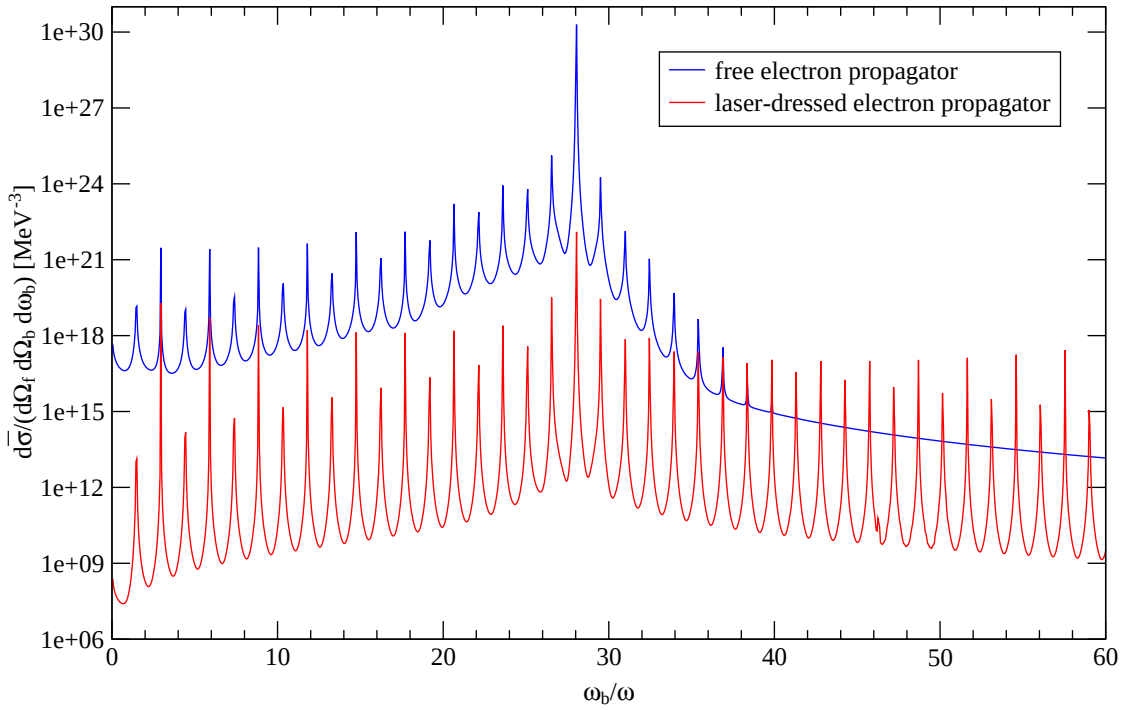

Figure 4.1: The comparison between the free and the laser-dressed electron propagator shows clearly that the free electron propagator is not a good approximation at all for laser-dressed processes such as bremsstrahlung.

time elapsed between the interaction of the electron with the nucleus and the emission of the bremsstrahlung photon (or vice versa) is so short that the intermediate electron cannot interact with the laser field. It would then propagate as a free electron, and the free propagator would be a good approximation.

Although this sounds reasonable at first glance, there is also strong evidence that this assumption does not hold. When we go back to the derivation of the S-matrix in equation (2.14), we see that the propagator depends on the space-time points x_1 and x_2 of the two interactions (namely the interaction with the nucleus and the emission of the bremsstrahlung photon). Thus, the time difference is $t_2 - t_1$ which has to be very small according to the assumption above. However, in order to calculate the S-matrix, we have to integrate over x_2 and x_1. Therefore, $t_2 - t_1$ can get both arbitrarily small and arbitrarily big. We conclude that the assumption does not seem to be justified from a mathematical point of view.

We will now compare cross sections calculated with the free and the full, laser-dressed propagator. We did not treat the derivation of the cross section with the free propagator in this thesis. Obviously, it is much easier since we just plug $S_F(x_2, x_1)$ instead of $G(x_2, x_1)$ into equation (2.14). We also replace $m_e \to m_e^*$ which seems to be a better approximation than the "pure" free propagator.

In diagram (4.1), we see a differential cross section evaluated with the free and the laser-dressed propagator. Although the explicit scattering geometry is of no interest at this point, we note that we set $\theta_f = (6 \times 10^{-4})°$, $\theta_b = 90°$, and $a = 20\,\mathrm{MeV}$.

Our mathematical explanation why the free propagator cannot be a good approximation is

obviously proved by the numerical comparison. The number of resonances in the free case is much lower. Moreover, the value of the cross section with the free propagator is several orders of magnitude higher than the one with the laser-dressed propagator. This enormeous increase of roughly ten orders of magnitude (even more compared to the laser-free, i.e. Bethe-Heitler cross section) also seems to be unphysical.

The reason why the free propagator cannot be a good approximation can also be explained in a more intuitive way. One laser cycle lasts $1060\,\mathrm{nm}/c = 3.5\,\mathrm{fs}$. The time scale t_b for photon emission can be estimated with the help of Heisenberg's uncertainty relation for time and energy: $E_b t_b \geq \hbar$. With $E_b = \hbar\omega_b = n\hbar\omega$, we get $t \geq 1/(n\omega) \gtrsim \mathrm{fs}/n$. For small n (e.g. of the order of 1), one laser cycle and the time scale of photon emission are both in the femto-second region. Thus, the influence of the external laser on the intermediate electron must not be neglected, and the full propagator must be used. However, if the energy of the bremsstrahlung photon exceeds the energy of the laser photons by several orders (very big n), the time scale of the emission of a bremsstrahlung photon will be very small or – in other words – the external field almost static during this short time interval. Then, we expect the free propagator to be a good approximation for our process. This rather naive argumentation can rigourously be proven and is confirmed in [23].

4.2 Comparison of the Cross Sections with and without the Imaginary Mass and Energy

We remember that we calculated the imaginary mass and energy shift of the electron in order to get finite peaks at the resonances. These shifts are only small contributions to the "normal" electron mass and energy. The influence of them will only be visible in a small region around the resonances. This is precisely what we get when we have a look at figure (4.2a). Both cross sections coincide more or less exactly.

To check whether the resonances are really finite we "zoom" into the first peak of the differential cross section. Indeed, we find the cross section with the imaginary shift to be finite in the next figure; the unregularized cross section seems to tend to infinity as we expect it.

4.3 Differential Cross Sections

In this section, we will have a closer look at differential cross sections – differential in the energy and the solid angle of the emitted bremsstrahlung photon and differential in the solid angle of the outgoing electron. We stated before that we are mainly interested in the total cross section. However, we expect differential and total cross sections to be qualitatively the same if we consider no deflection of the electron. This expectation is reasonable because of the strong decrease of the differential cross section with increasing θ_f (see section 3.3). Therefore, we can use the differential cross section for qualitative analysis of the bremsstrahlung process – the big advantage is that its evaluation is much faster than the one for the total cross section.

So, we will start with $\theta_b = 179°$ in the top diagram of figure (4.3). From now on, we will also show the field-free cross section (i.e. the Bethe-Heitler cross section) as a comparison. It is drawn as a solid black line. Since $\vec{k}_b$ and $\vec{k}$ are almost parallel, we expect the appearance of higher harmonics in the narrower sense[1]. We recognize that our expectation is fulfilled for all

[1] We remember from our theoretical discussion that all resonances are higher harmonics *in the rest frame of the electron*. For this scattering geometry, however, the resonances are also "higher harmonics" in the laboratory frame.

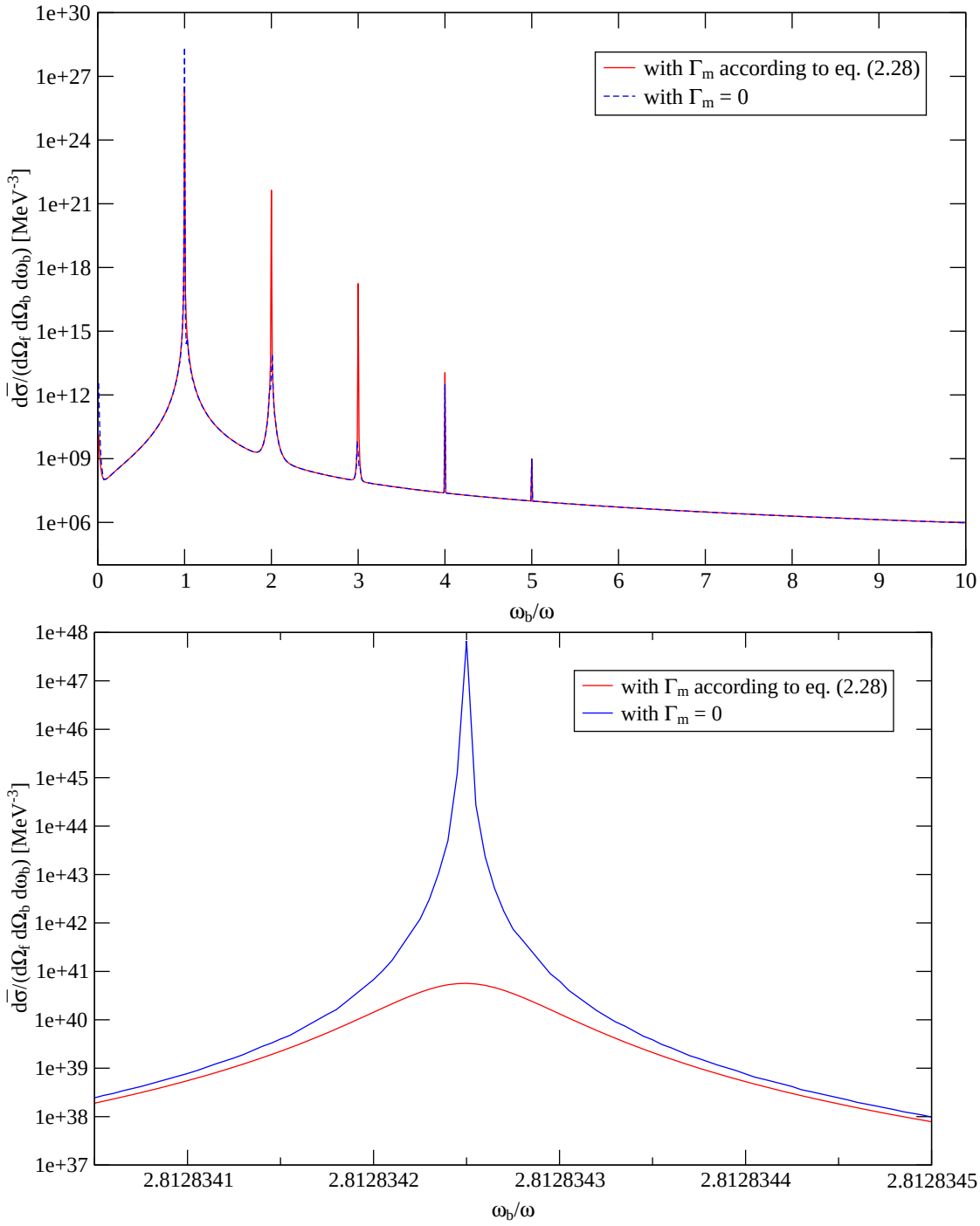

Figure 4.2: The comparison between the differential cross section with and without the imaginary mass and energy shift shows that the cross sections coincide (top, diagram (a) with $\theta_b = 179°$). Only around the resonances, the cross section with the imaginary shift yields a finite value whereas the other one goes to infinity (bottom, diagram (b) with $\theta_b = 90°$). This is the expected behaviour.

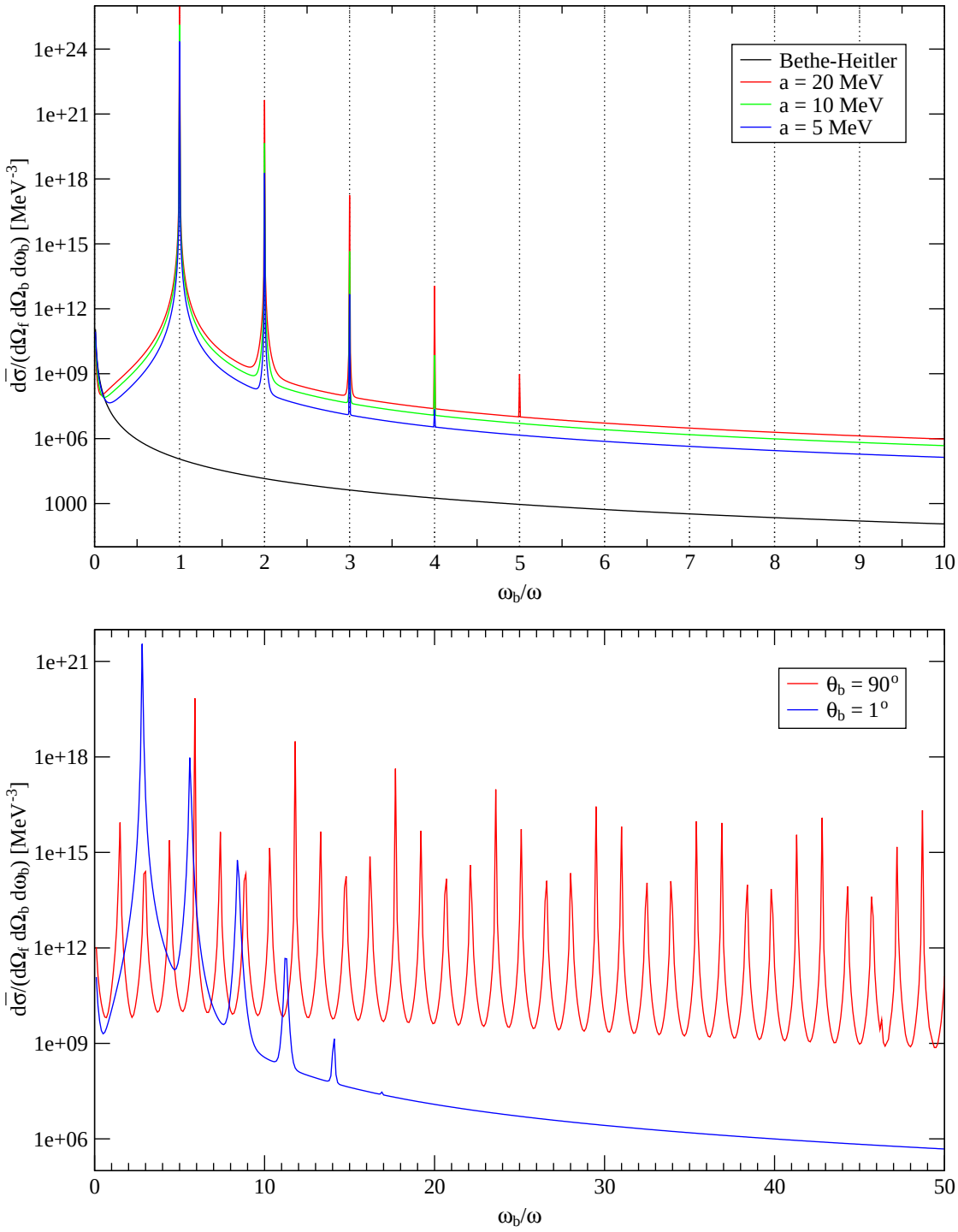

Figure 4.3: The differential cross section for $\theta_b = 179°$ (top diagram) shows resonance peaks at integer multiples of the laser frequency. If the bremsstrahlung photon is not emitted parallel to the laser photons (bottom diagram), the resonance peaks are not higher harmonics in the laboratory frame. The number of resonances strongly depends on the angle θ_b (here we set $a = 20\,\mathrm{MeV}$).

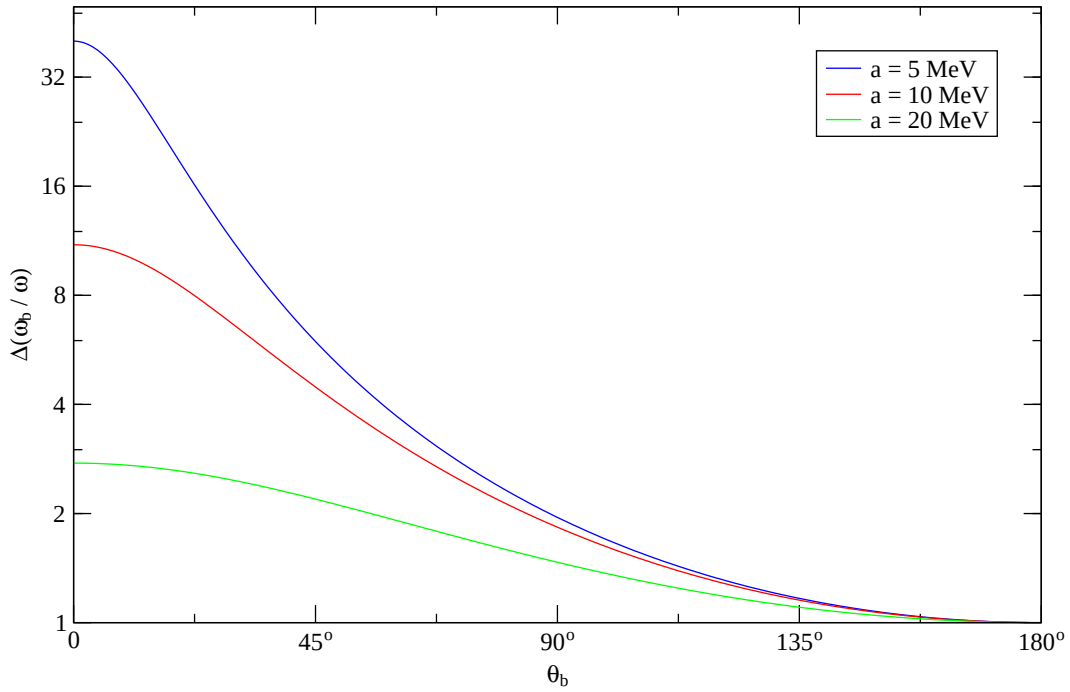

Figure 4.4: The dependence of the spacing between resonances on the polar angle θ_b is shown in this diagram. The greatest spacing is achieved for low laser intensities and anti-parallel emission of the bremsstrahlung photon compared to the laser photons.

intensities. Nevertheless, the resonances vanish after just four or five peaks.

In the bottom diagram of the same figure (4.3), we see the differential cross section for $a = 20\,\mathrm{MeV}$. The bremsstrahlung photon is in one case emitted with an angle $\theta_b = 90°$ and in the other case with $\theta_b = 1°$. We can calculate the spacing between the resonances with the formulas (2.27). For our approximation, it does not matter whether we take the first or the second formula since the electron is not deflected. We calculate a spacing of $\Delta(\omega_b/\omega) = 1.5$ for $\theta_b = 90°$ and $\Delta(\omega_b/\omega) = 2.8$ for $\theta_b = 1°$. These values are in very good agreement with the diagram.

We will have a closer look at the formulas (2.27) for the spacing of the resonances. We consider no deflection of the electron (which is – as explained above – the most interesting case) so that both formulas yield approximately the same result. We find

$$\Delta\left(\frac{\omega_b}{\omega}\right) = \frac{\tilde{E}_i + \sqrt{\tilde{E}_i^2 - m_e^{*2}}}{\tilde{E}_i - \sqrt{\tilde{E}_i^2 - m_e^{*2}}\cos\theta_b}. \tag{4.1}$$

We plot this as a function of θ_b and get diagram (4.4). We see from the graph (and we can also easily calculate it) that we get a minimum at $\theta_b = 180°$. The value at this point is always – independent of any other parameters – $\Delta\left(\omega_b/\omega\right)\big|_{\theta_b=180°} = 1$. This is of course the result we expected from our previous considerations. The maximum spacing we can get is at $\theta_b = 0°$ with $\Delta\left(\omega_b/\omega\right)\big|_{\theta_b=0°} = \left(\tilde{E}_i + \sqrt{\tilde{E}_i^2 - m_e^{*2}}\right)^2 / m_e^{*2}$. Therefore, for a fixed laser intensity a, we get a finite maximal spacing.

4.4 Total Cross Sections

The main reason why we calculate the total cross section – the cross section integrated over all directions of the outgoing electron – is that the emission of the bremsstrahlung photon and its features are the most interesting aspects of the whole process. Moreover, from an experimental point of view, it is much more demanding to measure the differential cross section since we would have to be able to detect electron and photon in coincidence. However, the calculations for the total cross sections last much longer than in the differential case (this is due to the numerical integration and the use of quadrupel precision); the calculations of the upcoming spectra took typically several weeks.

We first present spectra with $\theta_b = 179°$. After all, it is no surprise that we see higher harmonics at integer values of ω_b/ω in the top diagram of figure (4.5). If we compare this graph with the differential cross section (4.3) (top diagram), our assumption of the qualitative agreement in the previous section is confirmed. However, as we can see, the total cross section is of the same order of magnitude as the Bethe-Heitler cross section whereas the differential cross section (4.3) is enhanced by approximately three orders of magnitude. This enhancement in the differential case is due to the fact that we just considered final electrons without any deflection (i.e. $\theta_f = 0°$). As we saw, the differential cross section falls off rapidly with increasing polar angle θ_f so that the total cross section is of the same order as the Bethe-Heitler cross section.

So let us turn our attention to another spectrum, namely the bottom graph in figure (4.5) with the polar angle $\theta_b = 1°$. The first striking feature is probably the large difference in the spacing of the resonances of the two spectra. However, if we go back to our considerations in the previous chapter, this is not very amazing any more. According to diagram (4.4), the dependence of the spacing on a becomes greater with decreasing angle θ_b. Thus we expect a spacing of just below 3 for $a = 20\,\mathrm{MeV}$ and just below 12 for $a = 10\,\mathrm{MeV}$. This is in perfect agreement with figure (4.5).

Up to here, we just considered spectra where we varied the energy ω_b. We did not consider the angular distribution of the radiation so far. Of course, if we want to get resonances at certain multiples of the laser frequency, then we have to detect the bremsstrahlung photons at a specific polar angle θ_b which we can calculate with formula (4.1). Therefore, the experimentalist will probably fix θ_b according to his interests. Nevertheless, it is quite interesting to know the angular distribution of the bremsstrahlung radiation. For example, one could assume that some angles θ_b are favoured compared to others – similar to the case of a relativistically accelerated charge (the maximal intensity is found for a polar angle $1/(2\gamma)$; γ being the relativistic factor). For this purpose, we fix the energy ω_b and vary the angle θ_b. The calculations yield the next diagram (4.6). The peaks we see are resonances which are also caused by intermediate on-shell electrons. Hence, the equations (2.25) and (2.26) must be fulfilled at the peaks. As we know, it is enough for a first approximation to use just one of the equations; we will use (2.26). We neglect the $(k \cdot \tilde{n}_b)$-term in the denominator. With $q_i \cdot \tilde{n}_b = \tilde{E}_i - |\vec{q}_i| \cos\theta_b$, we get

$$\cos\theta_b = \frac{s}{\omega_b/\omega}\left(\frac{\tilde{E}_i}{|\vec{q}_i|} + 1\right) + \frac{\tilde{E}_i}{|\vec{q}_i|}.$$

The ratio $\tilde{E}_i/|\vec{q}_i|$ depends on the laser intensity a:

a [MeV]	$\tilde{E}_i/\lvert\vec{q}_i\rvert$
10	1.200
20	2.103
30	8.835

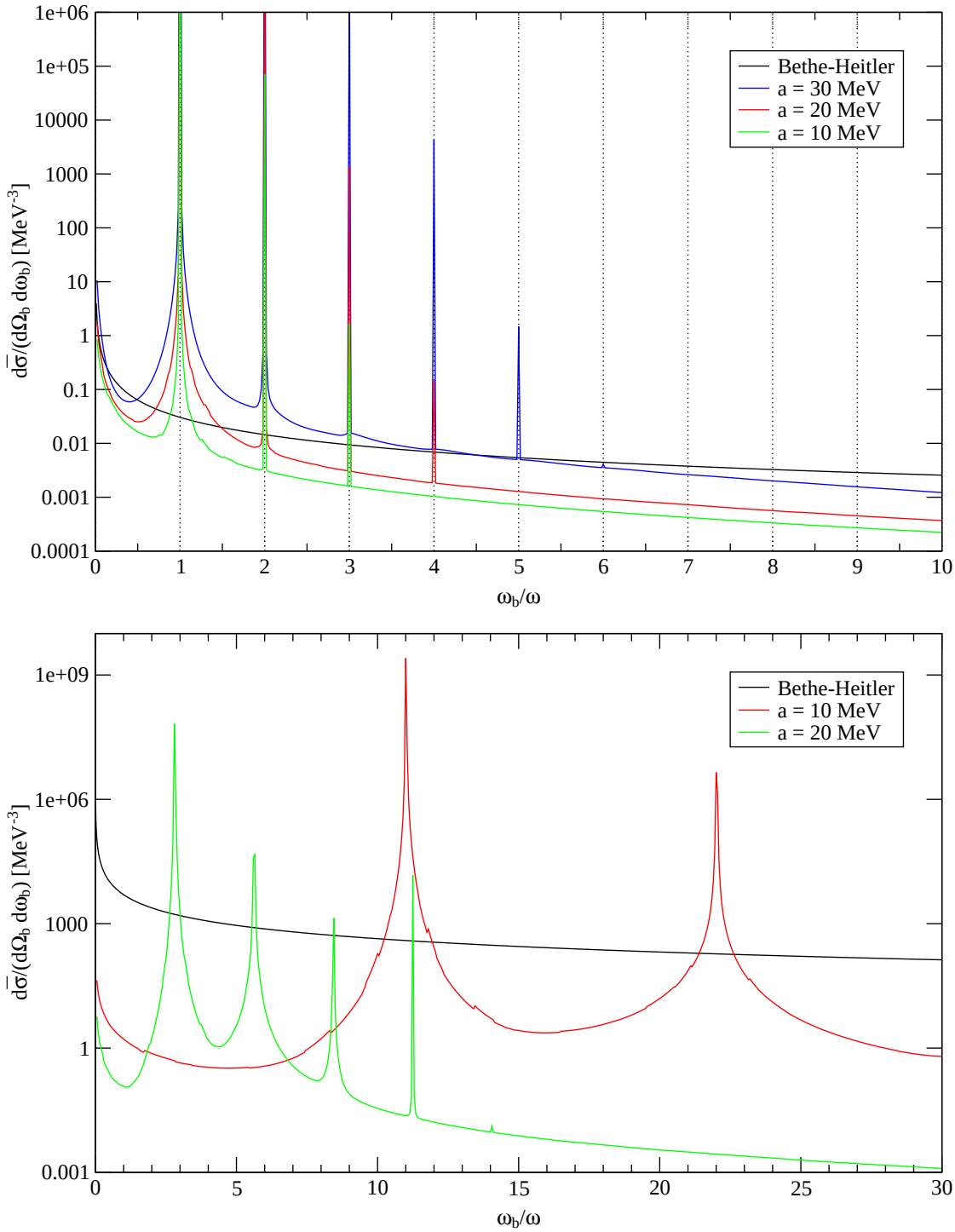

Figure 4.5: The total cross section for $\theta_b = 179°$ (top diagram) shows resonances at integer multiples of the laser frequency as it was expected from our theoretical considerations. In contrast to the differential cross section, the total cross section is not enhanced compared to the Bethe-Heitler cross section. As we can clearly see in bottom diagram with the polar angle $\theta_b = 1°$, the spacing of the resonances also depends on the laser intensity a.

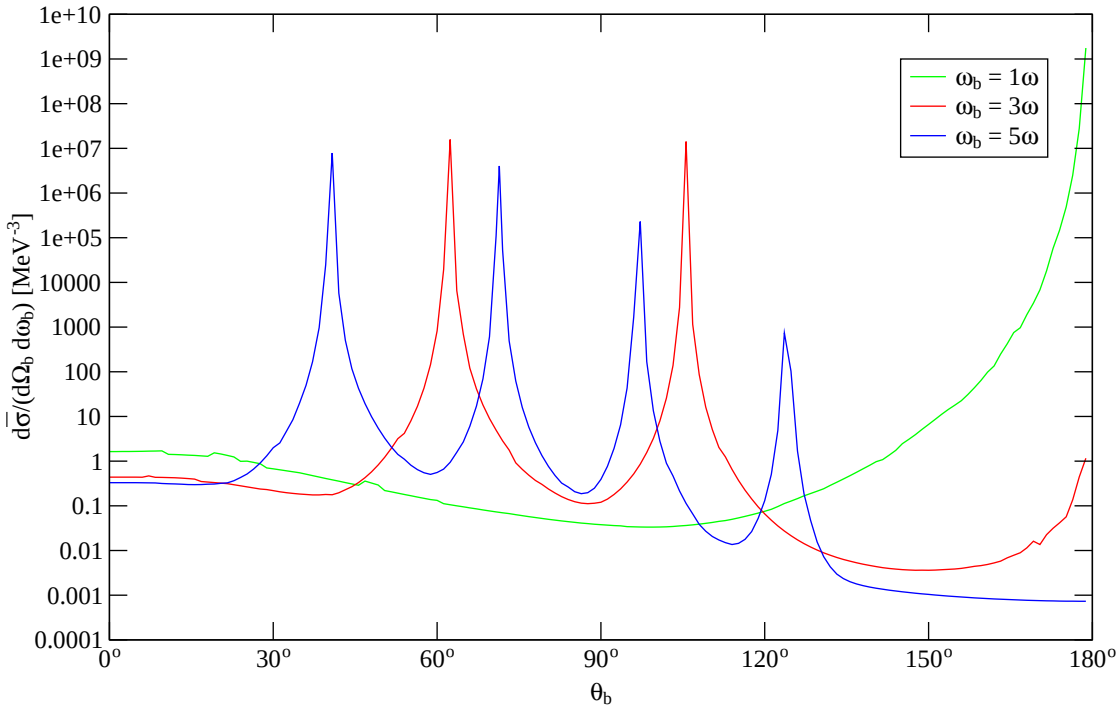

Figure 4.6: The angular distribution of the total cross section for the laser intensity $a = 10\,\mathrm{MeV}$ shows resonance peaks at various angles θ_b.

We chose $a = 10\,\mathrm{MeV}$ so that we can write

$$\theta_b = \arccos\left(2.2\frac{s}{\omega_b/\omega} + 1.2\right)$$

Let us choose $\omega_b = 5\omega$ as an example. Then, we can get resonances for $s = -5$, -4, -3, -2, and -1. For all other values of s, the argument of the arccos is either above $+1$ or below -1. The corresponding angles are $\theta_b = 180°$, $124°$, $97°$, $71°$, and $41°$. This can also be seen in the diagram[2].

4.5 The Peculiar Behaviour for a Varying Laser Intensity

At the end of this section, we want to have a look on the behaviour of the (differential) cross section in dependence of the laser intensity a. Consequently, we have to fix the energy of the bremsstrahlung photon; we set it to $\omega_b = 1.5\omega$[3]. The cross section will be plotted for the four different combinations of the two angles $\theta_b = 1°, 179°$ and $\theta_f = 0°, 180°$. The resulting plot can be seen in figure (4.7).

The peaks occur due to intermediate on-shell electrons; the fluctuations for higher intensities in the dashed graph is numerical noise which could be stopped by using a higher precision.

[2]The resonance at $\theta_b = 180°$ is suppressed due to other effects. There is no fifth higher harmonic in the top diagram of figure (4.5), either.

[3]This energy is arbitrarily chosen; a different energy does not change the overall behaviour and the feature we will examine in this subsection.

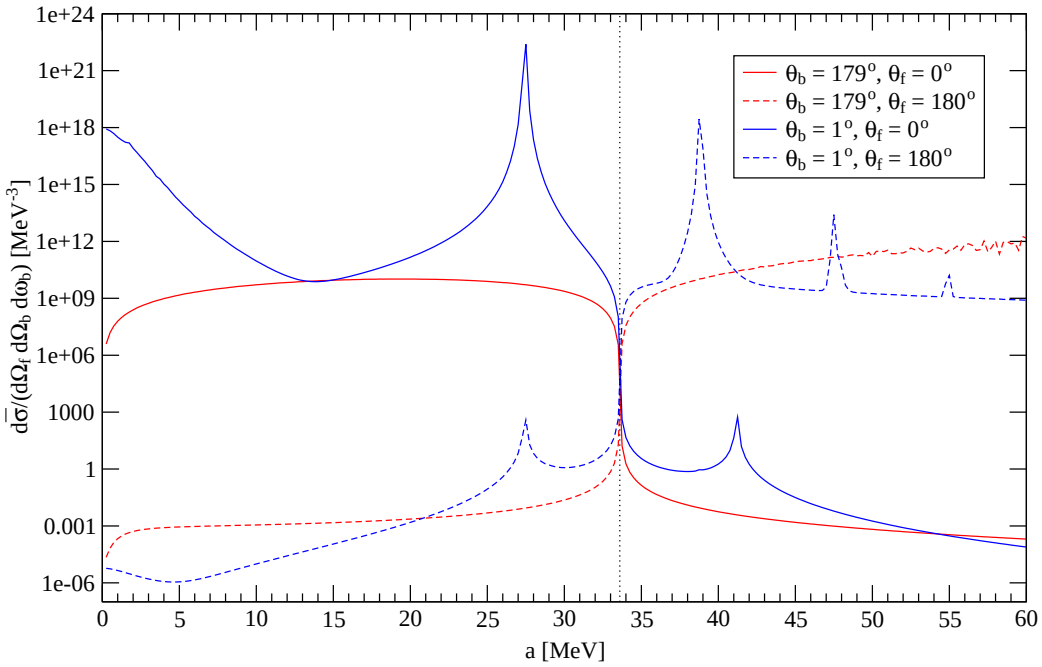

Figure 4.7: The cross section shows a step at $a \approx 33.5\,\mathrm{MeV}$ if we fix all angles and the energy and vary the laser intensity a. The position of this step does not depend on the angles or the energy of the bremsstrahlung photon.

However, this is not what we are interested in. As we can see in the diagram, there is a huge step of order $\mathcal{O}(10^{10})$ at an intensity of $a \approx 34\,\mathrm{MeV}$. The cross sections with final electrons which are not deflected ($\theta_f = 0°$) drop dramatically; whereas in the opposite case, when the final electron is reflected ($\theta_f = 180°$), the cross sections increase from very low up to very high values. How can this unexpected behaviour be explained?

For this reason, we go back to the definition of the effective momentum (2.5) and have a look at the x-component: $q_i^x = p_i^x - \frac{e^2 a^2}{2k\cdot p_i}\omega$. Obviously, q_i^x can become negative if a is large enough; the electron will then effectively travel backwards in the laser field. But if the electron travels backwards, we will hardly detect any electrons in the forward direction ($\theta_f = 0°$) but most of them in the backward direction ($\theta_f = 180°$). So, we expect the laser intensity $a_{\mathrm{tp}} \approx 34\,\mathrm{MeV}$ at which there is the huge step in figure (4.7) to be the "turning point", i.e. $q_i^x\big|_{a=a_{\mathrm{tp}}} = 0$.

$$
\begin{aligned}
0 &\stackrel{!}{=} p_i^x - \frac{e^2 a_{\mathrm{tp}}^2}{2k\cdot p_i}\omega \\
\Leftrightarrow a_{\mathrm{tp}} &= \sqrt{\frac{2p_i^x (k\cdot p_i)}{e^2\omega}} \\
&= \sqrt{\frac{2\sqrt{E_i^2 - m_e^2}\left(E_i + \sqrt{E_i^2 - m_e^2}\right)}{e^2}} \\
&\approx \frac{2\gamma m_e}{e} \qquad \text{for ultrarelativistic electrons } E_i = \gamma m_e \ggg m_e
\end{aligned}
$$

We see that a_{tp} depends only on the energy of the incoming electron. In our case with $\gamma = 10$,

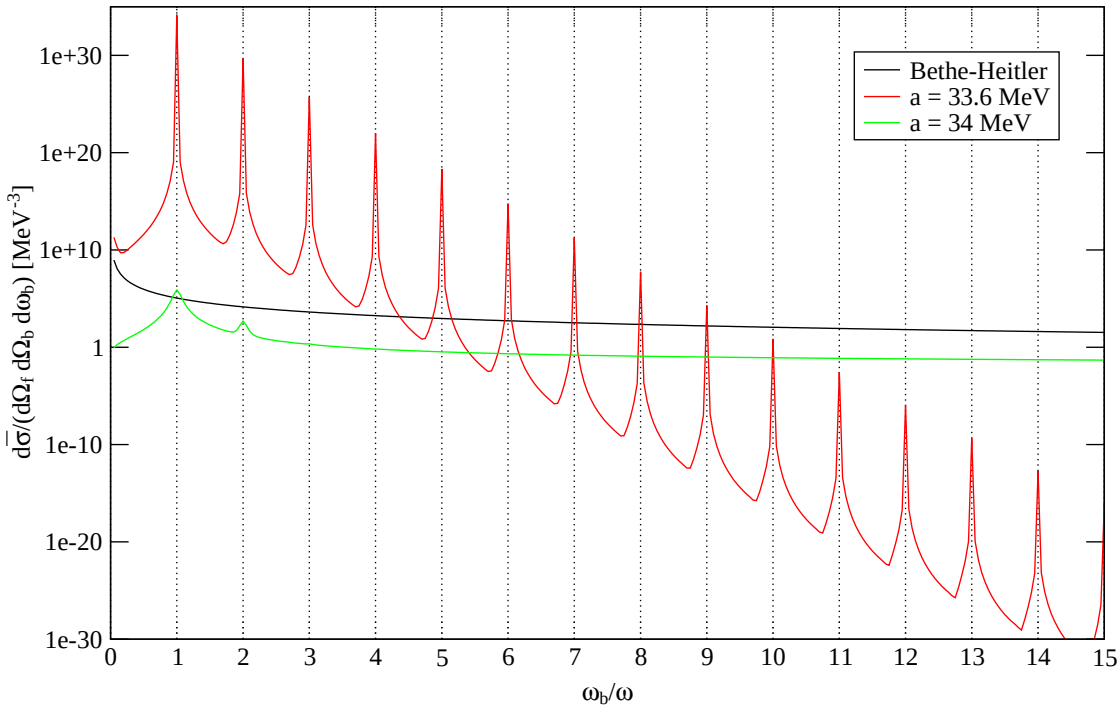

Figure 4.8: The differential cross section behaves significantly differently at laser intensities around a_{tp}.

the (exact) formula yields $a_{\mathrm{tp}} = 33.6\,\mathrm{MeV}$. This is in perfect agreement with figure (4.7)[4].

Let us shortly have a look at spectra of the differential cross section at laser intensities around a_{tp}. We set $\theta_b = 179°$ and $\theta_f = 0°$. The spectra are shown in the next diagram (4.8).

For $a = 34\,\mathrm{MeV}$, the cross section is very small. According to our previous discussion and the fact that $34\,\mathrm{MeV} > a_{\mathrm{tp}}$, this is easily understood. For $a = a_{\mathrm{tp}}$ we get many resonances; moreover the overall cross section decreases exponentially. However, one might wonder whether our calculations are valid at this particular laser intensity.

We want to stress again that this peculiar behaviour of the cross section depending on a is a special feature of the *differential* cross section. If we consider the total cross section, we will not be able to see the step at a_{tp}. The integration over θ_f will blur all traces.

[4]The approximated formula yields $a_{\mathrm{tp}} = 33.7\,\mathrm{MeV}$ with $\gamma = 10$.

Chapter 5

Summary and Outlook

At the end of this thesis, we want to discuss shortly what we found out during our analysis and what problems and questions arose.

The basic aim of the thesis was to derive analytically the bremsstrahlung cross section in a circularly polarized field. Hereby, a QED-approach had to be used. Moreover – as important as the derivation – in a second step, this cross section had to be numerically evaluated by using a Fortran 90 programme. These two steps were the requirements for all following discussions.

In the derivation, we used the solutions of the Dirac equation in an external plane-wave field – the so-called Volkov solutions – as initial and final electron states (2.6). Another focus was put on the use of the full, laser-dressed electron propagator (2.9). We found that the poles of the propagator are shifted to the effective mass shell. Furthermore, we showed that it is necessary to implement the laser-dressed propagator in order to make any useful predictions. This is obvious from figure (4.1) in chapter 4.1. An approximation with the free electron propagator can only be justified for high energies ω_b of the bremsstrahlung photon. In fact, we are the first who implemented and evaluated the laser-dressed electron propagator in a nontrivial, second-order process.

One of the great discoveries of laser-assisted experiments with bound electrons was the creation of higher harmonics. This can be qualitatively and quantitatively explained in the semiclassical *three-step-model* by considering recollision effects [13]. We were interested in the question whether higher harmonic generation could also occur in our unbound system. Recollision effects do not play any role as we showed in appendix B; a semiclassical approach could not be used. However, we showed analytically in section 2.5 that we expect resonances in the cross section for certain scattering geometries and energies. By choosing the proper parameters – namely bremsstrahlung emission parallel to the propagation of the laser photons –, we could create a system which indeed emits bremsstrahlung photons with frequencies preferable at integer multiples of the laser frequency. This happens for both the differential and the total cross section as it can be seen in figures (4.3) and (4.5). In fact, we showed in section 2.5 that all resonances are higher harmonics in the rest frame of the electron in a very good approximation. Resonances generally occur whenever the intermediate electron is on-shell, i.e. becomes real. Then, the second-order bremsstahlung process factorizes into a product of two first-order processes, namely laser-dressed Compton scattering [8, 10] and laser-assisted Coulomb scattering [19, 24].

Whenever the electron fulfills the on-shell condition, the denominator of the propagator becomes zero; as a result, the total expression is singular. In order to circumvent this unphysical behaviour, we included an imaginary mass shift according to equation (2.28). This we described in section 2.6. When implementing the imaginary mass shift, it is crucial to also introduce an

imaginary energy shift as in (2.30). Without doing this, the destructive interference between the exchange and the direct terms of the two transition amplitudes $S_{fi}^{(1)}$ and $S_{fi}^{(2)}$ (figure (1.4)) becomes constructive, and the overall cross section is increased by more then ten orders of magnitude – a result which is obviously incorrect. The imaginary energy follows immediately from the condition that, even for complex masses, the energy-momentum relation $q^2 = m_e^{*2}$ has to be fulfilled. On the other hand, it can also be motivated from the fact that the electron shows a level structure in an external laser field. Transitions between different levels are possible by absorbing or emitting laser photons. Thus, the electron in the laser field can be seen as a decaying system and therefore has a complex energy. With the implementation of the imaginary mass and energy, the singularities caused by intermediate on-shell electrons disappear. This can clearly be seen in figure (4.2).

Since laser-dressed Compton scattering and bremsstrahlung have the same initial and final states, one could assume that both processes interfere. However, we showed in appendix C that this not the case. This is due to the different energy conservation relations which the two processes obey.

At this point, we want to shortly point out a problem of our formalism. For this purpose, we remember that the cross section is divided by the absolute value of the momentum transfer $|\vec{q}_n|$ to the fourth power as in equation (2.23). If $|\vec{q}_n| = 0$, then the cross section will be infinite. $|\vec{q}_n|$ can only equal zero if each component equals zero, i.e. if $q_n^\mu = 0^\mu$. This means that we have four-momentum conservation $q_f = q_i + nk - k_b$ which is equivalent to $q_i \cdot k_b = n\, q_f \cdot k$. If we express this in terms of q_i, this is equal to $q_i \cdot k_b = n(q_i \cdot k - k \cdot k_b)$ which corresponds to the equation (2.26) for resonance peaks of the propagator for $n \to -s$. Expressed in terms of q_f, we end up with $n\, q_f \cdot k = q_f \cdot k_b - nk \cdot k_b$ which, in turn, equals (2.25) for resonance peaks for $n \to n + s$. It can be shown that, for certain (very small) angles θ_f, $|\vec{q}_n|$ really equals zero. Hence, the cross section will be singular at the resonances for this particular angle θ_f. This also explains why the peaks of the differential cross sections are in general finite as it can be seen in figure (4.2). On the other hand, the resonances of the total cross section will be singular since we integrate over θ_f. It should be stressed here that these infinities are due to the *Coulomb potential* we use. The imaginary mass and energy just regularize the propagators.

This behaviour is in fact not really unexpected. In the Bethe-Heitler formula, there is also an infinity for $\omega_b \to 0$ – the so-called *infrared divergence* or *infrared catastrophe*. For a (hypothetical) bremsstahlung photon with $\omega_b = 0$, the Bethe-Heitler cross section yields infinity because $|\vec{q}_n|$ will be zero. This is independent of regularizing the electron mass. The same happens in the laser-assisted case. Here, we get the infinity at $\omega_b = 0$ as well but also at the resonances for a particular θ_f. In the case of the Bethe-Heitler cross section, we know that it is not correct for very small ω_b; however, since we are not interested in this frequency regime, we do not have to worry about it. In the laser-assisted case, things change completely: We are especially interested in the regime where resonances occur. On the other hand, doubts might be appropriate whether our formalism describes the physical reality around the resonances correctly. A solution to this dilemma is the use of a *screened Coulomb potential*, i.e. a *Yukawa potential*. It modifies the Coulomb potential for small momentum transfer $|\vec{q}|$ and is of the form $A^0_{\text{Yukawa}}(x) \propto \exp\left[-|\vec{x}|/\lambda\right]/|\vec{x}|$ with the screening length λ. The Fourier-transformed Yukawa potential looks $A^0_{\text{Yukawa}}(q) \propto 1/\left(\vec{q}^2 + \lambda^{-2}\right)$. In the cross section (2.23), this yields the replacement $1/|\vec{q}_n|^4 \to 1/\left(\vec{q}^2 + \lambda^{-2}\right)^2$. Therefore, even if the momentum transfer onto the nucleus q is zero, the screening length λ prevents the expression from going to infinity.

Summarizing we can say that we accomplished our goal insofar as we could derive and numerically calculate the laser-dressed bremsstrahlung cross section. A more detailed analysis showed that bremsstrahlung does not compete with Compton scattering; both processes take place independently from each other. However, the use of the Coulomb potential leads to infinities at

the resonances. This is a problem which can be solved by using the Yukawa potential. Another problem which was only indicated in this thesis so far is the duration of the numerical integration. Since we have to use quadrupel precision to get reasonable results, the evaluation is slowed down considerably. Therefore, another problem for a future work on this topic is how the evaluation can be sped up even more.

An article in which the main results of this thesis will be published is in preparation [25].

Appendix A

Derivation of the Bethe-Heitler Cross Section

There are two approaches to QED – a more formal one starting from field theoretical considerations and another, more illustrative approach originating from *Stückelberg* and *Feynman*. Whereas the former one directly quantizes the occuring fields, the latter uses a propagator formalism. However, both approaches are equivalent and lead to a set of rules – the so-called *Feynman rules* – for writing down transition amplitudes for Feynman diagrams.

We will now derive the bremsstrahlung cross section in lowest, i.e. in second-order perturbation theory. We will basically follow the derivation in [12]. The Feynman rules in coordinate space we have to apply are:

1. In nth order of perturbation theory, one has to draw all possible, topologically distinct Feynman diagrams with n vertices and the specified external lines.
2. With each external line, one has to associate the following factors:
   (a) incoming electron: $\psi_i(x_1)$
   (b) outgoing electron: $\overline{\psi}_f(x_2)$
   (c) outgoing photon: $A^\mu_\lambda(x) = \frac{1}{\sqrt{2\omega V}}\epsilon^\mu_\lambda e^{ik\cdot x}$
   (d) interaction with external potential: $A^\mu_{\text{Potential}}(x)$
3. With each internal electron line connecting two vertices, one has to associate the electron propagator $iS_F(x_2 - x_1) = \int \frac{\mathrm{d}^4p}{(2\pi)^4} \exp\left[-ip\cdot(x_2-x_1)\right] \frac{i(\hat{p}+m_e)}{p^2-m_e^2+i\epsilon}$.
4. Each vertex is associated with a factor $-ie\gamma_\mu$.
5. Then, one has to integrate over the space-time x_i of all vertices $i = 1, 2, \ldots, n$.
6. Finally, one has to add the amplitudes of all possible Feynman-diagrams coherently.

In second order, there are only two distinct Feynman diagrams which are shown in figure (A.1). With the above rules, we can directly write down the transition amplitude S_{fi}:

$$\begin{aligned} S_{fi} = \int \mathrm{d}x_1 \int \mathrm{d}x_2 \overline{\psi}_f(x_2) \Big\{ \Big(-ie\gamma_\mu A^\mu_{b,\lambda}(x_2)\Big)\, iS_F(x_2-x_1)\, (-ie\gamma_\mu A^\mu_{\text{Coul}}(x_1)) + \\ (-ie\gamma_\mu A^\mu_{\text{Coul}}(x_2))\, iS_F(x_2-x_1) \Big(-ie\gamma_\mu A^\mu_{b,\lambda}(x_1)\Big)\Big\}\, \psi_i(x_1). \end{aligned} \tag{A.1}$$

Figure A.1: These two bremsstrahlung Feynman diagrams are the starting point for the derivation of the Bethe-Heitler formula.

We refer to section (2.3) for a more detailed discussion on the two vector potentials, especially how the Fourier-transformed Coulomb potential A_{Coul} looks like. The solution of the free Dirac equation is well-known: $\psi_i(x_1) = \sqrt{m_e/(E_i V)} u_{r_i}(p_i) \exp\left[-ip_i \cdot x_1\right]$ and hence $\overline{\psi}_f(x_2) = \sqrt{m_e/(E_f V)} \overline{u}_{r_f}(p_f) \exp\left[+ip_f \cdot x_2\right]$. We plug all these expressions into the above equation:

$$\begin{aligned} S_{fi} \;=\; & iZe^3 \sqrt{\frac{m_e^2}{2\omega_b E_i E_f V^3}} \int \mathrm{d}x_1 \int \mathrm{d}x_2 \int \frac{\mathrm{d}^4 p}{(2\pi)^4} \int \frac{\mathrm{d}^4 q}{(2\pi)^4} 2\pi\delta\left(q^0\right) \times \\ & \overline{u}_{r_f}(p_f) e^{ip_f \cdot x_2} \left\{ \left(\hat{\epsilon}_{b,\lambda} e^{ik_b \cdot x_2}\right) \frac{\hat{p} + m_e}{p^2 - m_e^2 + i\epsilon} e^{-ip\cdot(x_2 - x_1)} \left(\gamma^0 \frac{1}{|\vec{q}|^2} e^{-iq\cdot x_1}\right) + \right. \\ & \left. \left(\gamma^0 \frac{1}{|\vec{q}|^2} e^{-iq\cdot x_2}\right) \frac{\hat{p} + m_e}{p^2 - m_e^2 + i\epsilon} e^{-ip\cdot(x_2 - x_1)} \left(\hat{\epsilon}_{b,\lambda} e^{ik_b \cdot x_1}\right) \right\} u_{r_i}(p_i) e^{-ip_i \cdot x_1}. \end{aligned}$$

The integration over x_1, x_2, and p can be done without any problems. We consider the exponentials of the first summand:

$$\begin{aligned} & \int \mathrm{d}x_1 \int \mathrm{d}x_2 \int \frac{\mathrm{d}^4 p}{(2\pi)^4} \exp\left[i(p_f + k_b - p)\cdot x_2 + i(p - q - p_i)\cdot x_1\right] \\ =& \int \frac{\mathrm{d}^4 p}{(2\pi)^4} (2\pi)^4 \delta^{(4)}(p_f + k_b - p)(2\pi)^4 \delta^{(4)}(p - q - p_i) \\ =& (2\pi)^4 \delta^{(4)}(p_f + k_b - q - p_i). \end{aligned}$$

We note that the intermediate momentum can be expressed as $p = p_f + k_b$. The equivalent integration of the second summand yields the same result. However, here the intermediate momentum obeys the relation $p = p_i - k_b$. Now, it is also no problem to perform the integration over q, the momentum transfer onto the nucleus.

$$\int \frac{\mathrm{d}^4 q}{(2\pi)^4} 2\pi\delta\left(q^0\right) (2\pi)^4 \delta^{(4)}(p_f + k_b - q - p_i) = 2\pi\delta(E_f + \omega_b - E_i)$$

The momentum transfer is given by $\vec{q} = \vec{p}_f + \vec{k}_b - \vec{p}_i$ according to the δ-function. Energy is not transferred onto the nucleus since it was assumed to be infinitely heavy.

For the intermediate momenta, we plug in $p_f + k_b$ and $p_i - k_b$, respectively. The simplified transition amplitude now looks

$$S_{fi} = iZe^3 2\pi\delta(E_f + \omega_b - E_i) \sqrt{\frac{m_e^2}{2\omega_b E_i E_f V^3}} \frac{1}{|\vec{q}|^2} \epsilon^{\mu}_{b,\lambda} M_{\mu}(k_b)$$

with the matrix element

$$M_\mu(k_b) = \overline{u}_{r_f}(p_f)\left\{\gamma_\mu \frac{\hat{p}_f + \hat{k}_b + m_e}{2p_f\cdot k + i\epsilon}\gamma_0 + \gamma_0 \frac{\hat{p}_i - \hat{k}_b + m_e}{-2p_i\cdot k_b + i\epsilon}\epsilon_\mu\right\} u_{r_i}(p_i).$$

In the denominator, we used the energy-momentum relations $p_i^2 = p_f^2 = m_e^2$ and $k^2 = 0$.

The cross section is given by (for closer explanation, we refer to chapter 2)

$$\begin{aligned}\mathrm{d}\sigma &= \frac{1}{\frac{|\vec{v}_i|}{V}T}|S_{fi}|^2 \frac{V\mathrm{d}^3k_b}{(2\pi)^3}\frac{V\mathrm{d}^3p_f}{(2\pi)^3} \\ &= \frac{Z^2e^6m_e^2\pi}{\omega_b E_i E_f |\vec{v}_i|}\frac{1}{|\vec{q}|^4}\delta(E_f+\omega_b-E_i)\left|\epsilon^\mu_{b,\lambda}M_\mu(k_b)\right|^2\frac{\mathrm{d}^3k_b}{(2\pi)^3}\frac{\mathrm{d}^3p_f}{(2\pi)^3}\end{aligned}$$

For the square of the δ-function, we made the substitution according to (2.20). We want to determine the unpolarized differential cross section. This implies that we have to sum over the final electron spin r_f and over the photon polarization λ. Averaging over the incoming electron spins (since we consider an unpolarized electron beam) also results in summing over the (initial) spin r_i and dividing the whole expression by two. We obtain

$$\mathrm{d}\overline{\sigma} \equiv \frac{1}{2}\sum_{\lambda=1}^{2}\sum_{r_i,r_f=1}^{2}\mathrm{d}\sigma = \frac{1}{2}\sum_{\lambda=1}^{2}\sum_{r_i,r_f=1}^{2}\frac{Z^2e^6m_e^2\pi}{\omega_b E_i E_f|\vec{v}_i|}\frac{1}{|\vec{q}|^4}\delta(E_f+\omega_b-E_i)\left|\epsilon^\mu_{b,\lambda}M_\mu(k_b)\right|^2\frac{\mathrm{d}^3k_b}{(2\pi)^3}\frac{\mathrm{d}^3p_f}{(2\pi)^3}$$

We use the *completeness relation* of the photon polarization vector [12]

$$\sum_{\lambda=1,2}\epsilon^\mu_\lambda\epsilon^\nu_\lambda = -g^{\mu\nu} + \text{gauge terms}$$

to remove the λ-sum. Here, we can neglect the gauge terms since they do not contribute to any physical observable [12]. The sum over all spins can be rewritten as a trace with the help of equation (2.21). Finally, some of the prefactors will be expressed in terms of other quantities; we use the relations we wrote down in section (2.4). We can thus write:

$$\begin{aligned}\frac{\mathrm{d}\overline{\sigma}}{\mathrm{d}\Omega_b\mathrm{d}\Omega_f\mathrm{d}\omega_b} = -\frac{\alpha(Z\alpha)^2\omega_b}{8\pi^2}\frac{|\vec{p}_f|}{|\vec{p}_i|}\frac{1}{|\vec{q}|^4}\delta(E_f+\omega_b-E_i)\mathrm{d}E_f\times \\ \mathrm{Tr}\left[\left(\gamma^\mu\frac{\hat{p}_f+\hat{k}_b+m_e}{2p_f\cdot k_b}\gamma^0 + \gamma^0\frac{\hat{p}_i-\hat{k}_b+m_e}{-2p_i\cdot k_b}\gamma^\mu\right)(\hat{p}_i+m_e)\times\right. \\ \left.\left(\gamma^0\frac{\hat{p}_f+\hat{k}_b+m_e}{2p_f\cdot k_b}\gamma_\mu + \gamma_\mu\frac{\hat{p}_i-\hat{k}_b+m_e}{-2p_i\cdot k_b}\gamma^0\right)(\hat{p}_f+m_e)\right].\end{aligned}$$

We still have to integrate over the energy of the final electron. Because of the δ-function, this yields the energy conservation: $E_f = E_i - \omega_b$. Since the energy E_f of the outgoing electron has to be at least equal to its rest mass $E_f \geq m_e$, we find the inequality: $E_f = E_i - \omega_b \Leftrightarrow E_i - m_e - \omega_b \geq 0$. If this inequality is not fulfilled, then the cross section must be zero. This is implemented into the formula with a step-function. In this way, we derived the differential

Bethe-Heitler cross section:

$$\begin{aligned}\frac{\mathrm{d}\overline{\sigma}}{\mathrm{d}\Omega_b \mathrm{d}\Omega_f \mathrm{d}\omega_b} = &-\frac{\alpha(Z\alpha)^2\omega_b}{8\pi^2}\frac{|\vec{p}_f|}{|\vec{p}_i|}\frac{1}{|\vec{q}|^4}\Theta(E_i - m_e - \omega_b)\times \\ &\mathrm{Tr}\left[\left(\gamma^\mu\frac{\hat{p}_f + \hat{k}_b + m_e}{2p_f\cdot k_b}\gamma^0 + \gamma^0\frac{\hat{p}_i - \hat{k}_b + m_e}{-2p_i\cdot k_b}\gamma^\mu\right)(\hat{p}_i + m_e)\times\right. \\ &\left.\left(\gamma^0\frac{\hat{p}_f + \hat{k}_b + m_e}{2p_f\cdot k_b}\gamma_\mu + \gamma_\mu\frac{\hat{p}_i - \hat{k}_b + m_e}{-2p_i\cdot k_b}\gamma^0\right)(\hat{p}_f + m_e)\right].\end{aligned}$$

This representation of the Bethe-Heitler cross section is probably the best one if one wants to analyse the different parts. However, using standard methods for calculations with Dirac matrices, we can rewrite it without the trace. Nevertheless, this is a quite cumbersome procedure and does not give any new physical insight. We therefore refer to the literature [12] and just quote the result:

$$\begin{aligned}\frac{\mathrm{d}\overline{\sigma}}{\mathrm{d}\Omega_b \mathrm{d}\Omega_f \mathrm{d}\omega_b} = &-\frac{\alpha(Z\alpha)^2\omega_b}{4\pi^2}\frac{|\vec{p}_f|}{|\vec{p}_i|}\frac{1}{|\vec{q}|^4}\Theta(E_i - m_e - \omega_b)\times \\ &\frac{1}{(k_b\cdot p_i)^2(k_b\cdot p_f)^2}\left[4m_e^2\left(E_f k_b\cdot p_f - E_i k_b\cdot p_i\right)^2 + \right. \\ &\left((k_b\cdot p_f)^2 + (k_b\cdot p_i)^2\right)(2k_b\cdot p_i k_b\cdot p_f + q^2 m_e^2) + \\ &\left. 2q^2 k_b\cdot p_i k_b\cdot p_f\left(E_f^2 + E_i^2 - p_i\cdot p_f\right)\right].\end{aligned} \tag{A.2}$$

This expression can be integrated analytically over the solid angle $\mathrm{d}\Omega_f$ of the outgoing electron. We again just give the result of the total Bethe-Heitler cross section; see equation 2BN in [26][1]:

$$\begin{aligned}\frac{\mathrm{d}\overline{\sigma}}{\mathrm{d}\Omega_b \mathrm{d}\omega_b} = &\frac{\alpha(Z\alpha)^2}{8\pi\omega_b}\frac{|\vec{p}_f|}{|\vec{p}_i|}\left\{\frac{8m_e^2\sin^2\theta_b\left(2E_i^2 + m_e^2\right)}{|\vec{p}_i|^2\Delta^4} - \frac{2\left(5E_1^2 + 2E_i E_f + 3m_e^2\right)}{|\vec{p}_i|^2\Delta^2} - \right. \\ &\frac{2\left(|\vec{p}_i|^2 - \omega_b^2\right)}{Q^2\Delta^2} + \frac{4E_f}{|\vec{p}_i|^2\Delta} + \frac{L}{|\vec{p}_i||\vec{p}_f|}\left[\frac{4m_e^2 E_i\sin^2\theta_b\left(3m_e^2\omega_b - |\vec{p}_i|^2 E_f\right)}{|\vec{p}_i|^2\Delta^4} + \right. \\ &\frac{4E_i^2\left(E_i^2 + E_f^2\right)}{|\vec{p}_i|^2\Delta^2} + \frac{2m_e^4 - 2m_e^2\left(7E_i^2 - 3E_i E_f + E_f^2\right)}{|\vec{p}_i|^2\Delta^2} + \\ &\left.\frac{2\omega_b\left(E_i^2 + E_i E_f - m_e^2\right)}{|\vec{p}_i|^2\Delta}\right] - \frac{4\epsilon}{|\vec{p}_f|\Delta} + \\ &\left.\frac{\epsilon^Q}{|\vec{p}_f|Q}\left[\frac{4m_e^2}{\Delta^2} - \frac{6\omega_b}{\Delta} - \frac{2\omega_b\left(|\vec{p}_i|^2 - \omega_b^2\right)}{Q^2\Delta}\right]\right\}\end{aligned} \tag{A.3}$$

with the following definitions

$$L = \ln\left[\frac{E_i E_f - m_e^2 + |\vec{p}_i||\vec{p}_f|}{E_i E_f - m_e^2 - |\vec{p}_i||\vec{p}_f|}\right], \quad \Delta = E_i - |\vec{p}_i|\cos\theta_b, \quad \epsilon = \ln\left[\frac{E_f + |\vec{p}_f|}{E_f - |\vec{p}_f|}\right]$$

and

$$Q^2 = |\vec{p}_i|^2 + \omega_b^2 - 2|\vec{p}_i|\omega_b\cos\theta_b, \quad \epsilon^Q = \ln\left[\frac{Q + |\vec{p}_f|}{Q - |\vec{p}_f|}\right].$$

[1] In order to switch to our system of units, we set $r_0 = \alpha/m_e$ and use our definition of the energies.

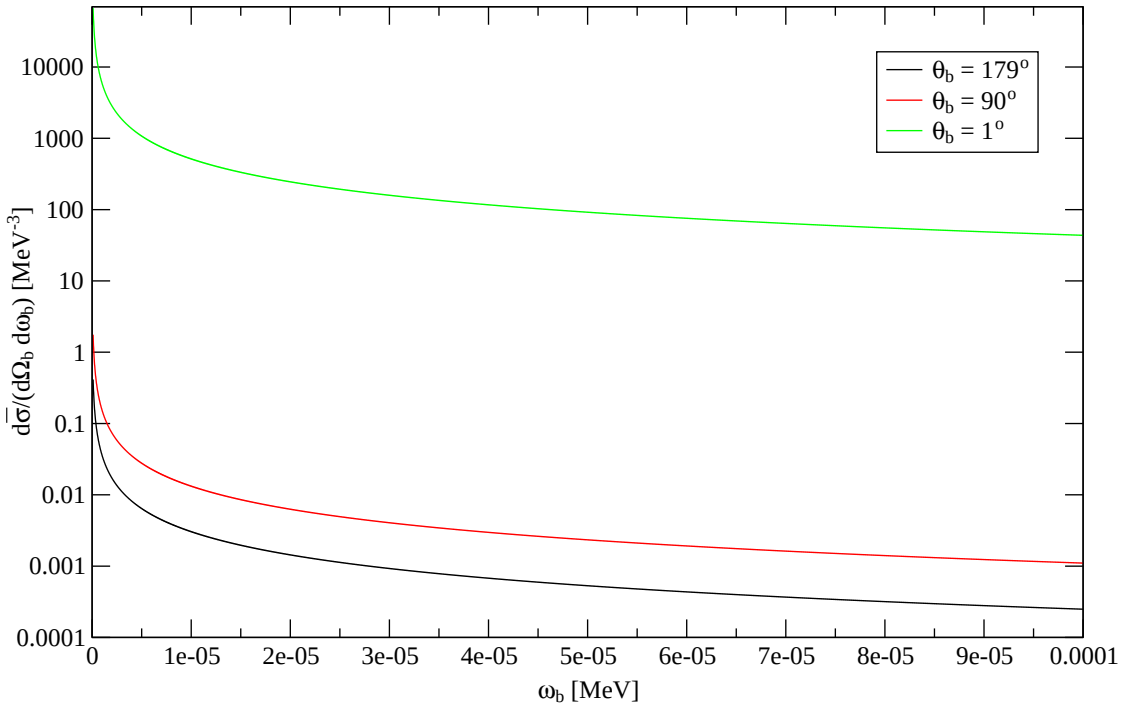

Figure A.2: The integrated Bethe-Heitler cross section for different emission angles θ_b of the bremsstrahlung photon goes to infinity for low energies of the bremsstrahlung photon. This is due to intermediate on-shell electrons and the Coulomb potential and is called the *infrared divergence*.

Figure (A.2) shows the total Bethe-Heitler cross section for three different angles θ_b (for the scattering geometry please consult section 2.7). We see that the cross section tends towards infinity for $\omega_b \to 0$. This unphysical behaviour is called *infrared divergence* or *infrared catastrophe*. Even if we regularize the mass, the total cross section will go to infinity. This is then due to the use of the Coulomb potential: $1/|\vec{q}|^4 = 1/q^4 = 1/(q_f - q_i)^4 \to \infty$ for certain angles of the final electron, namely if it is not deflected at all.

Appendix B

Classical Motion of an Electron in a Plane-Wave Field

We will derive the trajectory of an electron in a plane-wave field A^μ in a fully covariant way. We follow the derivation for linear polarization sketched in [27]. The external field looks $A^\mu(\phi) = a\,(\varkappa_1^\mu \delta \cos\phi + \varkappa_2^\mu \sin\phi)$ with $\phi = k\cdot x$. The different four-vectors obey relations which are stated in section 2.1. For $\delta = 0$, we retrieve linear polarization, $\delta = 1$ corresponds to circular polarization. We calculate the field-strength tensor: $F^{\mu\nu} = \partial^\mu A^\nu - \partial^\nu A^\mu = (k^\mu \varkappa_1^\nu - k^\nu \varkappa_1^\mu)\,(-a\delta\sin\phi) + (k^\mu \varkappa_2^\nu - k^\nu \varkappa_2^\mu)\,(a\cos\phi)$. The relativistic equation of motion in a covariant notation then looks

$$m_e \frac{\mathrm{d}u^\mu(\tau)}{\mathrm{d}\tau} = -eF^\mu{}_\nu u^\nu(\tau). \tag{B.1}$$

τ is the proper time – the time elapsed in the rest frame of the electron –, and u is the four-velocity of the electron: $u^\mu = \mathrm{d}x^\mu/\mathrm{d}\tau$. This is the differential equation we have to solve in order to find the electron trajectory $x^\mu(\tau)$.

We multiply both sides of (B.1) with k_μ and find $k\cdot u(\tau) = k\cdot u(0) = \text{const}$ because in our gauge $k_\mu F^\mu{}_\nu = 0$. We arbitrarily set $x^\mu(0) = 0$. With $x^\mu(\tau) = u^\mu(\tau)\tau$, we can write $\phi = k\cdot x(\tau) = k\cdot u(\tau)\tau = k\cdot u(0)\tau$. Thus, $\mathrm{d}\phi = k\cdot u(0)\mathrm{d}\tau$.

Now, we can rewrite (B.1) in the following way:

$$\frac{\mathrm{d}u^\mu(\phi)}{\mathrm{d}\phi} = -\frac{e}{m_e}\left[\left(\frac{\varkappa_1\cdot u(\phi)}{k\cdot u(0)}k^\mu - \varkappa_1^\mu\right)(-a\delta\sin\phi) + \left(\frac{\varkappa_2\cdot u(\phi)}{k\cdot u(0)}k^\mu - \varkappa_2^\mu\right)(a\cos\phi)\right].$$

After multiplication with $\varkappa_{1\mu}$ or $\varkappa_{2\mu}$ and integration over $\mathrm{d}\phi$, we obtain

$$\begin{aligned}\varkappa_1\cdot u(\phi) &= \varkappa_1\cdot u(0) - \frac{ea}{m_e}\delta(\cos\phi - \cos 0),\\ \varkappa_2\cdot u(\phi) &= \varkappa_2\cdot u(0) - \frac{ea}{m_e}(\sin\phi - \sin 0).\end{aligned}$$

We plug these two relations into the previous equation and end up with

$$\begin{aligned}\frac{\mathrm{d}u^\mu}{\mathrm{d}\phi} = -\frac{ea}{m_e}\Bigg[&\left(\frac{\varkappa_1\cdot u(0)}{k\cdot u(0)}k^\mu - \frac{ea}{m_e}\frac{\cos\phi - 1}{k\cdot u(0)}k^\mu - \varkappa_1^\mu\right)(-a\delta\sin\phi) +\\ &\left(\frac{\varkappa_2\cdot u(0)}{k\cdot u(0)}k^\mu - \frac{ea}{m_e}\frac{\sin\phi}{k\cdot u(0)}k^\mu - \varkappa_2^\mu\right)(a\cos\phi)\Bigg].\end{aligned}$$

This expression can now be integrated with respect to ϕ yielding $u^\mu(\phi)$. A second integration with respect to τ then gives x^μ. Hereby, we use the relations $\int \mathrm{d}\tau(\cos\phi - 1) = (\sin\phi - \phi)/(k\cdot u(0))$ and $\int \mathrm{d}\tau(\cos\phi - 1)^2 = \left(\frac{1}{4}\sin(2\phi) - 2\sin\phi + \frac{3}{2}\phi\right)/(k\cdot u(0))$. Our final result looks

$$\begin{aligned}
x^\mu(\phi) &= \int_0^\tau \mathrm{d}\tau' \int_0^\phi \mathrm{d}\phi' \frac{\mathrm{d}u^\mu(\phi')}{\mathrm{d}\phi'} \\
&= \int_0^\tau \mathrm{d}\tau' \left\{ u^\mu(0) - \frac{ea}{m_e}\delta\left(\cos\phi' - \cos 0\right)\left[\frac{\not{\kappa}_1 \cdot u(0)}{k\cdot u(0)} k^\mu - \not{\kappa}_1^\mu\right] - \right. \\
&\quad \frac{ea}{m_e}\left(\sin\phi' - \sin 0\right)\left[\frac{\not{\kappa}_2 \cdot u(0)}{k\cdot u(0)} k^\mu - \not{\kappa}_2^\mu\right] + \\
&\quad \left. \frac{e^2a^2}{2m_e^2}\left[\delta\left(\cos\phi' - \cos 0\right)^2 + \left(\sin\phi' - \sin 0\right)^2\right]\frac{k^\mu}{k\cdot u(0)} \right\} \\
&= \frac{u^\mu(0)}{k\cdot u(0)}\phi + \frac{ea}{m_e}\delta(\sin\phi - \phi)\frac{\not{\kappa}_1^\mu}{k\cdot u(0)} - \frac{ea}{m_e}(\cos\phi - 1)\frac{\not{\kappa}_2^\mu}{k\cdot u(0)} - \\
&\quad \frac{ea}{m_e}\left[\delta \not{\kappa}_1 \cdot u(0)(\sin\phi - \phi) - \not{\kappa}_2 \cdot u(0)(\cos\phi - 1) - \right. \\
&\quad \left. \frac{ea}{8m_e}\left\{(\delta - 1)\sin(2\phi) - 8\delta\sin\phi + (6\delta + 2)\phi\right\}\right]\frac{k^\mu}{\left(k\cdot u(0)\right)^2}.
\end{aligned}$$

This formula yields the position of the electron at the laser phase ϕ. This can be converted to the proper time with $\phi = k\cdot u(0)\tau$. $u(0)$ is the initial four-velocity and is derived from the initial momentum of the electron: $u^\mu(0) = p_i^\mu/m_e$. We can now plot the electron trajectory (using the scattering geometry introduced in section (2.7)) for three laser cycle and $a = 20\,\mathrm{MeV}$. In figure (B.1), we see that the electron moves along a spiral trajectory.

Since we consider relativistic intensities, the drift velocity induced by the $\vec{B}$-field must not be neglected. An electron which is initially at rest travels approximately $780 \times 10^3\,\mathrm{MeV}^{-1}$ during one laser cycle due to the drift velocity. If we compare this with the *first Bohr radius* $a_0 = 1/(Z\alpha m_e) \approx 270\,\mathrm{MeV}^{-1}$ $(Z = 1)$, we see that this distance is roughly 3000 times greater than the Bohr radius. Hence, there is only one interaction between electron and nucleus possible; a recollision will not happen. Therefore, our calculation taking just one interaction between the electron and the nucleus into account is well-justified.

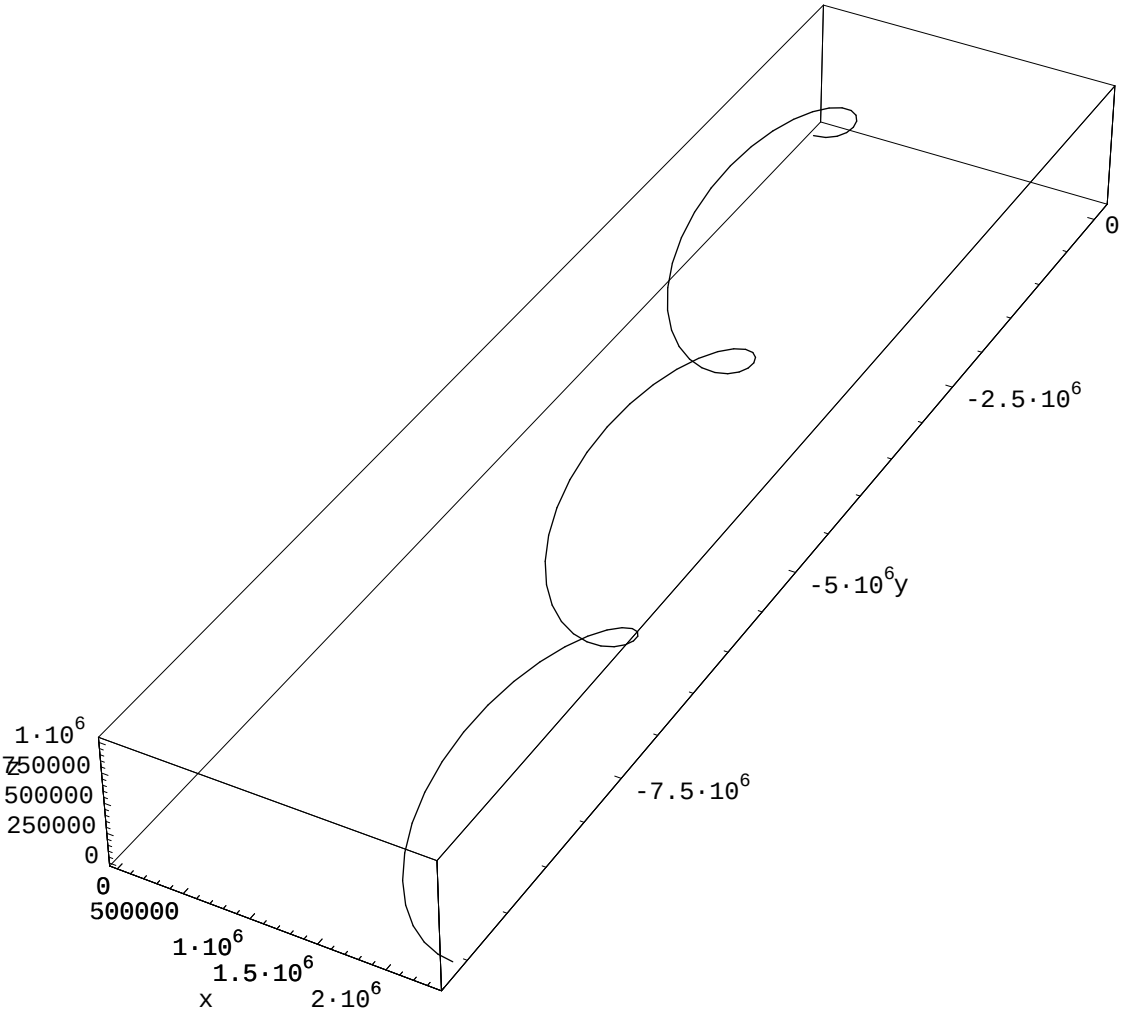

Figure B.1: A classical electron moves along a helix if it is exposed to an external, circularly polarized laser field.

Appendix C

The Role of the Interference Term

Bremsstrahlung is, as we already saw in the introduction, a second-order process. The corresponding first-order process – namely photon emission by an electron in an external field (laser-dressed Compton scattering) – is, in contrast to the field-free case, allowed, too. In our second-order bremsstrahlung process and in the first-order Compton scattering, we have the same in- and out-states (the initial and the final electron and the emitted photon). Hence, we could expect that these processes interfere with each other. The S-matrix has to be written in the following form then:

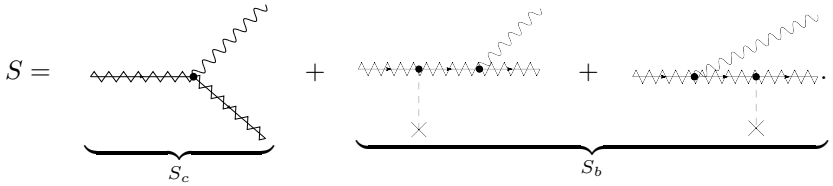

In all observables (e.g. cross sections), $|S|^2$ enters. Therefore, we get[1]

$$|S|^2 = |S_c + S_b|^2 = |S_c|^2 + |S_b|^2 + 2\Re(S_c S_b^*).$$

The first summand describes laser-dressed Compton scattering. This process was discussed quite a long time ago in [28] or, more recently, in [10]. Consequently, we will not discuss it here. The effects of the second summand are widely discussed in this thesis. The third summand finally is a term which describes quantum mechanical interference of the two processes laser-dressed Compton scattering and bremsstrahlung.

So, let us focus our attention on the interference term $\Re(S_c S_b^*)$. In S_c, we have four-momentum conservation at the vertex which yields a δ-function $\delta^{(4)}(q_f - q_i + k_c - mk)$. S_b is determined according to equation (2.15) with the momentum relation $\vec{q}_f = \vec{q}_i + n\vec{k} - \vec{k}_b + \vec{q}_n$. Therefore, we can write

$$\Re(S_c S_b^*) \propto \Re\left(\sum_{m,n} \frac{1}{\vec{q}_n^{\,2}} \delta^{(4)}\left(q_f - q_i + k_c - mk\right) \delta^{(1)}\left(q_f^0 - q_i^0 + k_b^0 - nk^0\right)\right).$$

In the interference case (i.e. the same in- and out-states), $k_c = k_b$ and hence, because of the two δ-functions, $n = m$. The spatial parts of the first δ-function in connection with the above

[1] The index c denotes Compton scattering in contrast to b meaning "bremsstrahlung".

momentum relation then yield $\vec{q}_n = \vec{0}$. Thus, $\Re(S_c S_b^*) \propto 1/0 \to \infty$. There must obviously be an error in our considerations; the only possibility is that in the physical reality these two processis do not interfere. The question remains: Why is there no interference despite the fact that we have the same in- and out-states?

The answer is quite simple. Interference occurs whenever the experimentalist cannot determine which of two (or more) processes takes place during an experiment. For example, if we defract an electron beam at two slits, we will get an interference pattern on a screen as long as we do not detect through which slit the electrons pass. If we do so, the interference pattern will vanish. It is somehow similar in our case here. Since we know the energies of all initial and final particles, we can deduce just because of the different energy conservation relation whether laser-dressed Compton scattering or the bremsstrahlung process took place. Because of this knowledge, interference is not possible. In contrast, the two bremsstrahlung amplitudes $S_{fi}^{(1)}$ and $S_{fi}^{(2)}$ obey the same energy conservation relation. Thus, they interfere with each other.

We can turn our argumentation around. In the special case of bremsstrahlung with zero momentum transfer onto the nucleus, i.e. $\vec{q}_n = \vec{0}$, laser-dressed Compton scattering and bremsstrahlung obey the same energy and momentum conservation relation. Do they intefere in this special case then? However, as in the above paragraph, we will get infinity. The reason is that the Coulomb potential (2.13) is an approximation which is not valid for zero momentum.

We conclude that laser-dressed Compton scattering and bremsstrahlung are two processes which take place completely independent of each other. An expansion of the S-matrix as in the beginning of this section is not correct.

Appendix D

Dirac Algebra and the Free Dirac Spinor

In this section, we want to remind of some important relations which can be derived from the Dirac equation. We will also prove relations which will be very useful in the evaluation of the cross section.

The γ-matrices form a *Clifford Algebra* and satisfy, independently of their particular representation, the anticommutation relation

$$\{\gamma^\mu, \gamma^\nu\} = 2g^{\mu\nu}\mathbb{1}$$

and the Hermiticity condition

$$\gamma^{\mu\dagger} = \gamma^0\gamma^\mu\gamma^0.$$

These are the constitutional relations for the γ-matrices. If we use a particular representation, we will use the Dirac representation which is given in the introduction.

The Dirac equation can easily be solved in the vacuum. For a general four-momentum p, one obtains two linearly independent solutions of positive frequency for the spinor [29]:

$$u_r(p) = \sqrt{\frac{p^0 + m_e}{2m_e}} \begin{pmatrix} \chi_r \\ \frac{\vec{\sigma}\vec{p}}{p^0+m_e}\chi_r \end{pmatrix}$$

with

$$\chi_1 = \begin{pmatrix} 1 \\ 0 \end{pmatrix} \qquad \text{and} \qquad \chi_2 = \begin{pmatrix} 0 \\ 1 \end{pmatrix}.$$

This solution depends on the particular representation of the γ-matrices. r labels the two possible spin directions. The components of the vector $\vec{\sigma} = (\sigma_1, \sigma_2, \sigma_3)$ are *Pauli's spin matrices*. The free Dirac spinors $u_r(p)$, which also enter into the Volkov solutions, satisfy the orthonormality relation $\overline{u}_r(p)u_s(p) = \delta_{rs}$ and $\overline{u}_r(p)\gamma^\mu u_r(p) = \frac{p^\mu}{m_e}$

In the following, we will prove some useful relations containing γ-matrices. From the anticommutation relation, one immediately gets:

$$\begin{aligned} \gamma^0\gamma^0 &= \mathbb{1}, \\ \gamma^0\gamma^0\gamma^0 &= \gamma^0, \\ \gamma^0\gamma^i &= -\gamma^i\gamma^0, \\ \gamma^0\gamma^i\gamma^0 &= -\gamma^i. \end{aligned}$$

For an arbitrary real four-vector $p = p^*$, we use the Hermiticity condition of the γ-matrices in order to obtain

$$\overline{\hat{p}} = \gamma^0 \hat{p}^\dagger \gamma^0 = \gamma^0 \left(\gamma^\mu\right)^\dagger p_\mu^* \gamma^0 = \gamma^\mu p_\mu = \hat{p}. \tag{D.1}$$

With this relation, we easily prove the following relation for any two real four-vectors a and b and a spinor u:

$$\overline{\hat{b}\hat{a}u} = \left(\hat{b}\hat{a}u\right)^\dagger \gamma^0 = u^\dagger \gamma^0 \gamma^0 \hat{a}^\dagger \gamma^0 \gamma^0 \hat{b}^\dagger \gamma^0 = \overline{u}\hat{a}\hat{b}. \tag{D.2}$$

In the following, the upper index i can take the values 1 and 2 in order to denote the two polarization vectors $\varkappa^1$ and $\varkappa^2$ of the external laser field.

$$\begin{aligned}
\hat{\varkappa}^i \hat{\varkappa}^i &= \gamma^\mu \gamma^\nu \varkappa_\mu^i \varkappa_\nu^i = 2g^{\mu\nu} \varkappa_\mu^i \varkappa_\nu^i - \gamma^\nu \gamma^\mu \varkappa_\nu^i \varkappa_\mu^i \\
&= 2\varkappa^{i\mu} \cdot \varkappa_\mu^i - \hat{\varkappa}^i \hat{\varkappa}^i = -2 - \hat{\varkappa}^i \hat{\varkappa}^i \qquad \text{using (2.4)} \\
\Rightarrow \hat{\varkappa}^i \hat{\varkappa}^i &= -1
\end{aligned}$$

In the same way, we can show that

$$\hat{k}\hat{k} = 0$$

for the wave vector k of the laser field. Using this, we can derive two useful rules for an arbitrary four-vector a:

$$\begin{aligned}
\hat{\varkappa}^i \hat{k}\hat{a}\hat{k}\hat{\varkappa}^i &= -\hat{k}\hat{\varkappa}^i \hat{a}\hat{k}\hat{\varkappa}^i && \text{with (2.2)} \\
&= -\hat{k}\left(2\varkappa^i \cdot a\right)\hat{k}\hat{\varkappa}^i + \hat{k}\hat{a}\hat{\varkappa}^i \hat{k}\hat{\varkappa}^i \\
&= -\left(2\varkappa^i \cdot a\right)\hat{k}\hat{k}\hat{\varkappa}^i - \hat{k}\hat{a}\hat{k}\hat{\varkappa}^i \hat{\varkappa}^i && \text{with (2.2)} \\
&= \hat{k}\hat{a}\hat{k} && (D.3)
\end{aligned}$$

and

$$\begin{aligned}
\hat{\varkappa}^2 \hat{k}\hat{a}\hat{k}\hat{\varkappa}^1 &= -\hat{k}\hat{\varkappa}^2 \hat{a}\hat{k}\hat{\varkappa}^1 && \text{with (2.2)} \\
&= -\left(2\varkappa^2 \cdot a\right)\hat{k}\hat{k}\hat{\varkappa}^1 + \hat{k}\hat{a}\hat{\varkappa}^2 \hat{k}\hat{\varkappa}^1 = -\hat{k}\hat{a}\hat{k}\hat{\varkappa}^2 \hat{\varkappa}^1 \\
&= \hat{k}\hat{a}\hat{k}\hat{\varkappa}^1 \hat{\varkappa}^2 && \text{with (2.3)} \\
&= -\hat{k}\hat{a}\hat{\varkappa}^1 \hat{k}\hat{\varkappa}^2 = \hat{k}\hat{\varkappa}^1 \hat{a}\hat{k}\hat{\varkappa}^2 - \left(2a \cdot \varkappa^1\right)\hat{k}\hat{\varkappa}^2 \\
&= -\hat{\varkappa}^1 \hat{k}\hat{a}\hat{k}\hat{\varkappa}^2. && (D.4)
\end{aligned}$$

We will need these rules for $a = (1, 0, 0, 0)$ so that $\hat{a} = \gamma^0$ and $a = \epsilon_{b,\lambda}$.

Appendix E

Bessel Functions and Generalized Bessel Functions

A definition of Bessel functions of the first kind is

$$J_n(x) = \left(\frac{x}{2}\right)^n \sum_{j=0}^{\infty} \frac{(-1)^j}{j!\,\Gamma(j+n+1)} \left(\frac{x}{2}\right)^{2j}.$$

Since we will only consider Bessel functions with integer index, the Γ-function can be written as a factorial $\Gamma(j+n+1) = (j+n)!$. The following properties of Bessel functions just hold for Bessel functions with integer indices.

One can easily verify the following relations for Bessel functions by plugging them into the above definition (and keeping in mind that $n! = \infty \; \forall n < 0$):

$$J_n(x) = (-1)^n J_{-n}(x), \tag{E.1}$$
$$J_n(x) = (-1)^n J_n(-x), \tag{E.2}$$
$$J_n(x) = J_{-n}(-x). \tag{E.3}$$

In particular, one gets $J_n(0) = \delta_{n,0}$ which can easily be derived from the the definition of the Bessel functions.

There are also well-known sum rules [30]:

$$J_{n-1}(x) + J_{n+1}(x) = \frac{2n}{x} J_n(x),$$
$$\sum_{k=-\infty}^{\infty} J_{s+k}(x) J_{t+k}(y) = J_{s-t}(x-y). \tag{E.4}$$

A generalisation of this sum rule is *Graf's addition theorem* [31]

$$J_s(z) \left(\frac{x - ye^{-i\phi}}{x - ye^{i\phi}}\right)^{\frac{1}{2}s} = \sum_{k=-\infty}^{\infty} J_{s+k}(x) J_k(y) e^{ik\phi} \tag{E.5}$$

with $\left|ye^{\pm i\phi}\right| < |x|$ and $z = (x^2 + y^2 - 2xy\cos\phi)^{\frac{1}{2}}$. One has to be very careful when implementing this theorem into a computer programme. The problem is the square root of a complex number

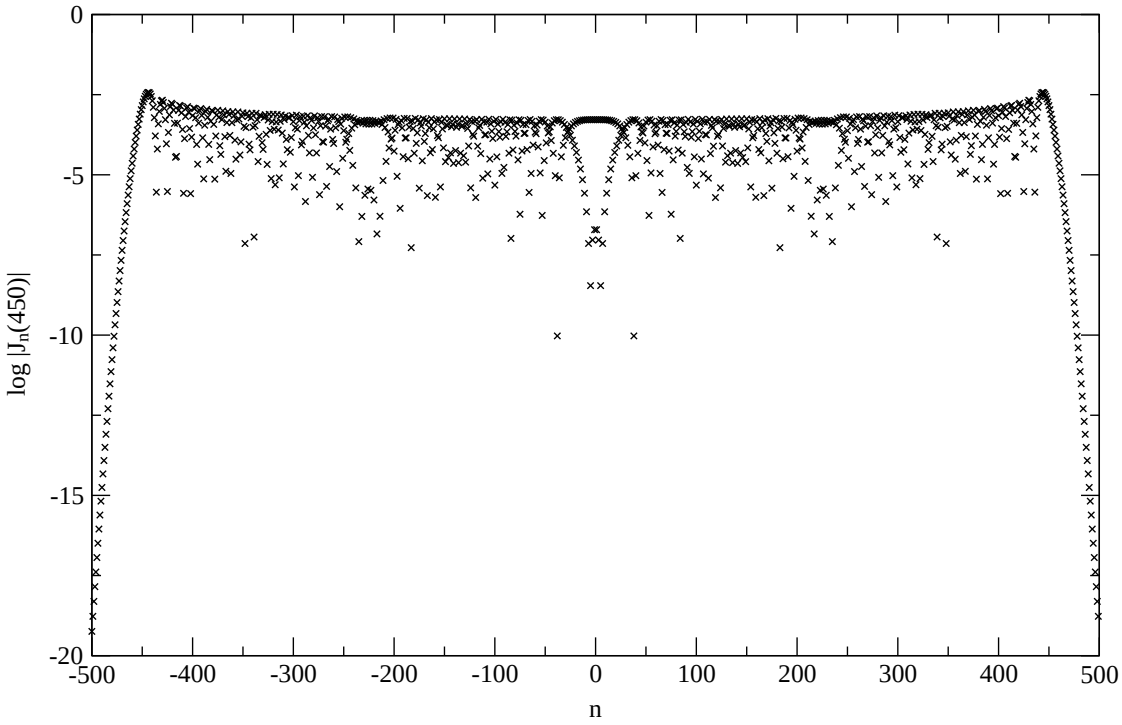

Figure E.1: From our theoretical considerations, we expect Bessel functions to show a cutoff if the index gets greater than the argument of the Bessel function. The progression of the function $\log|J_n(450)|$ reflects our expectation.

which is not well-defined:

$$\begin{aligned}\sqrt{x+iy} &= \left(\sqrt{x^2+y^2}\exp\left[i\arctan\frac{y}{x}+2\pi ik\right]\right)^{\frac{1}{2}} \\ &= \left(x^2+y^2\right)^{\frac{1}{4}}\exp\left[\frac{i}{2}\arctan\frac{y}{x}+\pi ik\right]\end{aligned}$$

with $k = 0, 1$.

We consider Bessel functions with large, but fixed argument $x = |x|$. We want to know the behaviour if the index n is of the order of x, i.e. also very large: $n \gtrsim x$. We can then rewrite the Γ-function with the well-known approximation formula (*Stirling's formula*) for large argument s: $\Gamma(s) \approx s^{s+1/2}\exp(-s)\sqrt{2\pi}$. We thus have

$$\begin{aligned}J_n(x) &\approx \left(\frac{x}{2}\right)^n \sum_{j=0}^{\infty}\frac{(-1)^j\exp(j+n)}{j!\,(j+n)^{j+n+1/2}\sqrt{2\pi}}\left(\frac{x}{2}\right)^{2j} \\ &\approx \frac{1}{\sqrt{2\pi}}\left(\frac{ex}{2n}\right)^n.\end{aligned}$$

From this approximation, we can conclude that there will be a fast decrease in the magnitude of the Bessel function whenever the index becomes greater than the argument of the Bessel function. This can be used to establish summation limits when we have to sum over the indices of Bessel functions. As an example, we recognise the expected behaviour in diagram (E.1). Because of

the relations (E.1) and (E.2), we can easily adapt this rule to negative indices or arguments. Consequently, we will find the decrease in the magnitude of a Bessel function whenever $|n| > |x|$.

Bessel functions can be used to expand plane waves. This is done by applying the so-called *Jacobi-Anger expansion* [30]:

$$e^{iz\cos\theta} = \sum_{s=-\infty}^{+\infty} i^s J_s(z) e^{is\theta}.$$

By replacing $\theta \to \theta - \pi/2$, we obtain

$$e^{iz\sin\theta} = \sum_{s=-\infty}^{+\infty} J_s(z) e^{is\theta}.$$

With $\theta = 0$, we get in particular

$$\sum_{s=-\infty}^{\infty} i^s J_s(z) = e^{iz},$$
$$\sum_{s=-\infty}^{\infty} J_s(z) = 1.$$

Using the Jacobi-Anger-expansions, we can easily derive the following formulas:

$$\begin{aligned} e^{i\xi\sin\phi + i\eta\cos\phi} &= \sum_{s=-\infty}^{\infty} B_s^0(\xi,\eta) e^{is\phi} \\ \text{with } B_s^0(\xi,\eta) &= \sum_{l=-\infty}^{\infty} i^l J_{s-l}(\xi) J_l(\eta), \qquad \text{(E.6)} \\ \cos\phi\, e^{i\xi\sin\phi + i\eta\cos\phi} &= \sum_{s=-\infty}^{\infty} B_s^1(\xi,\eta) e^{is\phi} \\ \text{with } B_s^1(\xi,\eta) &= \frac{1}{2}\left[B_{s-1}^0(\xi,\eta) + B_{s+1}^0(\xi,\eta)\right], \qquad \text{(E.7)} \\ \sin\phi\, e^{i\xi\sin\phi + i\eta\cos\phi} &= \sum_{s=-\infty}^{\infty} B_s^2(\xi,\eta) e^{is\phi} \\ \text{with } B_s^2(\xi,\eta) &= \frac{1}{2i}\left[B_{s-1}^0(\xi,\eta) - B_{s+1}^0(\xi,\eta)\right] \qquad \text{(E.8)} \end{aligned}$$

with the three *generalized Bessel functions* B^0, B^1, and B^2. They seem to be characteristical for the wave function in a circularly polarized field. Considering the special case $\phi = 0$, we obtain in particular

$$\sum_s B_s^0(\xi,\eta) = e^{i\eta},$$
$$\sum_s B_s^1(\xi,\eta) = e^{i\eta},$$
$$\sum_s B_s^2(\xi,\eta) = 0.$$

Having a closer look at the generalized Bessel functions, we see that we can apply Graf's addition theorem. We easily derive (by cross-checking in order to take the right solution of the root

operation):

$$B_s^0(\xi,\eta) = \begin{cases} J_s\left(\sqrt{\xi^2+\eta^2}\right)\frac{\exp\left[\frac{i}{2}s\cdot\arctan(\eta,\xi)\right]}{\exp\left[\frac{i}{2}s\cdot\arctan(-\eta,\xi)\right]} & \text{if } \xi\neq 0, \eta\neq 0, \\ J_s(\xi) & \text{if } \xi\neq 0, \eta = 0, \\ i^s J_s(\eta) & \text{if } \xi = 0, \eta\neq 0, \\ \delta_{s0} & \text{if } \xi = \eta = 0. \end{cases} \tag{E.9}$$

$\arctan(\eta,\xi)$ gives the arc tangent of $\frac{\eta}{\xi}$, taking into account in which quadrant the point (ξ,η) is. This is implemented into the Fortran code by using the function `atan2`(ξ,η).

It is not very hard to derive more useful relations containing the generalized Bessel function B^0, B^1, and B^2.

$$\begin{aligned} B_s^{0^*}(\xi,\eta) &= \sum_n (-i)^n J_{s-n}(\xi) J_n(\eta) \\ &= \sum_n i^n J_{s-n}(\xi) J_n(-\eta) \qquad \text{using (E.2)} \\ &= B_s^0(\xi,-\eta) \end{aligned} \tag{E.10}$$

$$\begin{aligned} B_{-s}^0(\xi,\eta) &= \sum_n i^n J_{-s-n}(\xi) J_n(\eta) \\ &= \sum_n i^n J_{s+n}(-\xi) J_n(\eta) \qquad \text{using (E.2)} \\ &= \sum_n i^{-n} J_{s-n}(-\xi) J_{-n}(\eta) \qquad \text{renaming } n\to -n \\ &= \sum_n (-1)^n i^n J_{s-n}(-\xi) J_{-n}(\eta) \\ &= \sum_n i^n J_{s-n}(-\xi) J_n(\eta) \qquad \text{using (E.2)} \\ &= B_s^0(-\xi,\eta) \end{aligned} \tag{E.11}$$

Similarly, we obtain

$$B_s^{1^*}(\xi,\eta) = B_s^1(\xi,-\eta), \tag{E.12}$$
$$B_s^{2^*}(\xi,\eta) = -B_s^2(\xi,-\eta), \tag{E.13}$$
$$B_{-s}^1(\xi,\eta) = B_s^1(-\xi,\eta), \tag{E.14}$$
$$B_{-s}^2(\xi,\eta) = -B_s^2(-\xi,\eta). \tag{E.15}$$

In the calculation of the cross section, we will also encounter infinite sums over generalized Bessel functions. The application of Graf's addition theorem leads to an enormous simplification of these sums. The derivation is not very instructive but rather technical and will be shown for

just one case. In the other cases, the derivation is done analogously.

$$
\begin{aligned}
&\sum_{k=-\infty}^{\infty} B^0_{k+s}(\alpha,\beta)B^0_{k+t}(\gamma,\delta) \\
=&\sum_k \left(\sum_n i^n J_{k+s-n}(\alpha)J_n(\beta)\right)\left(\sum_m i^m J_{k+t-m}(\gamma)J_m(\delta)\right) \\
=&\sum_{n,m}\left\{ i^{n+m}J_n(\beta)J_m(\delta)\sum_k J_{k+s-n}(\alpha)J_{k+t-m}(\gamma)\right\} \\
=&\sum_{n,m} i^{n+m}J_n(\beta)J_m(\delta)J_{-n+m+s-t}(\alpha-\gamma) \qquad \text{using (E.4)} \\
=&\sum_n i^n J_n(\beta)J_{-n+s-t}\left(\left(\delta^2+(\alpha-\gamma)^2\right)^{1/2}\right)\times \\
&\left(\frac{\alpha-\gamma+i\delta}{\alpha-\gamma-i\delta}\right)^{-\frac{1}{2}n+\frac{1}{2}s-\frac{1}{2}t} \qquad \text{using (E.5) and } |\alpha-\gamma|>|\delta| \\
\overset{\delta=0}{=}& B^0_{s-t}(\alpha-\gamma,\beta)
\end{aligned}
$$

We will show later that it is enough for the calculation of the cross section to restrict ourselves to the case where one argument (here δ) becomes zero[1]. Of course, $B^0_{s-t}(\alpha-\gamma,\beta)$ can be evaluated according to (E.9). The other sums yield

$$
\begin{aligned}
\sum_k B^1_{k+s}(\alpha,\beta)B^1_{k+t}(\gamma,\delta) &\overset{\delta=0}{=} \frac{1}{2}\left(B^1_{s-t+1}(\alpha-\gamma,\beta)+B^1_{s-t-1}(\alpha-\gamma,\beta)\right), \\
\sum_k B^2_{k+s}(\alpha,\beta)B^2_{k+t}(\gamma,\delta) &\overset{\delta=0}{=} \frac{1}{2i}\left(B^2_{s-t+1}(\alpha-\gamma,\beta)-B^2_{s-t-1}(\alpha-\gamma,\beta)\right), \\
\sum_k B^1_{k+s}(\alpha,\beta)B^0_{k+t}(\gamma,\delta) &= \begin{cases} B^1_{s-t}(\alpha-\gamma,\beta) & \text{if } \delta=0, \\ B^1_{s-t}(\alpha-\gamma,\delta) & \text{if } \beta=0, \end{cases} \\
\sum_k B^2_{k+s}(\alpha,\beta)B^0_{k+t}(\gamma,\delta) &= \begin{cases} B^2_{s-t}(\alpha-\gamma,\beta) & \text{if } \delta=0, \\ B^2_{s-t}(\alpha-\gamma,\delta) & \text{if } \beta=0, \end{cases} \\
\sum_k B^1_{k+s}(\alpha,\beta)B^2_{k+t}(\gamma,\delta) &= \begin{cases} \frac{1}{4i}\left(B^0_{s-t+2}(\alpha-\gamma,\beta)-B^0_{s-t-2}(\alpha-\gamma,\beta)\right) & \text{if } \delta=0, \\ \frac{1}{4i}\left(B^0_{s-t+2}(\alpha-\gamma,\delta)-B^0_{s-t-2}(\alpha-\gamma,\delta)\right) & \text{if } \beta=0. \end{cases}
\end{aligned}
$$

[1] see section 2.7

Appendix F

Derivation of $S_{fi}^{(1)}$

We start from

$$S_{fi}^{(1)} = e^2 \int \mathrm{d}^4x_1 \int \mathrm{d}^4x_2 \overline{\psi}_f(x_2) \left\{ \left(-i\hat{A}_{b,\lambda}(x_2) \right) iG(x_2, x_1) \left(-i\hat{A}_{\mathrm{Coul}}(x_1) \right) \right\} \psi_i(x_1)$$

and use the expressions (2.10) and (2.12) for the two vector potentials, the Volkov wave function (2.6) as initial and final states, and the laser-dressed electron propagator (2.9).

$$\begin{aligned}
S_{fi}^{(1)} \quad = \quad & i \frac{Ze^3 m_e}{\sqrt{2\omega_b \tilde{E}_i \tilde{E}_f V^3}} \sum_{s_1,s_2} \sum_{m_1,m_2} \int \mathrm{d}^4x_1 \int \mathrm{d}^4x_2 \int \frac{\mathrm{d}^4p}{(2\pi)^4} \int \frac{\mathrm{d}^4q}{(2\pi)^4} \left(2\pi\delta(q^0)\right) \times \\
& \overline{u}_{r_f}(p_f) \overline{U}(m_2, \xi_f, \eta_f, a, k, p_f) \exp\left[i\eta_f + iq_f \cdot x_2 - im_2 k \cdot x_2\right] \times \\
& \left(\hat{\epsilon}_{b,\lambda} \exp\left[ik_b \cdot x_2\right]\right) \left\{ B_{s_2}^0(\xi_p, \eta_p) + \frac{ea\hat{k}}{2k \cdot p} \left(\hat{\varkappa}^1 B_{s_2}^1(\xi_p, \eta_p) + \hat{\varkappa}^2 B_{s_2}^2(\xi_p, \eta_p) \right) \right\} \times \\
& \frac{\hat{p} - \frac{e^2a^2}{2k \cdot p}\hat{k} + m_e}{p^2 - m_e^{*2}} \left\{ B_{s_1}^{0*}(\xi_p, \eta_p) + \left(\hat{\varkappa}^1 B_{s_1}^{1*}(\xi_p, \eta_p) + \hat{\varkappa}^2 B_{s_1}^{2*}(\xi_p, \eta_p) \right) \frac{ea\hat{k}}{2k \cdot p} \right\} \times \\
& \exp\left[-ip \cdot (x_2 - x_1) + ik \cdot (s_2 x_2 - s_1 x_1)\right] \left(\gamma^0 \frac{1}{\vec{q}^2} \right) \exp\left[-iq \cdot x_1\right] \times \\
& U(m_1, \xi_i, \eta_i, a, k, p_i) u_{r_i}(p_i) \exp\left[-i\eta_i - iq_i \cdot x_1 + im_1 k \cdot x_1\right]
\end{aligned}$$

$$
\begin{aligned}
S_{fi}^{(1)} &= i\frac{Ze^3m_e}{\sqrt{2\omega_b\tilde{E}_i\tilde{E}_fV^3}}\exp\left[i(\eta_f-\eta_i)\right]\sum_{s_1,s_2}\sum_{m_1,m_2}\int \mathrm{d}^4x_1\int \mathrm{d}^4x_2\times\\
&\int\frac{\mathrm{d}^4p}{(2\pi)^4}\int\frac{\mathrm{d}^4q}{(2\pi)^4}\left(2\pi\delta(q^0)\right)\overline{u}_{r_f}(p_f)\overline{U}(m_2,\xi_f,\eta_f,a,k,p_f)\times\\
&\hat{\epsilon}_{b,\lambda}\left\{B^0_{s_2}(\xi_p,\eta_p)+\frac{ea\hat{k}}{2k\cdot p}\left(\hat{\varkappa}^1B^1_{s_2}(\xi_p,\eta_p)+\hat{\varkappa}^2B^2_{s_2}(\xi_p,\eta_p)\right)\right\}\times\\
&\frac{\hat{p}-\frac{e^2a^2}{2k\cdot p}\hat{k}+m_e}{p^2-m_e^{*2}}\left\{B^{0*}_{s_1}(\xi_p,\eta_p)+\left(\hat{\varkappa}^1B^{1*}_{s_1}(\xi_p,\eta_p)+\hat{\varkappa}^2B^{2*}_{s_1}(\xi_p,\eta_p)\right)\frac{ea\hat{k}}{2k\cdot p}\right\}\times\\
&\gamma^0\frac{1}{\vec{q}^2}U(m_1,\xi_i,\eta_i,a,k,p_i)u_{r_i}(p_i)\times\\
&\exp\left[i(q_f-m_2k+k_b-p+s_2k)\cdot x_2\right]\exp\left[i(p-s_1k-q-q_i+m_1k)\cdot x_1\right]
\end{aligned}
$$

We will evaluate some integrals before we proceed.

$$
\begin{aligned}
&\int \mathrm{d}^4x_1\int \mathrm{d}^4x_2\int\frac{\mathrm{d}^4p}{(2\pi)^4}\exp\left[i(q_f-m_2k+k_b-p+s_2k)\cdot x_2\right]\exp\left[i(p-s_1k-q-q_i+m_1k)\cdot x_1\right]\\
=&\int \mathrm{d}^4p(2\pi)^4\delta^{(4)}\left(q_f-m_2k+k_b-p+s_2k\right)\delta^{(4)}\left(p-s_1k-q-q_i+m_1k\right)\\
=&(2\pi)^4\delta^{(4)}\left(q_f-m_2k+k_b+s_2k-s_1k-q-q_i+m_1k\right)
\end{aligned}
$$

Since we integrated over a δ-function in the last step, we obtain the momentum relation for the intermediate electron

$$p=q_f-(m_2-s_2)k+k_b=q_i-(m_1-s_1)k+q.$$

Hence,

$$
\begin{aligned}
S_{fi}^{(1)} &= i\frac{Ze^3m_e}{\sqrt{2\omega_b\tilde{E}_i\tilde{E}_fV^3}}\exp\left[i(\eta_f-\eta_i)\right]\sum_{s_1,s_2}\sum_{m_1,m_2}\int \mathrm{d}^4q\left(2\pi\delta(q^0)\right)\times\\
&\overline{u}_{r_f}(p_f)\overline{U}(m_2,\xi_f,\eta_f,a,k,p_f)\hat{\epsilon}_{b,\lambda}\times\\
&\left\{B^0_{s_2}(\xi_p,\eta_p)+\frac{ea\hat{k}}{2k\cdot p}\left(\hat{\varkappa}^1B^1_{s_2}(\xi_p,\eta_p)+\hat{\varkappa}^2B^2_{s_2}(\xi_p,\eta_p)\right)\right\}\frac{\hat{p}-\frac{e^2a^2}{2k\cdot p}\hat{k}+m_e}{p^2-m_e^{*2}}\times\\
&\left\{B^{0*}_{s_1}(\xi_p,\eta_p)+\left(\hat{\varkappa}^1B^{1*}_{s_1}(\xi_p,\eta_p)+\hat{\varkappa}^2B^{2*}_{s_1}(\xi_p,\eta_p)\right)\frac{ea\hat{k}}{2k\cdot p}\right\}\gamma^0\frac{1}{\vec{q}^2}\times\\
&U(m_1,\xi_i,\eta_i,a,k,p_i)u_{r_i}(p_i)\delta^{(4)}\left(q_f-q_i-(m_2-s_2)k+(m_1-s_1)k+k_b-q\right)
\end{aligned}
$$

Since the indices run from negative infinity to positive infinity, they can be shifted or renamed. We choose

$$
\begin{aligned}
m_2-s_2&=m, \qquad s_2=m',\\
m_1-s_1&=s, \qquad s_1=s',
\end{aligned}
$$

and can write $p_m \equiv p = q_f - mk + k_b$. We perform the remaining integration over d^4q. This yields the energy and momentum conservation:

$$\begin{aligned}\tilde{E}_f &= \tilde{E}_i + (m-s)\omega - \omega_b,\\ \vec{q}_f &= \vec{q}_i + (m-s)\vec{k} - \vec{k}_b + \vec{q}_{m,s} \qquad \text{with} \quad q_{m,s} \equiv q.\end{aligned}$$

So, we get

$$\begin{aligned}S_{fi}^{(1)} \;=\;& 2\pi i \frac{Ze^3 m_e}{\sqrt{2\omega_b \tilde{E}_i \tilde{E}_f V^3}} \exp\left[i(\eta_f - \eta_i)\right] \sum_m \sum_{m'} \overline{u}_{r_f}(p_f) \times \\ & \left\{ B^{0*}_{m+m'}(\xi_f,\eta_f) + \left(\hat{\varkappa}^1 B^{1*}_{m+m'}(\xi_f,\eta_f) + \hat{\varkappa}^2 B^{2*}_{m+m'}(\xi_f,\eta_f)\right) \frac{ea\hat{k}}{2k\cdot p_f} \right\} \hat{\epsilon}_{b,\lambda} \times \\ & \left\{ B^0_{m'}(\xi_p,\eta_p) + \frac{ea\hat{k}}{2k\cdot p} \left(\hat{\varkappa}^1 B^1_{m'}(\xi_p,\eta_p) + \hat{\varkappa}^2 B^2_{m'}(\xi_p,\eta_p)\right) \right\} \frac{\hat{p}_m - \frac{e^2a^2}{2k\cdot p_m}\hat{k} + m_e}{p_m^2 - m_e^{*2}} \times \\ & \sum_s \sum_{s'} \frac{\delta(q^0)}{\vec{q}^{\,2}_{m,s}} \left\{ B^{0*}_{s'}(\xi_p,\eta_p) + \left(\hat{\varkappa}^1 B^{1*}_{s'}(\xi_p,\eta_p) + \hat{\varkappa}^2 B^{2*}_{s'}(\xi_p,\eta_p)\right) \frac{ea\hat{k}}{2k\cdot p} \right\} \gamma^0 \times \\ & \left\{ B^0_{s+s'}(\xi_i,\eta_i) + \frac{ea\hat{k}}{2k\cdot p_i} \left(\hat{\varkappa}^1 B^1_{s+s'}(\xi_i,\eta_i) + \hat{\varkappa}^2 B^2_{s+s'}(\xi_i,\eta_i)\right) \right\} u_{r_i}(p_i)\end{aligned}$$

Using the relations (E.10), (E.12), (E.13), this expression can be rewritten without any complex conjugated generalized Bessel functions.

$$\begin{aligned}S_{fi}^{(1)} \;=\;& 2\pi i \frac{Ze^3 m_e}{\sqrt{2\omega_b \tilde{E}_i \tilde{E}_f V^3}} \exp\left[i(\eta_f - \eta_i)\right] \sum_{m,m'} \overline{u}_{r_f}(p_f) \times \\ & \left\{ B^0_{m+m'}(\xi_f,-\eta_f) + \left(\hat{\varkappa}^1 B^1_{m+m'}(\xi_f,-\eta_f) - \hat{\varkappa}^2 B^2_{m+m'}(\xi_f,-\eta_f)\right) \frac{ea\hat{k}}{2k\cdot p_f} \right\} \hat{\epsilon}_{b,\lambda} \times \\ & \left\{ B^0_{m'}(\xi_p,\eta_p) + \frac{ea\hat{k}}{2k\cdot p} \left(\hat{\varkappa}^1 B^1_{m'}(\xi_p,\eta_p) + \hat{\varkappa}^2 B^2_{m'}(\xi_p,\eta_p)\right) \right\} \frac{\hat{p}_m - \frac{e^2a^2}{2k\cdot p_m}\hat{k} + m_e}{p_m^2 - m_e^{*2}} \times \\ & \sum_{s,s'} \frac{\delta(q^0)}{\vec{q}^{\,2}_{m,s}} \left\{ B^0_{s'}(\xi_p,-\eta_p) + \left(\hat{\varkappa}^1 B^1_{s'}(\xi_p,-\eta_p) - \hat{\varkappa}^2 B^2_{s'}(\xi_p,-\eta_p)\right) \frac{ea\hat{k}}{2k\cdot p} \right\} \gamma^0 \times \\ & \left\{ B^0_{s+s'}(\xi_i,\eta_i) + \frac{ea\hat{k}}{2k\cdot p_i} \left(\hat{\varkappa}^1 B^1_{s+s'}(\xi_i,\eta_i) + \hat{\varkappa}^2 B^2_{s+s'}(\xi_i,\eta_i)\right) \right\} u_{r_i}(p_i)\end{aligned}$$

Before we proceed, some remarks on the scattering geometry are necessary in order to use the sum rules derived at the end of appendix E. Without loss of generality, the incoming electron propagates in x-direction: $p_i = \left(E_f, \sqrt{E_f^2 - m_e^2}, 0, 0\right)$. Since it is the most interesting case, we will choose the laser to be antiparallel: $k = (\omega, -\omega, 0, 0)$. The effective four-momentum of the outgoing electron is given in its most general form (using spherical coordinates) by $q_f = \left(\tilde{E}_f, \sqrt{\tilde{E}_f^2 - m_e^{*2}}\cos\theta_f, \sqrt{\tilde{E}_f^2 - m_e^{*2}}\sin\theta_f\cos\rho_f, \sqrt{\tilde{E}_f^2 - m_e^{*2}}\sin\theta_f\sin\rho_f\right)$. Now, the question arises how to choose the laser polarization vectors. They must fulfill the relations (2.2), (2.3), and (2.4). Thus, an obvious choice would be $\varkappa^1 = (0,0,1,0)$ and $\varkappa^2 = (0,0,0,1)$. This is, of course,

possible. However, we can also choose $\varkappa^1 = (0, 0, \cos\rho_f, \sin\rho_f)$ and $\varkappa^2 = (0, 0, -\sin\rho_f, \cos\rho_f)$. Trivially, because of the scattering geometry, $\xi_i = \eta_i = 0$. Moreover, we now even obtain $\eta_f = 0$. Because of this result, it is possible to apply the sum rules of the generalized Bessel functions derived in appendix E. Besides, it will increase the speed of the computer programme. The scattering geometry will be presented in full detail in section (2.7). At this point, we know enough about it to go on with the derivation of $S_{fi}^{(1)}$.

So from now on, we have $\xi_i = \eta_i = \eta_f = 0$. We sum over s' and m' using the sum rules presented at the end of appendix E.

$$
\begin{aligned}
S_{fi}^{(1)} \;=\; & 2\pi i \frac{Ze^3 m_e}{\sqrt{2\omega_b \tilde{E}_i \tilde{E}_f V^3}} \sum_{m,s} \frac{\delta(q^0)}{\vec{q}_{m,s}^{\,2}} \overline{u}_{r_f}(p_f) \times \\
& \Big\{ \hat{\epsilon}_{b,\lambda} B^0_{-m}(\xi_p - \xi_f, \eta_p) + \frac{ea}{2k\cdot p_m} \hat{\epsilon}_{b,\lambda} \hat{k} \hat{\varkappa}^1 B^1_{-m}(\xi_p - \xi_f, \eta_p) + \\
& \frac{ea}{2k\cdot p_m} \hat{\epsilon}_{b,\lambda} \hat{k} \hat{\varkappa}^2 B^2_{-m}(\xi_p - \xi_f, \eta_p) + \frac{ea}{2k\cdot p_f} \hat{\varkappa}^1 \hat{k} \hat{\epsilon}_{b,\lambda} B^1_{m}(\xi_f - \xi_p, \eta_p) + \\
& \frac{ea}{2k\cdot p_f} \frac{ea}{2k\cdot p_m} \hat{\varkappa}^1 \hat{k} \hat{\epsilon}_{b,\lambda} \hat{k} \hat{\varkappa}^1 \frac{1}{2} \left(B^1_{-m+1}(\xi_p - \xi_f, \eta_p) + B^1_{-m-1}(\xi_p - \xi_f, \eta_p) \right) + \\
& \frac{ea}{2k\cdot p_f} \frac{ea}{2k\cdot p_m} \hat{\varkappa}^1 \hat{k} \hat{\epsilon}_{b,\lambda} \hat{k} \hat{\varkappa}^2 \frac{1}{4i} \left(B^0_{m+2}(\xi_f - \xi_p, \eta_p) - B^0_{m-2}(\xi_f - \xi_p, \eta_p) \right) - \\
& \frac{ea}{2k\cdot p_f} \hat{\varkappa}^2 \hat{k} \hat{\epsilon}_{b,\lambda} B^2_{m}(\xi_f - \xi_p, \eta_p) - \\
& \frac{ea}{2k\cdot p_f} \frac{ea}{2k\cdot p_m} \hat{\varkappa}^2 \hat{k} \hat{\epsilon}_{b,\lambda} \hat{k} \hat{\varkappa}^1 \frac{1}{4i} \left(B^0_{-m+2}(\xi_p - \xi_f, \eta_p) - B^0_{-m-2}(\xi_p - \xi_f, \eta_p) \right) - \\
& \frac{ea}{2k\cdot p_f} \frac{ea}{2k\cdot p_m} \hat{\varkappa}^2 \hat{k} \hat{\epsilon}_{b,\lambda} \hat{k} \hat{\varkappa}^2 \frac{1}{2i} \left(B^2_{-m+1}(\xi_p - \xi_f, \eta_p) - B^2_{-m-1}(\xi_p - \xi_f, \eta_p) \right) \Big\} \times \\
& \frac{\hat{p}_m - \frac{e^2a^2}{2k\cdot p_m}\hat{k} + m_e}{p_m^2 - m_e^{*2}} \times \\
& \Big\{ \gamma^0 B^0_{-s}(\xi_p, -\eta_p) + \frac{ea}{2k\cdot p_i} \gamma^0 \hat{k} \hat{\varkappa}^1 B^1_{s}(-\xi_p, -\eta_p) + \\
& \frac{ea}{2k\cdot p_i} \gamma^0 \hat{k} \hat{\varkappa}^2 B^2_{s}(-\xi_p, -\eta_p) + \frac{ea}{2k\cdot p_m} \hat{\varkappa}^1 \hat{k} \gamma^0 B^1_{-s}(\xi_p, -\eta_p) + \\
& \frac{ea}{2k\cdot p_m} \frac{ea}{2k\cdot p_i} \hat{\varkappa}^1 \hat{k} \gamma^0 \hat{k} \hat{\varkappa}^1 \frac{1}{2} \left(B^1_{-s+1}(\xi_p, -\eta_p) + B^1_{-s-1}(\xi_p, -\eta_p) \right) + \\
& \frac{ea}{2k\cdot p_m} \frac{ea}{2k\cdot p_i} \hat{\varkappa}^1 \hat{k} \gamma^0 \hat{k} \hat{\varkappa}^2 \frac{1}{4i} \left(B^0_{-s+2}(\xi_p, -\eta_p) - B^0_{-s-2}(\xi_p, -\eta_p) \right) - \\
& \frac{ea}{2k\cdot p_m} \hat{\varkappa}^2 \hat{k} \gamma^0 B^2_{-s}(\xi_p, -\eta_p) - \\
& \frac{ea}{2k\cdot p_m} \frac{ea}{2k\cdot p_i} \hat{\varkappa}^2 \hat{k} \gamma^0 \hat{k} \hat{\varkappa}^1 \frac{1}{4i} \left(B^0_{s+2}(-\xi_p, -\eta_p) - B^0_{s-2}(-\xi_p, -\eta_p) \right) - \\
& \frac{ea}{2k\cdot p_m} \frac{ea}{2k\cdot p_i} \hat{\varkappa}^2 \hat{k} \gamma^0 \hat{k} \hat{\varkappa}^2 \frac{1}{2i} \left(B^2_{-s+1}(\xi_p, -\eta_p) - B^2_{-s-1}(\xi_p, -\eta_p) \right) \Big\} u_{r_i}(p_i)
\end{aligned}
$$

This very long expression can be simplified considerably by using the relations (D.3), (D.4), (E.11), (E.14), (E.15), and the definition of the generalized Bessel functions (E.6), (E.7), and

(E.8).

$$
\begin{aligned}
S_{fi}^{(1)} \;=\; & 2\pi i \frac{Ze^3 m_e}{\sqrt{2\omega_b \tilde{E}_i \tilde{E}_f V^3}} \sum_{m,s} \frac{\delta(q^0)}{\vec{q}_{m,s}^{\,2}} \overline{u}_{r_f}(p_f) \times \\
& \left\{ \left(\hat{\epsilon}_{b,\lambda} + \frac{ea}{2k\cdot p_f} \frac{ea}{2k\cdot p_m} \hat{k}\hat{\epsilon}_{b,\lambda}\hat{k} \right) B^0_{-m}(\xi_p - \xi_f, \eta_p) + \right. \\
& \left(\frac{ea}{2k\cdot p_m} \hat{\epsilon}_{b,\lambda}\hat{k}\hat{\varkappa}^1 + \frac{ea}{2k\cdot p_f} \hat{\varkappa}^1 \hat{k}\hat{\epsilon}_{b,\lambda} \right) B^1_{-m}(\xi_p - \xi_f, \eta_p) + \\
& \left. \left(\frac{ea}{2k\cdot p_m} \hat{\epsilon}_{b,\lambda}\hat{k}\hat{\varkappa}^2 + \frac{ea}{2k\cdot p_f} \hat{\varkappa}^2 \hat{k}\hat{\epsilon}_{b,\lambda} \right) B^2_{-m}(\xi_p - \xi_f, \eta_p) \right\} \times \\
& \frac{\hat{p}_m - \frac{e^2a^2}{2k\cdot p_m}\hat{k} + m_e}{p_m^2 - m_e^{*2}} \times \\
& \left\{ \left(\gamma^0 + \frac{ea}{2k\cdot p_m} \frac{ea}{2k\cdot p_i} \hat{k}\gamma^0\hat{k} \right) B^0_{-s}(\xi_p, -\eta_p) + \right. \\
& \left(\frac{ea}{2k\cdot p_i} \gamma^0\hat{k}\hat{\varkappa}^1 + \frac{ea}{2k\cdot p_m} \hat{\varkappa}^1 \hat{k}\gamma^0 \right) B^1_{-s}(\xi_p, -\eta_p) - \\
& \left. \left(\frac{ea}{2k\cdot p_i} \gamma^0\hat{k}\hat{\varkappa}^2 + \frac{ea}{2k\cdot p_m} \hat{\varkappa}^2 \hat{k}\gamma^0 \right) B^2_{-s}(\xi_p, -\eta_p) \right\} u_{r_i}(p_i)
\end{aligned}
$$

We want the energy and momentum conservation to depend on only one index. Therefore we define $m - s =: n$. Then, $q_f = q_i + nk - k_b + q_n$ with $q_n \equiv q$. As a further result, we have $p_m \equiv p_{n,s} = q_f - (n+s)k + k_b$. With the definition (2.16) and (2.17) and using (D.1), (E.10), (E.12), and (E.13), this can be written in a more compact form:

$$
\begin{aligned}
S_{fi}^{(1)} =& 2\pi i \frac{Ze^3 m_e}{\sqrt{2\omega_b \tilde{E}_i \tilde{E}_f V^3}} \sum_{n,s} \frac{\delta(q_n^0)}{\vec{q}_n^{\,2}} \overline{u}_{r_f}(p_f) \times \\
& \left\{ F^{f,p_{n,s}}_{-n-s}(\xi_p - \xi_f, \eta_p) \frac{\hat{p}_{n,s} - \frac{e^2a^2}{2k\cdot p_{n,s}}\hat{k} + m_e}{p_{n,s}^2 - m_e^{*2}} \overline{G}^{i,p_{n,s}}_{-s}(\xi_p, \eta_p) \right\} u_{r_i}(p_i).
\end{aligned}
$$

A completely analogous calculation yields the second contribution $S_{fi}^{(2)}$ to the S-matrix. This calculation will not be presented in this thesis. Adding $S_{fi}^{(1)}$ and $S_{fi}^{(2)}$ up leads to the expression (2.15).

Appendix G

Main Structure of the Programme

In the following, the main structure of the programme will be presented. This does not mean that every definition or every calculation will be shown. Rather we want to present the most important parts like modules, functions, and loops, and how they are interconnected. One should note that we will present the programme for the calculation of spectra, i.e. the bremsstrahlung frequency ω_b is varied. For other graphs, the programme has to be modified accordingly. However, the overall structure remains the same in all cases. Lines which are written in a `typewriter font` are direct quotes from the programme code; the lines in-between written in normal letters are explanations of the preceding lines.

```
include 'bessel.f90'
include 'intlib.f90'
include 'variable_declaration.f90'

program int_brems

  use variable_declaration
  use Besselfunctions_GenBesselfunctions
  ...
```

The module `Besselfunctions_GenBesselfunctions` calculates the Bessel functions. In the other module `variable_declaration`, all variables are declared. With the help of the `use`-statement right at the beginning of the programme, both modules are made accessible to all parts (functions and subroutines) of the programme. They are included by the commands `include 'bessel.f90'`, `include 'variable_declaration.f90'`. The input file `intlib.f90` is a library of numerical integration routines which will be used later on.

```
!* Start of Executable Section

...

!* Start of Loop wb
!* (cross section in dependance on wb)

  open(unit=25,file='output.dat',status='new',action='write',iostat=status)
  ...
```

```
if (status == 0) then
   do wb = 0.01_QD*w,10._QD*w,0.01_QD*w
      ...
      call int_theta1(integrand_theta1,0._QD,0.0001_QD)
      ...
      write(25,*), real(wb/w), real(total,8)
   end do
else
   print*, "Error while trying to open file."
end if
close(unit=25)
```

Here, we can see the main loop over $\omega_b \equiv$ `wb` and how it is incremented after each cycle. The laser frequency $\omega \equiv$ `w` serves as a scaling factor. During each cycle, the integration routine `int_theta1` is called with the function to be integrated as an argument (for closer explanations, see section (3.3)). Afterwards, the result is written to a file called `output.dat`.

```
contains

!* Functions used for the Calculation

  function sum_n(rho1, theta1)
    ...
    do n= -nmax,nmax
       ...
       do lambda = 1,2
         sum_n = sum_n + cross(n,lambda,smax)
       end do
       ...
    end do
    ...
  end function sum_n
```

`sum_n` is the function which we use for the calculation of the differential cross section. The sums over $n \equiv$ `n` and $\lambda \equiv$ `lambda` take place in this function. For the calculation of the trace in (2.23), which also includes the s-sum, we call the following function.

```
  function cross(n, lambda, smax) result (intres)
    ...
    do s = -smax, smax
       ...
       qsum = qsum + prop(n,s,lambda)
       ...
       qsum = qsum + propprime(n,s,lambda)
       ...
    end do
    ...
  end function cross
```

The two propagators are calculated in separate functions `prop` and `propprime` which will be explained below. Their value is then summed up over $s \equiv$ `s`.

```
  function slash(p) result (slash_p)
  ...
  end function slash

  function diracadj(M) result (Mbar)
  ...
  end function diracadj

  function trace(m) result (trace_m)
  ...
  end function trace

  function g(x,y)
  ...
  end function g

  function step(x)
  ...
  end function step

  function norm(vec)
  ...
  end function norm
```

Those little functions are thoroughly discussed in section (3.2) and are used to implement the Minkowski metric and the four-vector calculation into Fortran.

```
!* Propagators prop (n,s,lambda) and
!* propprime(n,s,lambda)

  function prop(n,s,lambda)
    ...
    psn = q2-(n+s)*k+kb                    ! electron propagator p
    ...

  ! imaginary mass shift-------------------------------------------------------
    Wkp = 240._QD*g(k,psn)                 ! a = 30 MeV: b = 371 1/MeV
                                           ! a = 20 MeV: b = 240 1/MeV
                                           ! a = 10 MeV: b = 110 1/MeV

    propagator = (slash(psn)-e**2*atilde**2/(2._QD*g(k,psn))*slash(k)+m*unit)/&
            (2._QD*(-(n+s)*g(q2,k)+g(q2,kb)-(n+s)*g(k,kb)+&
            (0._QD,1._QD)*(n+s)*(m**2/Etilde2)*w*finestructure/8._QD*Wkp-&
            (0._QD,1._QD)*(m**2/Etilde2)*wb*finestructure/8._QD*Wkp))
  ! ---------------------------------------------------------------------------

    aa = (slash(epsilonb(lambda,:))+e**2*atilde**2/(4._QD*g(k,p2)*g(k,psn))*&
         matmul(matmul(slash(k),slash(epsilonb(lambda,:))),slash(k)))*&
         bessel1(0,-n-s)
```

```
    bb = ...
    cc = ...
    dd = ...
    ee = ...
    ff = ...

    prop = matmul(matmul(aa+bb+cc,propagator),diracadj(dd+ee+ff))
  end function prop


  function propprime(n,s,lambda)
  ...
  end function propprime
```

The propagator Q according to (2.22) is calculated in the Fortran programme by $Q^{\lambda}_{n,s}$ = `prop(n,s,lambda)` + `propprime(n,s,lambda)`. The two functions `prop` and `propprime` are very similar to each other. Therefore, we will only discuss `prop` here.

In (2.22), we have the two functions F and G which themselves consist of three summands (2.16), (2.17). Thus, we can write $F =$ `aa` + `bb` + `cc` and $G =$ `dd` + `ee` + `ff`. Again, we will just show the summand `aa` since all summands are all similar to each other. As arguments, the three summation indices n, s, and λ are assigned to `prop`. All other variables like $q_f \equiv$ `q2`, $k_b \equiv$ `kb` etc. are globally defined and can be accessed by all functions. First, the four-momentum $p_{n,s} \equiv$ `psn` of the intermediate electron is calculated. Then, we need the imaginary mass shift: $\tilde{W}_\gamma(k \cdot p_{n,s}) \equiv$ `Wkp = 240._QD*g(k,psn)`. Here, the slope is already set to 240 according to $a = 20\,\mathrm{MeV}$. Now, we can easily write down the propagator according to equation (2.31), here in a mixed mathematical–Fortran notation:

$$\texttt{propagator} = \frac{\texttt{slash(psn)} - \frac{\texttt{e}^2\texttt{a}^2}{2\texttt{g(k,psn)}}\texttt{slash(k)} + \texttt{m}\mathbb{1}}{2\texttt{(-(n+s)g(q2,k)+g(q2,kb)-(n+s)g(k,kb)} + i\frac{\texttt{m}^2\texttt{finestructure}}{8\,\texttt{Etilde2}}\,\texttt{((n+s)w-wb))}}.$$

Then, we have to calculate `aa` $= \left(\hat{\epsilon}_{b,\lambda} + \frac{ea}{2k\cdot p_i}\frac{ea}{2k\cdot p_{n,s}}\hat{k}\hat{\epsilon}_{b,\lambda}\hat{k}\right) B^0_n(\xi,\eta)$. The generalized Bessel functions are stored in an array: $B^0_{-n-s} \equiv$ `bessel1(0,-n-s)`[1].

According to (2.16), (2.17), and (2.22), we can finally write down the expression for the return value of the function `prop`:

$$\texttt{prop} = (\texttt{aa} + \texttt{bb} + \texttt{cc}) \cdot \texttt{propagator} \cdot \overline{(\texttt{dd} + \texttt{ee} + \texttt{ff})}.$$

```
!* subroutines for numerical integration
!* making use of libary intlib.f90

  function integrand_theta1(theta1)
    ...
    call int_rho1(sum_n, a, b, theta1)
    ...
  end function integrand_theta1

  subroutine int_theta1 ( func, a, b )
    ...
```

[1] The Bessel and generalized Bessel functions are calculated using an algorithm described in [18].

```
    call gaus8 ( func, a, b, err, result, ier )
    return
  end subroutine int_theta1

  subroutine int_rho1 ( func, a, b, theta1 )
    ...
    call quad (...)
    return
  end subroutine int_rho1

end program int_brems
```

These routines and functions are used for the numerical integration of the differential cross section. This is explained in section (3.3).

Bibliography

[1] T. Kinoshita, *Quantum Electrodynamics* (World Scientific, Singapore, 1990).

[2] B. Odom, D. Hanneke, B. D'Urso, and G. Gabrielse, Phys. Rev. Lett. **97**, 030801 (2006).

[3] U. D. Jentschura, S. Kotochigova, E.-O. L. Bigot, P. J. Mohr, and B. N. Taylor, Physical Review Letters **95**, 163003 (2005).

[4] H. Bethe and W. Heitler, Proc. Roy. Soc. A **146**, 83 (1934).

[5] D. M. Volkov, Z. Phys. **94**, 250 (1935).

[6] T. H. Maiman, Nature **187**, 493 (1960).

[7] M. Protopapas, C. H. Keitel, and P. L. Knight, Rep. Prog. Phys. **60**, 389 (1997).

[8] A. I. Nikishov and V. I. Ritus, JETP **19**, 529 (1964).

[9] N. B. Naroshnyi, A. I. Nikishov, and V. I. Ritus, JETP **20**, 622 (1965).

[10] P. Panek, J. Z. Kamiński, and F. Ehlotzky, Phys. Rev. A **65**, 022712 (2002).

[11] W. B. Berestetski, E. M. Lifschitz, and L. P. Pitajewski, *Quantenelektrodynamik (Band IV der Lehrbuchreihe über Theoretische Physik von L. D. Landau und E. M. Lifschitz)*, 5 ed. (Akademie-Verlag, Berlin, 1986).

[12] W. Greiner and J. Reinhardt, *Quantum Electrodynamics*, 3 ed. (Springer, Berlin – Heidelberg – New York, 2003).

[13] P. B. Corkum, Phys. Rev. Lett. **71**, 1994 (1993).

[14] H. R. Reiss and J. H. Eberly, Phys. Rev. **151**, 1058 (1966).

[15] V. I. Ritus, Ann. Phys. (N.Y.) **69**, 555 (1972).

[16] H. Mitter, Acta Phys. Austriaca Suppl. **XIV**, 397 (1975).

[17] S. Zakowicz, J. Math. Phys. **46**, 032304 (2005).

[18] U. D. Jentschura, K. Z. Hatsagortsyan, and C. H. Keitel, internal report (unpublished).

[19] M. M. Denisov and M. V. Fedorov, JETP **26**, 779 (1968).

[20] H. B. G. Casimir, Helv. Phys. Acta **6**, 287 (1933).

[21] S. P. Roshchupkin, Sov. J. Nucl. Phys. **41**, 796 (1985).

[22] P. Davis and P. Rabinowitz, *Methods of Numerical Integration*, 2 ed. (Blaisdell Publishing, New York – Toronto – London, 1967).

[23] E. Lötstedt, U. D. Jentschura, and C. H. Keitel, submitted to Physical Review Letters (unpublished).

[24] C. Szymanowski, V. Véniard, R. Taïeb, A. Maquet, and C. H. Keitel, Phys. Rev. A **56**, 3846 (1997).

[25] S. Schnez, E. Lötstedt, U. D. Jentschura, and C. H. Keitel, in preparation (unpublished).

[26] H. W. Koch and J. W. Motz, Rev. Mod. Phys. **31**, 920 (1959).

[27] C. Itzykson and J.-B. Zuber, *Quantum Field Theory*, 2 ed. (Dover Publications, Mineola, NY, 2006).

[28] V. A. Lyul'ka, JETP **40**, 815 (1974).

[29] F. Mandl and G. Shaw, *Quantum Field Theory, Revised Edition*, 1 ed. (J. Wiley & Sons, Chichester – New York – Brisbane – Toronto – Singapore, 1993).

[30] M. Abramowitz and I. A. Stegun, *Handbook of Mathematical Functions* (Dover Publications, Mineola, NY, 1972).

[31] H. Bateman, *Higher Transcendental Functions, Volume II* (McGraw-Hill Book Company, Inc., New York, 1953).

Acknowledgement

At the end of this work, it is time to say thank you to all persons who helped me and contributed somehow to the outcome of the thesis. First of all, I want to thank Professor Christoph Keitel. He gave me the possibility to work as a project student in the theory group before I started my diploma thesis. I do not know whether I would have dared to write a theoretical diploma thesis without this prior insight. My second supervisor Privatdozent Dr. Ulrich Jentschura gave valuable hints and suggestions whenever I had questions concerning my thesis. But moreover – and this is not self-evident –, he helped and advised me while I was on my search for a PhD position. I worked closely together with Erik Lötstedt. The discussions with him lead to crucial improvements of my thesis. I do not know what the outcome of my work would have been without his help. My biggest thanks go to these three persons.

Of course, there are other persons I talked to and asked questions: Andreas, Andrey, Carsten, Michael, Zoltán, ... I thank them for their advice and help. Special thanks also go to my room mates Chirag, Matthias, and Stefan. Countless discussions on physics and life in general, on the differences between Germany and India lead to a friendly, amicable, but also agitated atmosphere in our room. Working at the MPI would have been boring without their company. And finally, it was always a pleasure to meet the other group members during the coffee break.

Physics affected my life quite strongly during the last year. However, there is – fortunately – life in addition to physics. All persons, my family and my friends, I spent time with helped and supported me by their means. They all know how valuable they are for me. I thank them for being my family and friends and for just being there.

Erklärung gemäß Prüfungsordnung

Ich versichere, daß ich diese Arbeit selbständig verfaßt und keine anderen als die angegebenen Quellen oder Hilfsmittel benutzt habe.

Heidelberg, den

(Stephan Schnez)